

REAL-TIME fMRI DECODING

READING MINDS USING BRAIN IMAGING



UNIVERSITEIT TWENTE 

Master's Thesis by
Adnan Muhammad Niazi * ‡
s1029789

External Supervisors

Marcel van Gerven *
Philip van den Broek *
Peter Desain *

Internal Supervisors

Mannes Poel ‡
Femke Nijboer ‡

*Donders Centre for Cognition,
Donders Institute for Brain, Cognition and Behavior,
Radboud University, Nijmegen, The Netherlands.

‡Human Media Interaction Group,
Faculty EEMCS, University of Twente, The Netherlands

REAL-TIME fMRI DECODING

READING MINDS USING BRAIN IMAGING

Adnan Muhammad Niazi

s1029789

a.m.niazi@student.utwente.nl

Human Media Interaction Group, Faculty of Electrical Engineering, Mathematics and Computer Science (EEMCS)
University of Twente, Enschede, The Netherlands

Thesis submitted to obtain the degree of
MASTERS OF SCIENCE IN COMPUTER SCIENCE
with specialization
HUMAN MEDIA INTERACTION

Date: August 01, 2012

External Supervisors

Dr. Marcel van Gerven

ir. Philip van den Broek

Prof. Dr. Peter Desain

Donders Centre for Cognition, Donders Institute for Brain, Cognition and Behavior
Radboud University, Nijmegen, The Netherlands.

Internal Supervisors

Dr. Mannes Poel

Dr. Femke Nijboer

Human Media Interaction Group, Faculty of Electrical Engineering, Mathematics and Computer Science (EEMCS)
University of Twente, Enschede, The Netherlands

Download a PDF version of this thesis including detailed videos and supplementary materials

www.analyze4d.com/misc_adnan/masters_thesis_adnan.rar



Front page picture by:

Melissa Clark

Stella Harper Events

The picture is inspired by Mercedes Benz 'Left Brain, Right Brain' advertisement.

<http://stellaharperevents.blogspot.nl/2012/02/left-brain-right-brain-painting.html>

ACKNOWLEDGMENTS

I would like to thank a few people for helping and supporting me during the course of this research project.

First of all, I would like to thank my weekly supervisor, Marcel van Gerven, for his feedback and input, and for keeping me motivated throughout the duration of this study. With his positive attitude, even at the most disappointing and disheartening junctures in this project, he always lifted my morale and set me on the right track.

I also highly appreciate the support from Philip van den Broek for the countless number of times that he had to modify the stimulus presentation scripts for me and for expanding my understanding of BrainStream. I thank him for his time, effort, and patience.

Kudos to Paul Gaalman from the MRI Lab for being so accommodating in giving me tonnes of extra scanning time beyond my assigned quota, and for broadening my understanding of rtfMRI architecture at Donders. With his jovial personality, it was always fun to run experiments at the MRI lab.

I am also highly grateful to Mannes Poel, Femke Nijboer and Peter Desain for their continued supervision and guidance through out this process.

Last by not least, I would like to thank my friends and family for supporting me. In particular, I would like to thank my sister Fariha Atta, for thinking along with me when encountering specific problems.

*Adnan Niazi
August 01, 2012*

ABSTRACT

REAL-time functional magnetic resonance (rtfMRI) imaging is a relatively new technique to compute moment-to-moment changes in brain activations corresponding to a particular experimental manipulation. When coupled with modern machine learning techniques, rtfMRI becomes a powerful tool to read brain states in real time. Two separate experiments were conducted in this study to answer two broad research goals.

The first experiment was conducted to investigate if visual perception and imagination can be decoded in real-time and if presenting neurofeedback of the decoding results can help improved decoding/task performance. 25 elastic net logistic regression classifiers were trained on fMRI responses for 100 random flickering random patterns on a 5 x 5 grid in order to learn the stimulus to cortical activation mapping. The trained classifiers were then used to predict novel stimuli perceived and imagined on the same 5 x 5 grid used in training. Each perception and imagination conditions were performed twice once with feedback and once without it. The results of the study indicate that visual perception can be decoded in real-time with an average accuracy of 55%. No significant decoding accuracy was obtained for imagined stimuli. Furthermore, lower decoding accuracies were obtained for conditions with feedback than the same conditions

without feedback. However, the results of this experiment cannot be trusted as some critical mistakes were made in its design and implementation including selecting a wrong voxel size and using a very long visual cortex stimulation (12s) during training. All this led to poor performance in the experiment. Furthermore, the results indicate that subject motivation and experiment duration have a significant impact on task performance during the experiment.

The second experiment was conducted to find if one of the two competing stimulus categories can be attended to and decoded in real-time and if presenting feedback of the decoding can assist in improving task performance. The classifier was trained on pictures of famous faces and places. Subjects were then shown a 50/50 hybrid of a picture of famous face and a famous place and asked to attend to only one of them. The attended picture was then decoded in real-time and the hybrid mix was updated at every TR such that if the prediction was right, the non-target picture will fade out whereas the target picture will get enhanced and vice versa. This is what happened in trials in feedback. In trials without feedback, the hybrid mix remained at 50/50 % at all time during a trials. The results of the study indicate that the attended category can be decoded with very high accuracy (78.5%). Furthermore, the feedback of the decoded category has no influence on the decoding accuracy. The feedback does however, induce a snow ball effect where one classification leads to a stream of similar classifications in subsequent TRs in a trial. The results also indicate that the transition period of the BOLD activity has a reliable structure that can be decoded with above chance level accuracies, thereby decreasing the real-time fMRI delay by as much as 6s.

Apart from these two experiments, the real-time fMRI architecture used for executing real-time fMRI experiments was developed and refined. Moreover, tools for efficient analysis and visualization of fMRI and rtfMRI data were also developed.

CONTENTS IN BRIEF

1	Introduction	1
2	Background	5
3	Real-time decoding of visual perception and imagery	19
4	Online voluntary control of category-selective brain regions	51
5	Hardware/Software Development	81
6	Summary and General Discussion	91
	Bibliography	94
	Appendices	102

CONTENTS

Acknowledgments	i
Abstract	iii
List of Figures	xi
Acronyms	xv
Glossary	xvii
1 Introduction	1
1.1 Project motivation and goals	2
1.2 Structure of the thesis	3
2 Background	5
2.1 Functional Magnetic Resonance Imaging (fMRI)	5
2.1.1 Hemodynamic response function (HRF)	6
2.1.2 fMRI terminologies and procedure	7
2.2 Real-time functional Magnetic Resonance Imaging (rtfMRI)	8
2.2.1 Real-time data acquisition and streaming	9
2.2.2 Preprocessing	9
	vii

2.2.3	Real-fMRI design constraints	13
2.3	Decoding	13
2.3.1	Elastic Net Logistic Regression	16
3	Real-time decoding of visual perception and imagery	19
3.1	Introduction	19
3.2	Method	23
3.2.1	Subjects	23
3.2.2	Experimental task	24
3.2.3	Experimental protocol	33
3.2.4	MRI Acquisition parameters	35
3.2.5	Real-time fMRI processing	35
3.2.6	Data analysis	36
3.3	Results	38
3.4	Discussion	44
3.5	Suggestions for future improvements	48
4	Online voluntary control of category-selective brain regions	51
4.1	Introduction	52
4.2	Method	54
4.2.1	Subjects	54
4.2.2	Experimental Task	54
4.2.3	Experimental protocol	62
4.2.4	MRI Acquisition parameters	63
4.2.5	Real-time fMRI processing	64
4.2.6	Data Analysis	64
4.3	Results	67
4.4	Discussion	76
4.5	Conclusion	79
5	Hardware/Software Development	81
5.1	Distributed real-time fMRI pipeline	81
5.2	Shortcomings of distributed real-time fMRI pipeline	83
5.3	Integrated real-time fMRI pipeline	83
5.4	Analyze4D	85
5.4.1	Features of Analyze4D	87
5.5	Analyze4D RT	88
5.6	Significance of developed hardware/software	88

6	Summary and General Discussion	91
6.1	Future of real-time fMRI	93
	Bibliography	94
	References	94
	Appendices	102
	Appendix A	105
	Appendix B	107
	Appendix C	109
	Appendix D	110
	Appendix E	118
	Appendix F	126
	Appendix G	130
	Appendix H	131

LIST OF FIGURES

2.1	Hemodynamic response function (HRF)	6
2.2	Voxels, Slices and Volume	7
2.3	Slit-scan photography analogue to the slice timing problem	9
2.4	Prospective Acquisition CorrEction (PACE)	11
2.5	Boundary slice masking	12
2.6	Timeline of a real-time fMRI experiment	13
2.7	Timeline of a conventional (non real-time) fMRI experiment	13
3.1	Dorsal and ventral pathways in the brain	20
3.2	Retinotopic organization of visual cortex in a monkey	21
3.3	Basic building blocks of the stimulus	26
3.4	Stimuli used for training	28
3.5	Stimuli used in ‘Visual perception with no feedback condition’	29
3.7	Basis set of letters used in the experiment	30
3.6	Stimuli used in ‘Visual perception with feedback condition’	31

3.8	Stimuli used in ‘Visual imagery with no feedback condition’	32
3.9	Stimuli used in ‘Visual imagery with feedback condition.	34
3.10	Slice positioning	35
3.11	Decoding accuracy per subject	38
3.12	Decoding accuracy per TR with cumulative averaging of scan data	39
3.13	Decoding accuracy per TR without averaging of scan data	40
3.14	Vividness of Visual Imagery(VVIQ) score for each subject	40
3.15	Reconstructions for visual perception condition averaged across group	41
3.16	Reconstructions for visual imagery condition averaged across group	42
3.17	Reconstructions for visual perception condition averaged across subject 02 and 03	43
3.18	Classifier Weights	46
3.19	Voxel for time course analysis	46
3.20	Voxel time course	47
4.1	Structure of the training phase	55
4.2	Structure of face, place and rest blocks in the training phase	56
4.3	Face-place pair selection	58
4.4	Basis set of 15 picture pairs used in the test phase	59
4.5	Structure of feedback and non-feedback trial in the test phase	60
4.6	Test phase	61
4.7	Slice positioning	63
4.8	Accuracy of feedback and non-feedback trials for all subjects	68
4.9	Accuracy of face and place trials in feedback and non-feedback condition	68
4.10	Accuracy of feedback and non-feedback trials in transition period	69
4.11	Accuracy of feedback and non-feedback trials in stable period	70
4.12	Accuracy as a function of TR for feedback and non-feedback conditions	70
4.13	Accuracy as a function of TR for place and face trials in feedback and non-feedback conditions	71
4.14	Classifier bias	71

4.15	All brain regions activated across subjects	72
4.16	All brain regions activated for more than two subjects	73
4.17	Brain region activated during the experiment	73
4.18	Region of interest (ROI) analysis	74
4.19	Region of interest (ROI) analysis	74
4.20	Classifier weights	75
4.21	Voxel time course	75
4.22	Snow ball effect of feedback	77
4.23	Some examples of pictures of famous places and faces	78
4.24	Example pictures of supposedly famous places unfamiliar to most of the subjects	79
5.1	Distributed real-time fMRI pipeline	84
5.2	Integrated real-time fMRI pipeline	86
5.3	A screenshot of Analyze4D	87

ACRONYMS

AAL	Automated Anatomical Labeling
AC-PC	Anterior and Posterior commissure
AFNI	Analysis of Functional NeuroImages
BCI	Brain Computer Interface
BET	Brain Extraction Tool
BOLD	Blood Oxygenation Level-Dependent
BITSI	Bits to Serial Interface
CSF	Cerebral Spinal Fluid
DICOM	Digital Imaging and Communications in Medicine
DMLT	Donders Machine Learning Toolbox
EEG	Electroencephalography
EPI	Echo Planar Imaging
FA	Flip Angle
FFA	Fusiform Face Area
fMRI	Functional Magnetic Resonance Imaging

FSL	Functional MRI of the Brain Software Library
GBVS	Graph Based Visual Saliency
GLM	General Linear Model
HRF	Hemodynamic Response Function
M	Mean
MEG	Magnetoencephalography
MOCO	MOtion CORrected
MNI	Montreal Neurological Institute
MPRAGE	Magnetization Prepared RAPid Gradient Echo
MRI	Magnetic Resonance Imaging
MTL	Medial Temporal Lobe
NIFTI	Neuroimaging Informatics Technology Initiative
OFA	Occipital Face Area
ROI	Region of Interest
rtfMRI	Real-time functional Magnetic Resonance Imaging
PACE	Prospective Acquisition CorrEction
PPA	Parahippocampal Place Area
PET	Positron Emission Tomography
PTB	Psychtoolbox
RLSGLM	Recursive Least Square General Linear Model
SD	Standard Deviation
SEM	Standard Error of the Mean
SPM	Statistical Parametric Mapping
T	Tesla
TTL	Transistor Transistor Logic
TE	Echo Time
TR	Repetition Time
VOI	Volume of interest

GLOSSARY

AAScout Stands for AutoAlign Scout. It is a sequence that compares the acquired image to a reference atlas that allows automated placement of the preceding sequences.

BrainStream BrainStream is a MATLAB-based software package for real-time processing of continuous data streams.

BOLD BOLD or Blood Oxygenation Level Dependent functional magnetic resonance imaging is a form of magnetic resonance imaging of the brain that registers blood flow to functioning areas of the brain.

BITSI stands for Bits to Serial Interface. It is used to send and receive trigger and response signals in EEG, MEG, fMRI and Behavioral studies. It is a simple building block that has a serial port and two eight bit ports: input and output. The two ports can be used for responses (input) and stimulus triggers (output). By using the serial port, the BITSI can be used platform independent, i.e. it works on Windows, Linux and Mac OSX. In virtually any programming language, it is possible to communicate with the serial port.

Channels A channel in fMRI refers to the time course data of one voxel. A typical fMRI volume contains thousands of these channels.

EPI The EPI is a T2 sequence that is sensitive to the changes in oxy-hemoglobin and therefore is used to generate brain activated areas.

FieldTrip FieldTrip is the MATLAB software toolbox for EEG, MEG and fMRI analysis that is being developed at the Center for Cognitive Neuroimaging of the Donders Institute for Brain, Cognition and Behavior together with collaborating institutes.

HRF HRF or Hemodynamic response function is the predicted BOLD response to an instantaneous neuronal signal. Its shape and delay varies between individuals, across brain areas, with alertness etc. The sluggishness or inertia of the HRF limits the temporal resolution of fMRI.

Matrix or Display Matrix The total number of pixels in the selected matrix, which is described by the product of its phase and frequency axis. For example if the readout and phase resolution of an fMRI is 64 and 48 respectively then the display matrix would be 64 x 48.

fMRI fMRI or Functional magnetic resonance imaging, is a technique for measuring brain activity by detecting the changes in blood oxygenation and flow that occur in response to neural activity. When a brain area is more active it consumes more oxygen and to meet this increased demand blood flow increases to the active area. fMRI can be used to produce activation maps showing which brain regions are involved in a particular mental process.

MPRAGE The MPRAGE is a 3D gradient echo sequence which acquires a high resolution T1 sagittal structural data set. These images are used to define functional slices to make sure they are covering the required anatomy. This structural scan is also what is used to overlay activations on.

PACE PACE or Prospective Acquisition CorrEction is Siemens implementation of online motion correction in which MRI gradients are changed whenever head motion occurs such that the same spatial location in the brain are scanned no matter where the head moves inside the scanner.

Longitudinal equilibrium When a scanner is first started the MR signal is much higher than what it will be later on during the experiment. It takes about at least 3s before a quasi stable MR signal level (equilibrium) is reached. Because the scans collected till the longitudinal equilibrium has reached have higher contrast then the scans that follow, therefore these few scans need to be discarded from analysis.

Preprocessing data buffer The preprocessed data buffer is a FieldTrip buffer which receives data from raw data buffer, one sample at a time, and applies all

the preprocessing steps to it. The preprocessed data is stored so that another application down the line can access it whenever needed.

Phase resolution The two axes in an image are thus the "readout" axis and the "phase-encode" axis. For a transaxial image in the traditional orientation (z-axis along the main magnetic field), the z-gradient is used to select the slice. The y-gradient may be used for "phase-encoding" and the x-gradient for "frequency-encoding" or "readout" (or vice versa). The number of voxels in the y direction, is known as the phase resolution.

Readout resolution The two axes in an image are thus the "readout" axis and the "phase-encode" axis. For a transaxial image in the traditional orientation (z-axis along the main magnetic field), the z-gradient is used to select the slice. The y-gradient may be used for "phase-encoding" and the x-gradient for "frequency-encoding" or "readout" (or vice versa). The number of voxels in the x direction, is known as the readout resolution.

Raw data buffer Raw data buffer is a FieldTrip buffer that can receive raw neurological data from a data acquisition client such EEG, MEG or fMRI. The FieldTrip buffer is a network transparent TCP server that allows the acquisition client to stream data to it per sample or in small blocks, while at the same time previous data can be analyzed.

Real-time In streaming applications, an operation on a data sample is said to be real-time if it is completed before the next sample becomes available.

Repetition time or TR TR is the time interval between two successive scans. One scan is acquired in each TR. Each scan contains N slices as specified in the acquisition protocol.

StimBox A toolbox (in development) which uses Psychtoolbox for developing dynamically updateable agenda-based stimulus presentation designs.

Scan A scan refers to the one acquisition of the whole/ partial brain data. Each scan contains N different slices as specified in the fMRI scanner setting.

Sample A sample in real-time fMRI refers to one volume of MRI brain data.

SPM SPM is a MATLAB software package implementing Statistical Parametric Mapping for neuroimaging data. Statistical Parametric Mapping refers to the construction and assessment of spatially extended statistical processes used to test hypotheses about functional imaging data.

Slice A slice is one slab of brain voxels. Each slice contain $R \times P$ voxels, where R is the readout resolution and P in the phase resolution. N slices of the brain constitute one volume or scan.

Volume A volume is the same as a Scan. Each volume contains N slices as specified in the MRI sequence. In normal 2D-EPI sequences, each volume is acquired slice by slice. In 3D Flash sequences, all the slices are acquired at once.

Voxel Voxel or *Volume Element* is the basic measured entity in fMRI and it represents the BOLD activity in a small 3D brain area.

CHAPTER 1

INTRODUCTION

READING human thoughts and intention has been one of the biggest fantasies of many in recent decades. Over the years, these fantasies have also trickled in the entertainment media as well. In the 1983 film *Brainstorm*, Christopher Walken playing a scientist, was able to record movies of people's mental experiences, then play them back into the minds of other people. More recently, in 2010, in the episode *Black Hole* of the popular TV series, *House M. D.*, Dr. Gregory House was able to make a medical diagnosis of a patient suffering from hallucinations. By using a fictitious fMRI-based gadget, the 'Cognitive Pattern Recognition' device, the doctor was able to tap into the patient's brain and see the reconstructions of the hallucinogenic thoughts, as they were happening in the patient's brain. Although these might seem like a leap of imagination, one step too many, the current state of the art is getting fairly close to making these fictions a reality. In 2011, researchers at the Gallant Lab in UC, Berkeley, by utilizing functional Magnetic Resonance Imaging (fMRI) and computer models, demonstrated the visual reconstructions of brain activity of human subjects watching movie trailers; in other words, they could see what the people's brains were seeing. Hence mind reading is no longer a thing of science fiction.

Formally, mind reading refers to the ability to ascribe mental states based on the information derived from neuroimaging [12]. Although there are many neuroimaging techniques such as CT, PET, MEG, and fMRI, but none is more suited to the mind reading problem than *functional Magnetic Resonance Imaging* (fMRI). With its high spatial resolution coupled with its ability to measure moment-to-moment changes in the brain activity patterns, fMRI is ideally suited to gauge cognitive activities in the human brain.

Although mind reading is still in its infancy, the technology will make a profound impact on the lives of many. It would permit the profoundly handicapped, those paralyzed by conditions such as motor-neuron disease and cerebral palsy, to communicate more easily. It might unlock the mental prison of patients suffering from diseases like *Locked in Syndrome* (LIS). For the able-bodied, it could allow workers to dictate documents silently to computers simply by thinking about what they want to say. And most importantly, such a device might one day be able to detect lies and help judicial systems to prosecute criminals and deliver justice.

1.1 PROJECT MOTIVATION AND GOALS

Although decoding of mental activity has been demonstrated in many studies [83, 87, 121, 129], none of them were performed in real time. Data was collected from the subjects in a scanner in long scanning sessions. After all the data had been acquired, it would take several hours to build the models or train the classifiers, and then these models/classifiers were used offline on a portion of the previously collected data to predict the perceived stimulus. If brain reading is to be viable for any future application, then the decoding has to be done on-the-fly. In other words, decoding the mental activity of a person should be done while these mental states are being generated. Therefore, our first research goal is:

R1: *To demonstrate an online decoding of perceived stimuli using real-time fMRI*

Furthermore, although past studies have demonstrated the decoding of perceived stimuli, i.e., these studies tried to decode the brain activity elicited by pictures [115], or letters [83, 121], or movies [87]; the real-time decoding of mental activity of purely imagined percepts has never been attempted. Decoding imagination in real time is the essence of mind reading. Future mind reading devices would only be useful if they could read imagined percepts/intentions on-the-fly. Therefore, this study will investigate if an imagined percept can be decoded in real time using models that were previously trained on perceived stimuli. This brings us to our second objective:

R2: *To demonstrate online decoding of imagined stimuli using a classifier which is trained only on perceived stimuli*

Because decoding can never be 100% perfect, therefore, it would be interesting to see how performance of subjects is affected when the classifier prediction is being fed back to them (using real-time fMRI neurofeedback) while they are actively engaged in the mental task which is being decoded. So our third research goal is:

R3: To investigate the influence of real-time fMRI neurofeedback on decoding accuracy and hence subject's task performance.

In our daily life, we are always faced with situations where we are flooded with multiple sensory information but somehow we always manage to filter out the pertinent information from the non-pertinent. So in the presence of two competing retinal inputs, we will investigate if it is possible to voluntarily attend to only one of them and try to decode the attended stimuli in real time. So our fourth research objective is:

R4: To investigate if the attended stimuli, in a scenario in which two competing sensory inputs are presented, could be decoded in real time.

Because real-time fMRI is a relatively new technology, there is always a room for improvement by way of newer and faster processing algorithms and better data visualization and analysis tools. This brings us to our fifth and the last research objective which is:

R5: To improve the existing real-time fMRI architecture and design new tools for easy visualization and analysis of fMRI and real-time fMRI data.

1.2 STRUCTURE OF THE THESIS

Two separate experiments were conducted in this study to address the aforementioned research goals. Therefore, the thesis has been structured into five chapters. In chapter 2, a general introduction to functional magnetic resonance imagining (fMRI) will be given. Then, we will describe real-time fMRI (rtfMRI) along with the various preprocessing steps involved in preparing raw fMRI data so that it is ready to be decoded. In the end we will briefly describe decoding and the *Elastic Net Logistic Regression* classifier that will be used in both experiments to decode the fMRI data.

Chapter 3 addresses research goals R1, R2, and R3 and describes the first experiment which aims to decode visual perception and visual imagination in real time and also investigates the effect of real-time fMRI neurofeedback.

Chapter 4 tackles the research objectives R3 and R4 and describes the second experiment which aims to decode the attended stimulus when two competing stimuli are presented. In this experiment as well, the influence of real-time neurofeedback on subject and decoding performance is investigated.

Chapter 5 focuses on research goal R5 and briefly describes the *distributed real-time fMRI pipeline* which was used to execute the first experiment. Then the *integrated real-time fMRI pipeline* is described, the development of which was prompted by the inherent design flaws in the *distributed real-time fMRI pipeline*. This new improved pipeline was used to run the second experiment. Furthermore, we will describe a new tool *Analyze4D*, a software venture that emerged as a result of this project and which is now a bonus deliverable for the BrainGain Work Package 6. The tool is designed specifically for easy and intuitive visualization and analysis of fMRI and rtfMRI data. In closing, we will describe the impact that the hardware and software developed in this project will have on the fMRI and rtfMRI research community.

Chapter 6 summarizes the important findings of this project and proposes ideas for future work.

CHAPTER 2

BACKGROUND

IN this chapter, we will first briefly introduce conventional fMRI along with some common terminologies used in fMRI literature. Then we will describe real-time fMRI starting with literature review of all pertinent studies. We will then give a detailed explanation of real-time fMRI implementation at the Donders Institute which was used to conduct both experiments (Chapter 3 and 4) in this thesis. Then we will give a brief overview of fMRI decoding starting with a literature review. Finally, we will describe classification and explain *Elastic Net Logistic Regression* classifier because this classifier will be used in both upcoming experiments.

2.1 FUNCTIONAL MAGNETIC RESONANCE IMAGING (fMRI)

Magnetic resonance imaging (MRI) is a non-invasive technique that uses strong magnetic fields to form high resolution images of brain and body. *Functional* magnetic resonance imaging (fMRI) is an extension of MRI to measure quick and tiny metabolic changes that take place in the active brain. More specifically,

fMRI signals reflect differences in the paramagnetic properties of oxygenated and deoxygenated blood as a consequence of activation [50]. Thus, fMRI studies are capable of providing not only an anatomical view of the brain, but a moment-to-moment recording of actual brain activity based on blood-oxygen-level-dependent (BOLD) signal changes related to neuronal activity across the entire brain [90]. The ability of fMRI to track changes in the neuronal activity has proved very useful in localizing task-related brain activations and hence in the functional mapping of brain.

2.1.1 Hemodynamic response function (HRF)

The time course of the BOLD signal as it evolves over time in response to an impulse is called the hemodynamic response function (HRF). HRF has three phases [47], as plotted in Figure 2.1:

- 1. Initial dip:** As neurons consume oxygen in response to the stimulus, there is a small rise in the amount of deoxyhaemoglobin, which results in a reduction of the BOLD signal. This increase in deoxyhaemoglobin is because the capillaries supplying blood to the brain cannot instantaneously fulfill the increased demand for the oxygenated blood.

- 2. Overcompensation:** In response to the increased consumption of oxygen, the blood flow to the region increases. The increase in blood flow is greater than the increased consumption, which results in significant increase in the BOLD signal. This is the component that is normally measured in fMRI.

- 3. Undershoot:** Finally, the blood flow and oxygen consumption dips before returning to their original levels. This may reflect a relaxation of the venous system, causing a temporary increase in deoxyhaemoglobin again.

The hemodynamic response function is relatively stable across sessions for the same participant in the same region, but is more variable across different brain regions for the same individual and more variable among individuals [5].

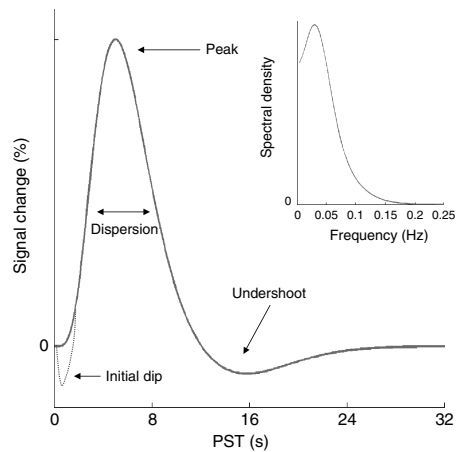
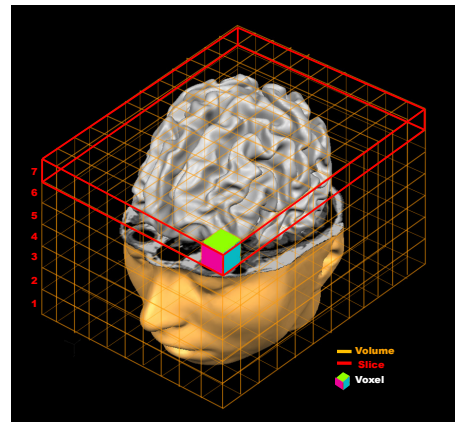


Figure 2.1 | Hemodynamic response function (HRF). The BOLD response as it evolves over time in response to an impulse at time $t = 0$ s. The signal reaches its peak around 5 to 6 s. The initial dip is not observable on 1.5T or lower strength scanners. Picture adapted from [93]

As can be seen on the HRF curve in Figure 2.1, the BOLD signal lags behind the stimulus by about 5 to 6 seconds. This limits the temporal resolution of fMRI and has important implications for timing of the real-time fMRI neurofeedback. Furthermore, after the HRF peaks, it takes about 6 to 12 seconds for it to decay back to baseline level. This effects how quickly a new trial can be started after the previous one and hence directly impacts the duration of a real-time fMRI experiment.

2.1.2 fMRI terminologies and procedure

In a typical fMRI experiment, a participant performs a cognitive task inside a scanner while being scanned. During scanning, the scanner takes snapshots of brain activity every few seconds. The captured image is called a *Scan* or *Volume*. A scan contains a number of *slices* and each slice contains a couple of thousands of voxels. A voxel is a basic measuring unit of fMRI and its value represents the BOLD activity in the small 3D brain region it encompasses, as shown in Figure 2.2.



The entire volume cannot be acquired instantaneously. Instead, the volume is acquired one slice at a time. Once all the slices have been acquired, the volume gets constructed. The time required to acquire all the slices in a volume is called the *Repetition Time* (TR). Therefore, the TR depends on the number of slices acquired. Fewer number of slices will take less time to acquire but at the cost of reduced brain coverage.

Figure 2.2 | Voxels, Slices and Volume. The cube highlighted in green, magenta and blue is a *Voxel* and its value represents the magnitude BOLD signal of the 3D brain region that it encompasses. The slab, highlighted in the red, is called a *Slice*. A typical slice contains thousands of voxels. A number these slices when combined make up a *Volume* or *Scan*. The volume is shown by the orange grid.

Once the experiment is over, the scan data can be retrieved from the scanner and then analyzed. The crucial point to note here is that the scan data cannot be retrieved during the experiment while the subject is being scanned. Hence real-time analysis of data in traditional fMRI is out of question.

2.2 REAL-TIME FUNCTIONAL MAGNETIC RESONANCE IMAGING (rtfMRI)

Unlike conventional fMRI that only allows analysis of images long after the subject has left the MR scanner, real-time fMRI allows data analysis simultaneously with image acquisition. Therefore, real-time fMRI provides additional information not readily available from conventional fMRI. For instance, activation maps obtained by the conventional approach are static and represent the sum of the effects agreeing with the assumed hypothesis for the entire session. On the other hand, real-time fMRI activation maps are dynamic and can reflect the temporal changes of the cognitive or motor processes occurring during the experiment, that may be manipulated by attention, optimization of strategy, or learning for task performance [9]. This enables the experimenter to use the available streaming data to derive a feedback signal that can be used for any neurofeedback application.

This ability of real-time fMRI systems to derive a feedback signal from brain images makes it ideal for neurofeedback training and fMRI-based brain computer interfaces. For instance, earlier this year (2012), researchers at Maastricht University used real-time fMRI to design an online speller suitable for patients with locked-in syndrome (LIS) [117]. The speller was reported to perform at 82%, which is more than sufficient for communication purposes given that spelling accuracies of 70% are usually regarded as the lower limit for spelling with an assistant device [108]. In a related study, researchers were able to move a computer cursor with five degree of freedom using activations emanating from hand and foot movements and utilizing it for selecting letters on an on-screen keyboard [24]. Another study demonstrated the use of real-time fMRI in controlling a dynamical system in which subjects were able to balance an inverse pendulum using brain activation from actual hand movements [25]. In a similar study, researchers used of real-time fMRI and activations from motor imagery of hands to control 2-dimensional movements of a robotic arm [68].

Real-time fMRI has also been experimented with for treatment of various medical ailments. Studies have demonstrated the use of real-time fMRI for self regulation of brain regions involved in Parkinson's disease [119], depression [70], contamination anxiety [40], chronic tinnitus [39], pain [18], and substance abuse [42, 69]. Real-time fMRI is also being used in neuropharmacological studies on animals to observe the dynamic signal changes to an acute drug administration [73]. Furthermore, real-time fMRI has been in presurgical planning to isolate lesions from important functional regions. For example, in patients with tumours in or near the motor cortex reliable intra-operative identification of the precentral gyrus can be difficult due to anatomical dislocation. In such cases, real-time fMRI can be very effective in guiding the neurosurgeon safely through minimally invasive craniotomies to tumours in eloquent areas without setting

lesions to functional areas [28, 107]. Similarly, real-time fMRI is shown to be effective in presurgical evaluation of intractable paediatric epilepsy [54].

The studies mentioned above have shown how real-time fMRI can be used in plethora of different applications. We will now describe how real-time fMRI, as implemented the Donders Institute, works. This general setup will be used for all experiments described in this report.

2.2.1 Real-time data acquisition and streaming

On SIEMENS scanners, as soon as the last slice of a volume is acquired, the raw pixel data of the acquired volume gets written to a folder in the drive of the scanner console. A custom designed software constantly polls this folder for any new files and as soon as a new file is detected, its contents are read and streamed over the ethernet along with the information about the fMRI protocol which was used to acquire the scan. The protocol information helps the remote computer which receives the streaming data to reconstruct the volume.

2.2.2 Preprocessing

The raw fMRI data received from the scanner needs to undergo certain preprocessing steps that improve the quality of the acquired scans. These steps include:

2.2.2.1 Slice time correction In fMRI, a brain volume is acquired one slice at a time and the last slice is acquired almost one TR^1 later then the first slice. This results in different voxels in the same brain volume being sampled at different time points on the Hemodynamic Response Function (HRF) curve. The problem is illustrated in Figure 2.3. Slice time correction solves this problem by shifting the voxel time courses to align them with sample time of the first slice.

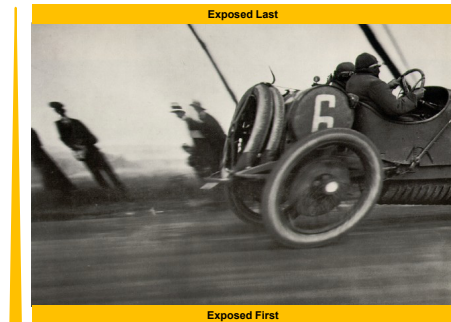


Figure 2.3 | Slit-scan photography analogue to the slice timing problem. In slit-scan photography, different portions of a scene are captured at different instants of time resulting in distorted representation of the moving objects. The same happens in fMRI as each slices in a volume is acquired at different instance of time. *Photography By: Henri Lartigue.*

¹Actually it is slightly less than one TR . To be more specific, the last slice is acquired $[(nSlices-1)/(nSlices)]*TR$ after the first slice.

This changes the data in a way as if the whole volume would have been measured at the same moment in time as the first slice. Slice time correction uses interpolation (Linear or Sinc) to align all the voxel sample point to the same location on the HRF curve.

2.2.2.2 Motion correction Head motion is a major problem during fMRI data acquisition. No matter how much care is taken to fixate the head, some head motion is bound to occur. Any motion causes the brain voxels to shift. For example if a voxel is in slice 22, then after motion this voxel may shift into the adjacent slice (slice 21 or 23).

Head motion is a huge problem in fMRI. For example, in scenarios where decoding algorithms are applied to voxel time courses, if voxels continuously shift their position, then it becomes difficult for decoding algorithms to learn any meaningful pattern of activity because the voxels would not represent activity from one location of the brain but would represent activity from many different regions of the brain.

There are two approaches for correcting motion:

Retrospective motion correction *Retrospective motion correction* tries to correct for motion after it has happened. This kind of motion correction has its limitations because it cannot correct for large movements. It applies rigid body transformation to align all the brain volumes to a reference volume. In our implementation of retrospective motion correction, this reference volume is the very first scan acquired. It uses interpolation to move all the voxels in all subsequent volumes to their position in the reference volume/scan.

Prospective motion correction Retrospective motion correction cannot correct for any motion larger than the slice thickness. Therefore, *prospective motion correction* or correcting the motion as it occurs, was introduced by Siemens. PACE or Prospective Acquisition CorrEction [74, 120], is a technique in which the MRI gradients are adjusted if head motion occurs, such that the slice position changes with shifts in the head position. Thus the slices always remain glued to the same spatial location in the brain no matter where and by how much² the brain moves in the scanner. This is depicted in Figure 2.4.

2.2.2.3 PACE series selection Whenever motion is detected, PACE recalculates the new gradients and then uses these new gradients for the next scan. Thus, there is a gap of two TRs between the detection of motion and its correction. Any motion that does occur in this two TR interval, cannot be corrected by PACE. This is removed by retrospective motion correction which Siemens calls

²There is a limit how much motion PACE can correct. On Siemens MAGNETOM Trio 3T scanner, this limit is 20 mm.

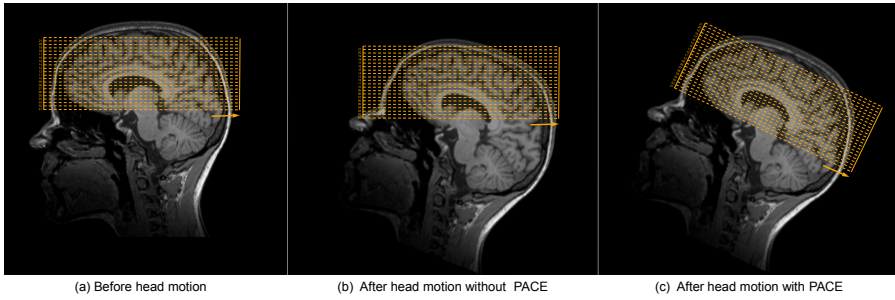


Figure 2.4 | Prospective Acquisition CorrEction (PACE). (a) Shows the slice positioning before any motion has occurred. (b) Shows what happens if motion occurs without any PACE correction. The slices remain in their original position but as the head has moved, therefore, the slices are sampling different region of the brain than originally intended. (c) With PACE, the MRI gradients are adjusted in real-time such that the slices remain glued to the same spatial locations in the brain no matter where the head moves.

MoCo. Hence if the PACE sequence is used, it not only corrects the images prospectively but also retrospectively. Therefore, the pace sequence spits out two series of images:

- the first series is just PACE (prospectively) corrected
- the second series is both PACE (prospectively) and MoCO (retrospectively) corrected.

In our experiments, we will use the second series as it has the least amount of residual motion.

2.2.2.4 Boundary slice Masking Retrospective motion correction always corrupts slices at the boundary of each volume because no interpolation data is available for these boundary slices. How many boundary slices get corrupt depends on the amount of motion incurred during the experiment. If PACE is enabled, a very small motion occurs. For instance, in a 70 minutes long experiment, on average only half of the first and last slice gets damaged due to motion. Hence by masking the entire first and last slice (as shown in Figure 2.5), it can be ensured that none of the damaged voxels get used in training and test sessions. Masking removes these bad voxels by setting the voxels in each of these bad slices to zero.

2.2.2.5 Nuisance regressors removal This step is applied to remove scanner drifts, offsets, and motion related activations. A *Recursive Least Square Gen-*

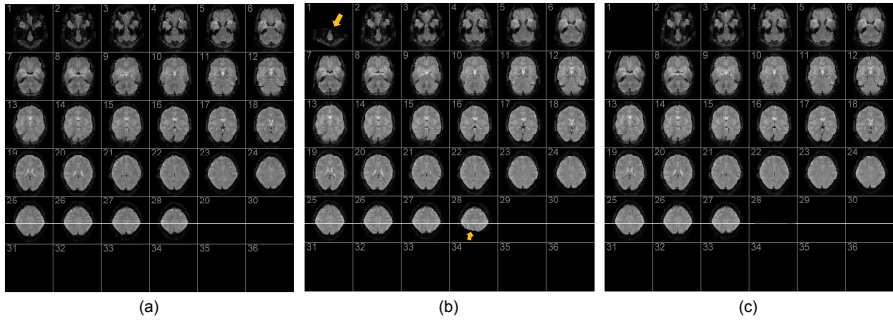


Figure 2.5 | Boundary slice masking. (a) The figure shows all the slices in the very first scans of the experiment (b) As time goes on and the subject moves, the first and the last slice start to get corrupt (shown by the arrows) as no interpolation data is available at these boundary slices to correct for the motion that has occurred. The more the motion, the more the damaged areas spreads. The picture was taken 70 minutes into the fMRI run and is the last scan (2095th) of a typical experiment with a PACE MR sequence. (c) Boundary slice masking masks out slice 1 and 28 so that the voxels corresponding to these slices are not used in training and testing phase of the experiment.

eral Linear Model (RLSGLM) is used for this purpose [8]. RLSGLM is similar to traditional GLM, the only difference being that RLSGLM updates the model every TR rather than recalculating the full model at every TR which could be very time consuming and may compromise the real-time operation of the pipeline.

2.2.2.6 Grey matter masking The brain contains three distinct tissue types i.e. grey matter, white matter, and cerebral spinal fluid (CSF). Only the voxels in the grey matter respond to the experimental manipulation while the rest of the voxels show only random activity patterns. Grey matter masking removes these white matter and CSF voxels.

2.2.2.7 Spatial smoothing In spatial smoothing, neighboring voxel values are averaged which essentially low pass filters the data, thereby removing high frequency fluctuations from the data. As a result, sharpness of the image is reduced which is why this process is called smoothing. In real-time experiments, better results are obtained if no smoothing is applied.

2.2.3 Real-fMRI design constraints

In conventional fMRI, first all scans for an experiment are acquired first and then these scans are preprocessed and analyzed in batch and the whole process may take several hours after the data has been acquired (as depicted in Figure 2.7). On the other hand, in real-time fMRI every scan is processed within a TR of being acquired (see Figure 2.6). In others word, each scans is completely dealt with before the next one becomes available and all this happens while the experiment is up and running. If for any reasons a scan takes more than a TR to be completely processed, then a lag starts to build up in the whole pipeline which jeopardizes the real-time operation of the pipeline.

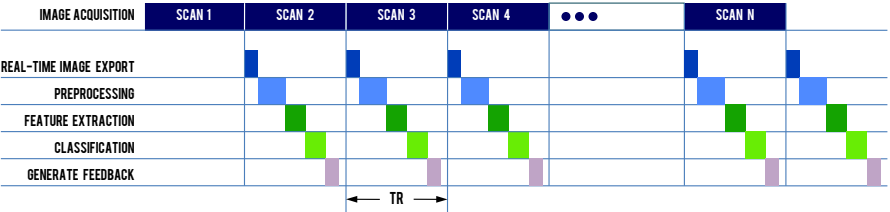


Figure 2.6 | Timeline of a real-time fMRI experiment. Every scan is completely processed within one TR of being acquired and hence a new feedback update is available every TR.

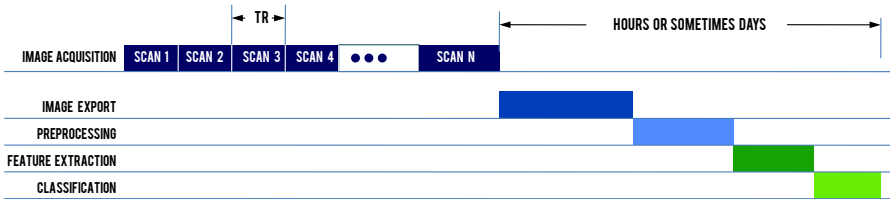


Figure 2.7 | Timeline of a conventional (non real-time) fMRI experiment. All scans acquired during the experiment are processed after the experiment is over. The process may take hours or sometimes even days. Note that there is no feedback in these experiments because by the time feedback gets calculated, the experiment is already over and test subject is already out of the scanner. This is what differentiates real-time fMRI from conventional fMRI.

2.3 DECODING

Once the fMRI data has been preprocessed, it is ready to be decoded. Decoding is at the heart of mind reading and involves figuring out on an abstract level as to what is happening in the brain. Many studies have used machine learning techniques to learn what the fMRI time series represents. A study by Naselaris et

al. [86] demonstrated a Bayesian decoder that used fMRI signals from early and anterior visual areas to reconstruct complex natural images [131]. In a related study, researchers reconstructed visual images by combining local image bases of multiple scales, whose contrasts were independently decoded from fMRI activity by automatically selecting relevant voxels and exploiting their correlated patterns [83]. Binary-contrast, 10 x 10-patch images (2(100) possible states) were accurately reconstructed without any image prior on a single trial or volume basis by measuring brain activity only for several hundred random images. Another study [91] used linear support vector machine to decode each syllable from human fMRI activity suggesting the possibility of using non-invasively measured brain activity to read the intended speech of patients disabled in speech motor control. A recent study by Mitchell et al. [94] used a variety of classifier (Gaussian Naive Bayes, Support Vector Machine and k Nearest Neighbors) to decode (1) whether the human subject was looking at a picture or a sentence, (2) whether the subject was reading an ambiguous or non-ambiguous sentence, and (3) whether the word the subject was viewing was a word describing food, people, buildings, etc. In an another study, Rodriguez et al. demonstrated that multivoxel pattern analysis of fMRI can be used to decode place-related information in spatial navigation [105]. All these studies have shown that machine learning techniques can be an invaluable tool to decode cognitive states.

Broadly speaking, Decoding techniques for fMRI can be divided into three categories:

1. Classification
2. Reconstruction
3. Identification

We will focus here only on the classification technique since it will be used that in all the experiments in this study.

In classification, a pattern of activity across many voxels is used to determine the discrete class from which the stimulus was drawn [16, 20, 43, 44, 52]. The most commonly used computational technique is the linear classifier [13, 22, 30, 45, 82, 92, 95]. The linear classifier is an algorithm that uses patterns of activity across an array of voxels to discriminate between different levels of stimulus, experimental, or task variables. Because classifiers exploit systematic differences in voxel selectivity within a region of interest (ROI), therefore they can detect information that would be missed by conventional analyses involving spatial averaging [65].

A linear classifier makes a classification decision based on the value of a linear combination of the feature values. In this study, the preprocessed time courses of the voxels would be used as features. If \vec{x} represents vector of all features, then the output of the linear classifier can be written as:

$$y = f(\vec{w}\vec{x}) = f\left(\sum_k w_k x_k\right)$$

where \vec{w} is a real vector of weights and f is a function that converts the dot product of the two vectors into the desired output. In other words, \vec{w} is a linear functional mapping of \vec{x} onto \mathbb{R} . The weight vector \vec{w} is learned from a set of labeled training examples. If f is a simple function, then it will map all values above a certain threshold to the first class and all other values to the second class. A more complex f will give the probability that an item belongs to a certain class.

Because a real-time mind reading experiment needs a classifier that can train fast and predict fast as well, a linear classifier is well suited for it as it is often the fastest classifier, especially when \vec{x} is sparse. Linear classifiers often work very well when the number of dimensions in \vec{x} is large, as in the case of fMRI where a typical voxel time series is thousands of samples long. In such cases, the classifier should be well-regularized to avoid overfitting.

There are two broad classes of methods for determining the parameters of a linear classifier \vec{w} .

1. **Discriminative models:** A discriminative algorithm does not care about how the data was generated, it simply categorizes a given signal. *Logistic Regression*, *Perceptron* and *Support Vector Machines (SVM)* are some of the classifiers in this category.
2. **Generative models:** A generative algorithm models how the data was generated in order to categorize a signal. It asks the question: based on generation assumptions, which category is most likely to generate this signal? *Linear Discriminant Analysis (LDA)* and *Naive Bayes* classifier are some of the classifiers in this category.

Imagine the task is to classify a speech to a language. It can be done either by:

1. Learning each language and then classifying it using the knowledge you just gained or
2. Determining the difference in the linguistic models without learning the languages and then classifying the speech

The first approach is generative and the second one is the discriminative. In this study, a derivative of logistic regression classifier called the *Elastic Net Logistic Regression* classifier will be used.

2.3.1 Elastic Net Logistic Regression

Regression is a technique which tries to estimate the value of a target variable based on a set of known values corresponding to one or more predictor variables and it does so by finding a target function f that best matches the target variable given the input data. An error function can then be used to assess how good or otherwise the fit is. One commonly used error function is the sum of squared error.

$$\text{Sum Squared Error (SSE)} = \sum_p (y_p - f(x_p))^2$$

where y_p corresponds to the target (or response) variable of the p^{th} observation x_p . The best matching target function is the one that minimizes this error function.

Linear regression is a specific form of regression which learns a linear target function f that best matches the target variable given the set of predictor variables.

Given p predictors x_1, x_2, \dots, x_p , the response \hat{y} is predicted by

$$\hat{y} = \hat{\beta}_0 + x_1\hat{\beta}_1 + x_2\hat{\beta}_2 + \dots + x_p\hat{\beta}_p \quad (2.1)$$

Logistic regression is another form of regression used the modeling of dichotomous categorical outcomes (e.g., dead vs. alive, cancer vs. none, etc.). Logistic and linear regression are both based on many of the same assumptions and theory. While convenient in many ways this presents a minor problem with regard to the outcome. Since the outcome is dichotomous, predicting unit change has little or no meaning. As an alternative to modeling the value of the outcome, logistic regression focuses instead upon the relative probability (odds) of obtaining a given result category. As it turns out the natural logarithm of the odds is linear across most of its range, allowing us to continue using many of the methods developed for linear models. The result of this type of regression can be expressed as follows:

$$\ln \left[\frac{P}{1-P} \right] = \hat{\beta}_0 + x_1\hat{\beta}_1 + x_2\hat{\beta}_2 + \dots + x_p\hat{\beta}_p \quad (2.2)$$

Where P represents the probability of an event (e.g., death, cancer, ..).

A model-fitting procedure produces the vector of coefficients $\hat{\beta} = (\hat{\beta}_0, \hat{\beta}_1, \dots, \hat{\beta}_p)$.

The criteria for evaluating the quality of a model will depend on the particular problem at hand but typically the following two aspects [134] are important:

- Accuracy of prediction on future data
- Interpretation of the model

OLS often performs poorly in prediction on future data samples and also yield models that hard to interpret. Therefore, penalizing approaches were introduced to counter these two problems. Depending on the type of penalty applied, there can be three types of regression:

1. Ridge regression (L2 penalty)
2. Lasso regression (L1 penalty)
3. Elastic net regression (Elastic net penalty)

The ridge regression minimizes SSE by putting a bound on the L2 norm of the coefficients. As a continuous shrinkage method, ridge regression achieves its better prediction performance through a bias-variance trade-off. One limitation of ridge regression is that it cannot produce a parsimonious model because it always keeps all the predictors in the model [134]. Therefore, the Lasso regression [123] was introduced. The Lasso is a penalized least squares method imposing an L1 penalty on the regression coefficients. Due to the nature of L1 penalty, the lasso regression does both continuous shrinkage and automatic variable selection simultaneously which comes in very handy in situations where sparse representation is required. However, the lasso has its limitation too as pointed out in [134]. For example, in fMRI where the number of scans is far less than the number of voxels (in other words $p \gg n$), the lasso selects at most n variables before it saturates, because of the nature of the convex optimization problem. Furthermore, if there is a group of variables with very high pairwise correlations, then the lasso tends to select only one variable from the group and does not care which one is selected. To counter these problems the elastic net penalty was introduced [134]. Similar to the lasso, the elastic net penalty P simultaneously does automatic variable selection and continuous shrinkage, but is also able to select groups of correlated variables. This makes the elastic net regression a perfect choice for fMRI decoding. The entire family of P_α creates a useful compromise between ridge and lasso regression [32]. The elastic net regression solves the following problem:

$$\hat{\beta} = \arg_{\beta \in \mathbb{R}^{p+1}} \left[\frac{1}{2N} \sum_{i=1}^N (y_i - x_i^T \beta)^2 + \lambda P_\alpha(\beta_1, \dots, \beta_p) \right] \quad (2.3)$$

where

$$P_\alpha = \sum_{j=1}^p \left[\frac{1}{2} (1 - \alpha) \beta_j^2 + \alpha |\beta_j| \right] \quad (2.4)$$

If $\alpha = 1$, then the regression is lasso and if $\alpha = 0$ the regression is ridge. Any value of α between 0 and 1 yields an elastic net regression.

The classifier in this study was an Elastic Net Logistic Regression classifier as implemented in the Donders Machine Learning Toolbox (DMLT). The mixing pa-

parameter α parameter was fixed to 0.99. For the regularization parameter λ , the whole regularization path was calculated with maximum number of allowed iterations set to 100. Optimal setting of λ was then computed using nested cross-validation on 75% of the training data.

CHAPTER 3

REAL-TIME DECODING OF VISUAL PERCEPTION AND IMAGERY

THIS chapter describes the first of the two experiments conducted during this study. The experiment tries to investigate if visual perception and imagination can be decoded in real-time and if presenting neurofeedback of decoded patterns has any influence on task performance of subject. The chapter begins with a literature review of visual perception and imagery studies. The experiment is then described in the methods section along with a description of the statistical analysis carried out on the data offline. We then discuss the important findings of this experiment including the design mistakes that were made during this experiment which will be used to refine the implementation of the second experiment described in Chapter 4).

3.1 INTRODUCTION

Visual perception is the ability to interpret information about the surroundings from the effects of visible light reaching eye allowing an individual to assimilate information from the environment. When light falls onto retina, the rod and cone

receptors transform it into electrical signals which travel via the optic nerve and optic chiasm to the Lateral Geniculate Nucleus (LGN). From there the signals travel to the occipital lobe, at the back of the brain. This is called the visual cortex [36]. In primates, nearly all visual information enters the cortex via area V1 which is also known as the *primary visual cortex*, *Brodmann area 17* or *striate cortex* due to its stripy appearance. From V1, the information travels to the *Extrastriate cortex* which includes V2, V3, V4, and V5/MT.

The primary visual cortex is the starting point of visual processing in the cortex. From the visual cortex, signals follow two different pathways, the *ventral* pathway to the temporal lobe and the *dorsal* pathway to the parietal lobe of the brain, as shown in Figure 3.1. The ventral and dorsal pathways each have been attributed with a different function. The ventral pathway is said to be involved in processing of object identity (the “what” pathway) and the dorsal stream is involved in the processing of location and spatial features (the “where” pathway) [128].

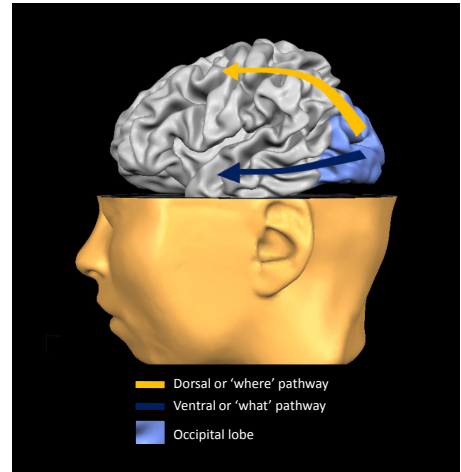


Figure 3.1 | Dorsal and ventral pathways in the brain.

Evidence for this dichotomy stems from decades of research into monkey and human brain. Tasks involving spatial processing, such as judging the spatial layout of a scene, activate regions in the dorsal pathway. Damage in this part of the brain in monkeys or human patients was found to lead to difficulties in spatial judgements [81]. In the ventral pathway, many regions have been discovered that respond optimally to certain object categories. For example, seeing faces extensively activates a region in the *fusiform gyrus* (part of the ventral pathway), while this region responds less optimally to other object categories [53, 99]. Other regions in the ventral pathway have also been identified to be optimally responsive to other object categories such as places or tools. Whether this suggests a modular organization of ventral temporal cortex or whether objects are represented in a continuous manner, is still under debate [1].

Although we now know which regions respond to what kind of stimuli, it is even more important to know how this information is internally encoded in brain. Since the 1970s, researchers have been trying to uncover the mechanics of how visual stimuli are represented in the visual cortex. One of the major breakthrough in this field was the finding by Tootell et al. [125] that the visual cortex is retinotopically organized. A geometric pattern of flashing lights

was shown to a monkey after it was injected with a radioactive sugar, which is taken up into brain cells in proportion to their level of activity. This stains the brain cell which are active. The animal was trained to stare at the stimulus and was then sacrificed so that its brain could be examined. The occipital cortex of the monkey showed dark bands revealing the neurons that were most activated while the animal viewed the pattern. A pattern of activation corresponding to the geometric structure of the stimulus can be seen clearly in Figure 3.2.

Tootell's experiment is a remarkable and beautiful demonstration of how the V1 area of the brain is retinotopically organized. That is, this part of the brain is organized similarly to how the light hits our retinas. The fact that the stimulus is retinotopically mapped on the visual cortex has opened new ways of decoding perceived stimulus. For example, Thirion et al. [121] argued that if a controlled stimulus (e.g. a flashing checkerboard) produces a known pattern of activation in the visual cortex, then the stimulus-to-activation chain can be identified and inverted, leading to activation-to-

stimulus inference. The inverse problem consisted of predicting the spatial layout of an activation pattern (stimulus) given a functional activation image of the visual cortex, a technique termed as *inverse retinotopy*. It comprised of first estimating a forward model using the receptive field model, and then inverting the model in a Bayesian framework. Thirion also compared the performance of inverse retinotopy to the classical linear SVM approach. The results of the study revealed that the supervised learning technique performed better than the inverse retinotopy technique, implicating that there is sizeable amount of discriminative information in fMRI data that can be learned by machine learning techniques.

One of the most notable aspects of the work by Thirion is that they reported good decoding performance not only for perceived stimuli but also for imagined stimuli. Visual mental imagery or *seeing through the mind's eye* can be defined as the manipulation of visual information that comes not from perception but from memory [58]. Imagery helps provide meaning to experience and understanding to knowledge; it is a fundamental facility through which people make sense of the world around them. For example, if asked which is greener, a pea or a cucumber, most people would imagine seeing a pea and cucumber before answering the question. Similarly, when deciding if the new table that one is about to buy would pass through the narrow door of the room back home, one would probably project the table onto the mental image of the door to figure out

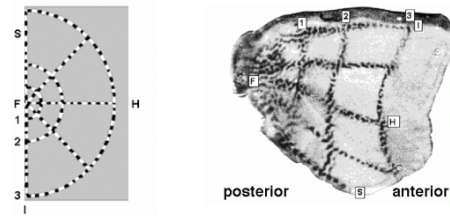


Figure 3.2 | Retinotopic organization of visual cortex in a monkey The stimulus is shown on the left and the brain in shown on the right. The brain stains have the same structures as the stimuli, indicating that the visual cortex is retinotopically organized. Picture adapted from [125]

the answer. A mental image occurs when a representation of the type created during the initial phases of perception is present but the stimulus is not actually being perceived; such representations preserve the perceptible properties of the stimulus and ultimately give rise to the subjective experience of perception [63].

Many parallels can be drawn between visual perception and visual imagery because a similar organization of object and spatial information into two processing streams has been found during visual mental imagery. Studies have indicated, e.g., that psychophysically, a visual mental representation can be manipulated in a similar fashion as a visual percept [113] and that patients with imagery deficits often have accompanying deficits in the perceptual domain [27, 126]. Moreover, neuroimaging studies in healthy individuals showed that the distributed cortical networks, active during specific mental imagery tasks, are also activated during corresponding perceptual processes [33, 49, 62, 78, 88]. Parts of the organizational structure of mental imagery, such as the division in 'what' and 'where' processing pathways, are very similar to that of perception while other aspects such as the involvement of the early visual cortex, are more disputed. The first study reporting primary visual cortex (V1) activation during a mental imagery task dates back to 1993 [59]. Since then conflicting results have been found. Several studies found no evidence for activation of the early visual cortex during imagery [31, 57, 79, 80], while others confirmed primary visual cortex activation [56, 60, 122]. Kosslyn [61] reviewed many of these studies containing a variety of different tasks and paradigms and extracted three essential components underlying early visual cortex activation. According to his analysis, three variables explained all systematic differences in the probability of early visual cortex activation across studies: imagining with high resolution details, imagining shapes instead of spatial arrangements and the sensitivity of the measurement technique. Forming a more detailed mental representation or mentally "zooming-in" on a picture might more frequently depend on the early visual cortex, although a study by Thompson et al. [122] showed no difference in the extent of early visual cortex activation when imagining a lower or higher resolution image. This suggests that the presence of either of these variables by itself might not be enough to find early visual cortex activation, but rather a combination of these variables enhances the probability. Because spatial imagery strongly relies on the parietal cortex and spatial properties are topographically stored there [109], this might explain why spatial imagery studies less often report early visual cortex activation. Although mental imagery and perception share certain neural mechanisms [118], the information flow between brain regions in the visual imagery network differs from visual perception. After all, we do not experience our mental images as being exogenous, but rather as internally generated. To generate, maintain, and manipulate these mental images, we also rely on memory processes in the frontal, parietal, and temporal lobes of the brain.

If same neural substrates are shared by visual perception and imagination, then any classifier trained on perceived stimuli might also be used to decode imagined

stimuli [103]. Therefore, in this study we will first present random patterns (on a 5x5 grid) to the subjects. Each element of the grid will act as an independent stimulation source. The fMRI data collected in this training part will be used by 25 classifiers to learn the stimulation to cortical activation mapping. The cortical activation is therefore a dependent variable and the stimulus impinging on the retina is the independent variable. Once all the classifier are ready, they will be used to decode novel perceived and imagined stimuli. To find if the real-time fMRI neurofeedback has any impact on the decoding performance, the perception and imagination tasks will be performed twice, once with feedback and once with out any feedback. We expect that the reconstruction accuracy for perceived stimuli will be higher compared to the imagined stimuli. This is because previous studies have shown that activation for imagined stimuli are not as strong as perceived stimuli [89]. Furthermore, we expect that a condition with feedback will be decoded with higher accuracy than similar condition with no neurofeedback. This is because the neurofeedback of the decoded pattern might drive the subjects perception or imagination so that next decoded pattern more accurately reflects the perceived or imagined stimuli. Because this experiment is purely visual, we expect the classifier to learn majority of its regression weights from voxels in visual cortex. So by examining the classifier weights, we should be able to see the visual cortex voxels being recruited for training.

We can now sum up our expected outcomes in three hypotheses:

H1: The decoding/reconstruction accuracy for perceived stimuli will be higher than the imagined stimuli

H2: Decoding accuracy will be higher for feedback conditions compared to the corresponding non-feedback condition

H2: Classifier will learn most of its weights from voxels in the visual cortex

3.2 METHOD

3.2.1 Subjects

Four Dutch female subjects participated in the experiment. The average age of the sample was 23.75($SD = 0.96$) years. Subjects were recruited from a web-based human subject pool management system (SONA). All subjects had normal or corrected-to-normal vision. For their participation, subjects received either a cash compensation or study credits. The study was approved by the ethical committee of the Donders Institute and all subjects gave a written informed consent (see Appendices A and C).

3.2.2 Experimental task

The goal of this experiment is to find out if visual perception can be decoded in real time and if a classifier trained on perceived stimuli can also be used to decode imagined stimuli as well. Furthermore, the effect of feeding the reconstructed (or decoded) patterns back to subjects, while they are actively engaged in the perception or imagination task, is also investigated. Naturally, if a subject is perceiving or imagining something (let's say the letter D), then feeding back the reconstructed or decoded letter might interfere with the ongoing perception or imagination task which the subject is currently engaged in. This because the reconstruction can not be perfect all the time. So subjects might see a reconstruction C, instead of the letter D that they are currently perceiving or imagining. Not only will the feedback distract subjects from mentally focusing on the task at hand, but more importantly attending to the feedback might induce feedback related visual activation. This feedback related visual activation is especially problematic for imagery condition because then the line between perception and imagery becomes murky. The imagery condition no longer remains purely imagery with visual neurofeedback. However, in this experiment presenting the neurofeedback in a modality other than visual is not feasible due to the nature of the reconstructed patterns itself. For example if the auditory modality is to be used to give neurofeedback of the reconstructed patterns, then how could one define the auditory equivalent of a jumbled up letter C? Therefore, it was decided to resort to visual neurofeedback of the reconstructed patterns but subject to the following constraints:

- The feedback itself should not invoke significant visual activation
- The feedback should be minimally intrusive and should not distract the subject too much from the task at hand
- The cues during imagination should not invoke any visual activation. For example, if a letter D is to be imagined during the task, then presenting a cue letter D before the start of the trial might result in activations due to perception of letter D, and then again the line between perception and imagination becomes murky.

To satisfy these constraints, the content for the stimulus for the entire experiment was generated using three building blocks (as shown in Figure 3.3), each performing a distinct function. These building blocks along with their respective function is mentioned below:

The fixation dot The fixation was presented in the middle of the screen and the subjects were instructed to always fixate on it. Apart from providing the subject a locus to fixate on, its color also served to indicate the beginning or end of the imagination period during visual imagery conditions. When

it turned from red to green the subjects had to start imagining and when it turned from green to red they had to stop imagining

The stimulation block The stimulation block of the stimuli was used to activate the visual cortex during training and perception conditions. This block consisted of a 5x5 grid of white rectangles subtending an angle of 8.2° on the visual cortex and flickering with a frequency of 8 Hz to induce maximal BOLD response [2]. Each of the 25 rectangles could be turned on/off independently of one another and hence any pattern could be constructed on the 5 x 5 grid. The stimulation block were all turned off during imagery condition and also during rest periods.

The feedback block The feedback block contained a 5x5 grid of empty grey rectangles with very low contrast which prevents significant visual cortex activation due to feedback. In conditions with feedback, each of these 25 rectangles were toggled depending on the classification result from the 25 binary classifiers (more on that in section 3.2.2.1) thereby giving subject a feedback on how the reconstructed pattern looked like. Each of these grey rectangles resided inside the white rectangles of the stimulation block and therefore had a smaller dimension than the rectangles of the stimulation block. This resulted in feedback being minimally intrusive because subjects could focus on task at hand while at the same time viewing the stimulus. Unlike the stimulation blocks which were made to flicker with 8 Hz, the feedback blocks did not flicker at all. This was to ensure minimal activation of visual cortex due to feedback [2].

The entire experiment was designed by manipulating just these three building blocks. The experiment itself was conducted in five conditions. In the first condition the stimuli for training the classifier was presented and after all the training stimuli had been presented, 25 binary classifiers, one for each element of 5x5 grid, were trained on the collected fMRI data. In the second and third condition, the previously trained classifiers were used decode visual perception without feedback and with feedback, respectively. In the fourth and fifth condition, the same classifiers were again used to decode visual imagery without and with feedback, respectively. The order of these conditions was not randomized across subjects. The decision to conduct experiment in contiguous block of conditions and not to intermix trials from different conditions, was motivated by the fact that had trials from the four aforementioned conditions been intermixed, an instruction screen would have been required before each trial to explain the task in that trial to the subject. Considering that the experiment was already 2.5 hours long without these instruction screens, had we gone to randomizing the trials and conditions, it would have easily extended the experiment duration by another 1 hour. This would have resulted in not only subject feeling extremely exhausted but would have also resulted in violation of MRI scanning laws which do not allow more than 3 hours of continuous scanning. Therefore, the experiment was conducted in five big conditions and an instruction screen was presented only at

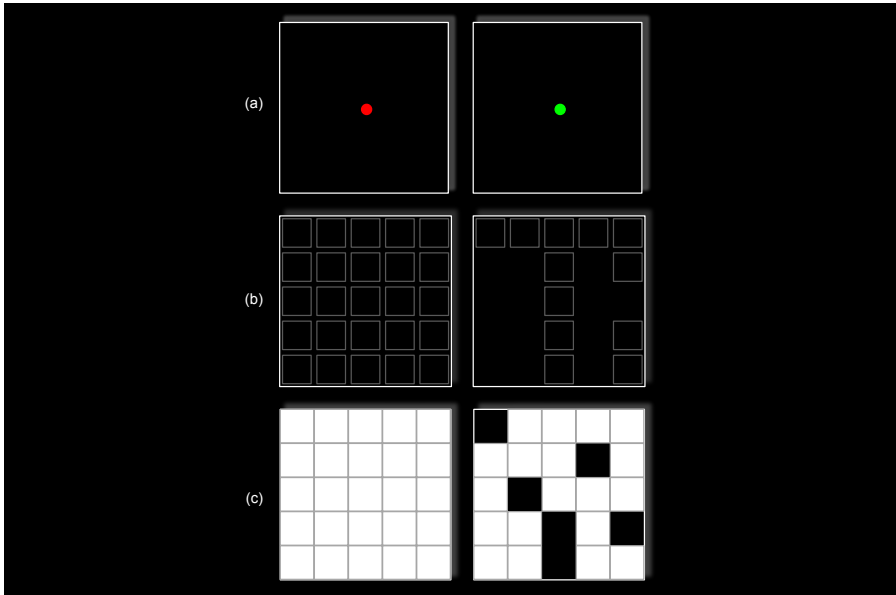


Figure 3.3 | Basic building blocks of the stimulus. (a) Fixation Dot. Apart from providing the subject a locus to fixate on, its color also served to indicate the beginning or end of the imagination period during visual imagery conditions. When it turned from red to green the subjects had to start imagining and when it turned from green to red they had to stop imagining (b) Feedback blocks. These 25 blocks could be manipulated independently of each other hence any pattern could be formed using these blocks. These blocks were used to provide feedback during perception and imagination feedback conditions by turning them on/off according to the classifier prediction. During the rest and non-feedback conditions, all feedback boxes are always visible (c) Stimulation blocks. These 25 white boxes could be made to appear or disappear independently of each other. Thus any pattern could be formed. The stimulation blocks were used in the training and also in the visual perception conditions. The pattern formed by these blocks was made to flicker at 8 Hz for maximal BOLD signal.

the start of each of these condition. Furthermore, by not intermixing trials from different conditions, the chances of subjects learning a strategy that works best for them, increased. We will now describe these conditions in detail.

3.2.2.1 Training Condition To learn the mapping from stimulus to cortical activation, the training condition was used in which 100 random patterns were presented to the subject. Each pattern was presented for 12 seconds followed by 12 seconds of rest to allow the hemodynamic activity from the previous pattern to return to baseline (see Figure 3.4). During each 12 second long stimulation period, the pattern was made to flicker with 8 Hz in order to induce maximal BOLD response [2]. Each random pattern was constructed such that exactly twelve of the stimulation blocks were ON and the rest OFF. To ensure that cortical areas corresponding to the each stimulation block was activated equally, in all 100 patterns each of the 25 stimulation blocks was ON for half of the patterns and OFF for the rest of the half. The red fixation dot and the 25 feedback block (grey rectangles) were always visible during training.

Classifier training The scans collected during training were used to train the elastic net logistic regression classifier. The mixing parameter α parameter was fixed to 0.99. For the regularization parameter λ , the whole regularization path was calculated with maximum number of allowed iterations set to 100. Optimal setting of λ was then computed using nested cross-validation on 75% of the training data. For more details about elastic net, please refer to Chapter 2, Section 2.3. The training data for the classifier was constructed by first shifting all the scans collected in the training session by four TRs to counter the hemodynamic delay. Then all the scans corresponding to the rest period were dropped. After this, all 8 scans in each stimulation block were averaged together and these 100 averaged time series were then used to train 25 classifier, one for each element of the grid. These trained classifiers were then used to predict the stimuli in incoming scans of all the subsequent test sessions.

3.2.2.2 Visual perception with no feedback condition This condition was used to assess the decoding performance for perceived stimuli when no decoding feedback was presented. Each trial contains 12 TRs (18 s) of task followed by 12 TRs of rest in which the subjects were allowed to close their eyes. The task in each trial consists of fixating on the letter flickering with 8 Hz. Sixteen trials were conducted in this manner, one trial for each of the letter in the word DON-DEERSINSTITUTE.

3.2.2.3 Visual perception with feedback condition This condition was used to investigate the decoding of perceived stimuli when the classifier prediction is fed back to the subject during the task. Each trial contains 12 TRs (18 s) of task followed by 12 TRs of rest in which the subjects were allowed to close

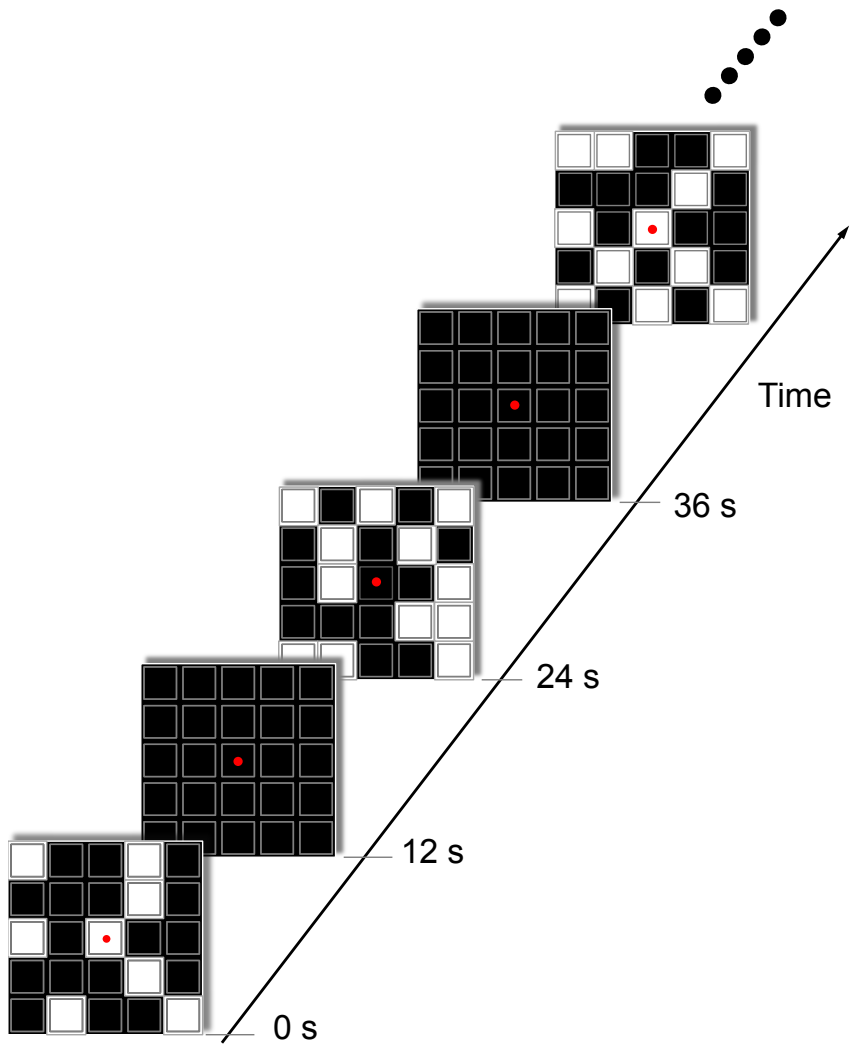


Figure 3.4 | Stimuli used for training. The stimuli contains 100 random patterns. Each pattern flickers with 8 Hz for 12 seconds followed by 12 seconds of rest in which subjects were allowed to close their eyes.

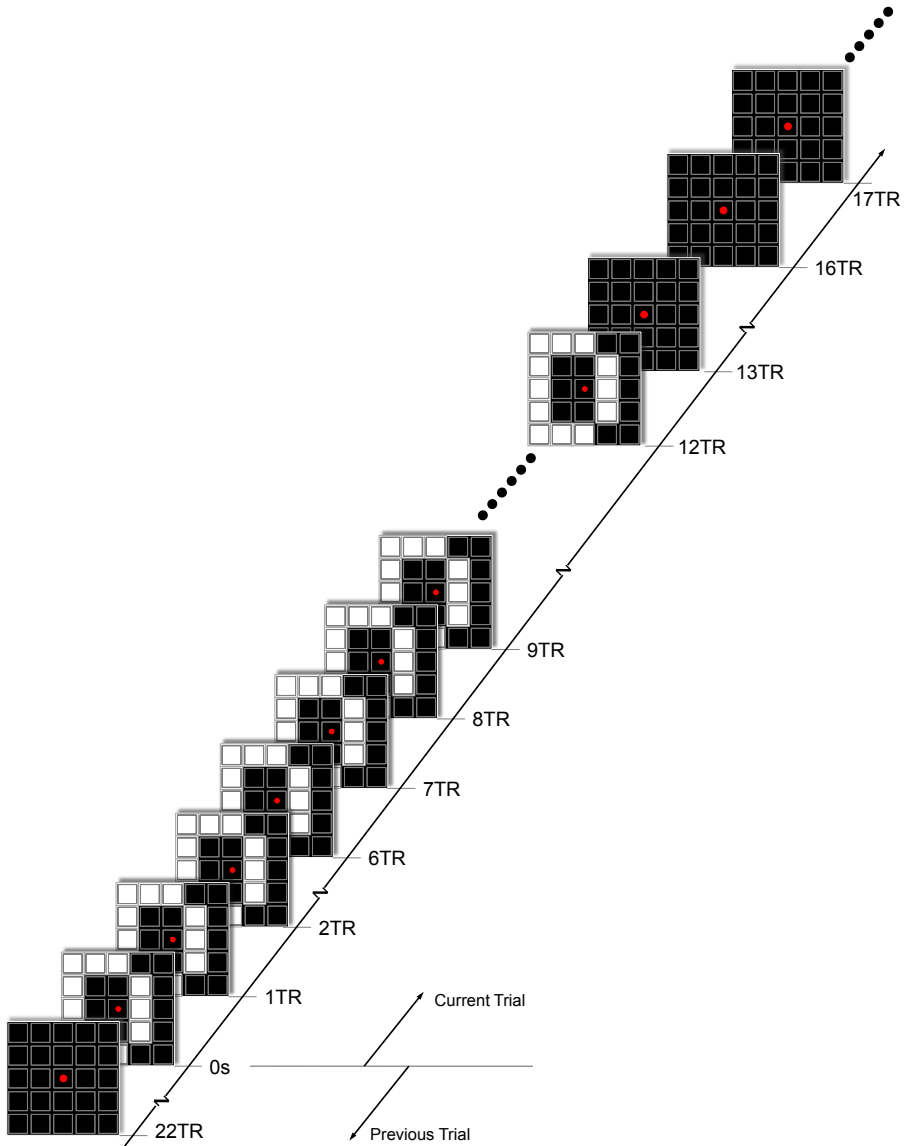


Figure 3.5 | Stimuli used in ‘Visual perception with no feedback condition’. The figure shows an example of one trial. Each trial contains 12 TRs (18 s) of task followed by 12 TRs of rest in which the subjects were allowed to close their eyes. The task in each trial consists of fixating on a letter, in this case ‘D’, flickering with 8 Hz. Sixteen trials were conducted in this manner, one trial for each of the letters in the word DONDERSINSTITUTE.

their eyes. The task consists of fixating on a letter flickering with 8 Hz. In the first two TRs, highlighted in yellow in Figure 3.6, there is no feedback due to pipeline delay. Similarly, in the four TRs that follow, highlighted in red, there is no feedback due to hemodynamic delay. The feedback starts from the 7th TR and is presented until the 16th TR although the task/visual stimulation stops after the 12th TR. This is due to the aforementioned hemodynamic lag. The feedback was such that if the classifier prediction for the grid element was below 0.5, the corresponding feedback block was turned off and turned on if above 0.5. Sixteen trails were conducted in this manner, one for each of the letter in the word DONDER SINSTITUTE.

3.2.2.4 Visual imagination with no feedback condition

This condition was used to assess the decoding performance for imagined stimuli when no decoding results were presented to the subject. Because no feedback is shown in this condition, therefore, the feedback grid remains static throughout the duration of the trial as shown in Figure 3.8. The cue letter was presented two TRs before the beginning of each trial in the rest period of the preceding trial. After the cue was over, the fixation dot turned from red to green, giving an indication to subjects that they have to start imagining the capital letter corresponding to the letter they saw in the cue. The exact pattern to imagine (shown in figure 3.7) was already memorized and thoroughly practiced by the participants in the pre-experiment briefing. The imagery task ended at the 12th TR and was indicated by a change of color the fixation dot from green to red. Thus, each trial contained 12 TRs of task followed by 12 TRs of rest. Sixteen trails were conducted in this manner, one trial for each of the letter in the word DONDER SINSTITUTE.

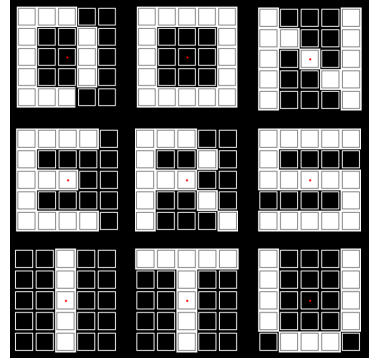


Figure 3.7 | Basis set of letters used in the experiment. These 9 letters were used to form a 16 letter word DONDER SINSTITUTE. These 16 letters were then used for the 16 trials of each of the four test conditions of the experiment. These 9 patterns were memorized by the subjects.

3.2.2.5 Visual imagination with feedback condition

This condition was used to assess the decoding performance for imagined stimuli while the reconstruction of the classifier prediction is being simultaneously fed back to the subject. The cue was presented two TRs before the beginning of each trial in the rest period of the preceding trial. After the cue was over, the fixation dot turned from red to green, giving an indication to the subjects that they have to start imagining the capital letter corresponding to the letter they saw in the cue. In the first two TRs, highlighted in yellow in Figure 3.9, no feedback was shown due to pipeline delay. Similarly, no feedback was shown in the four TRs that followed due to

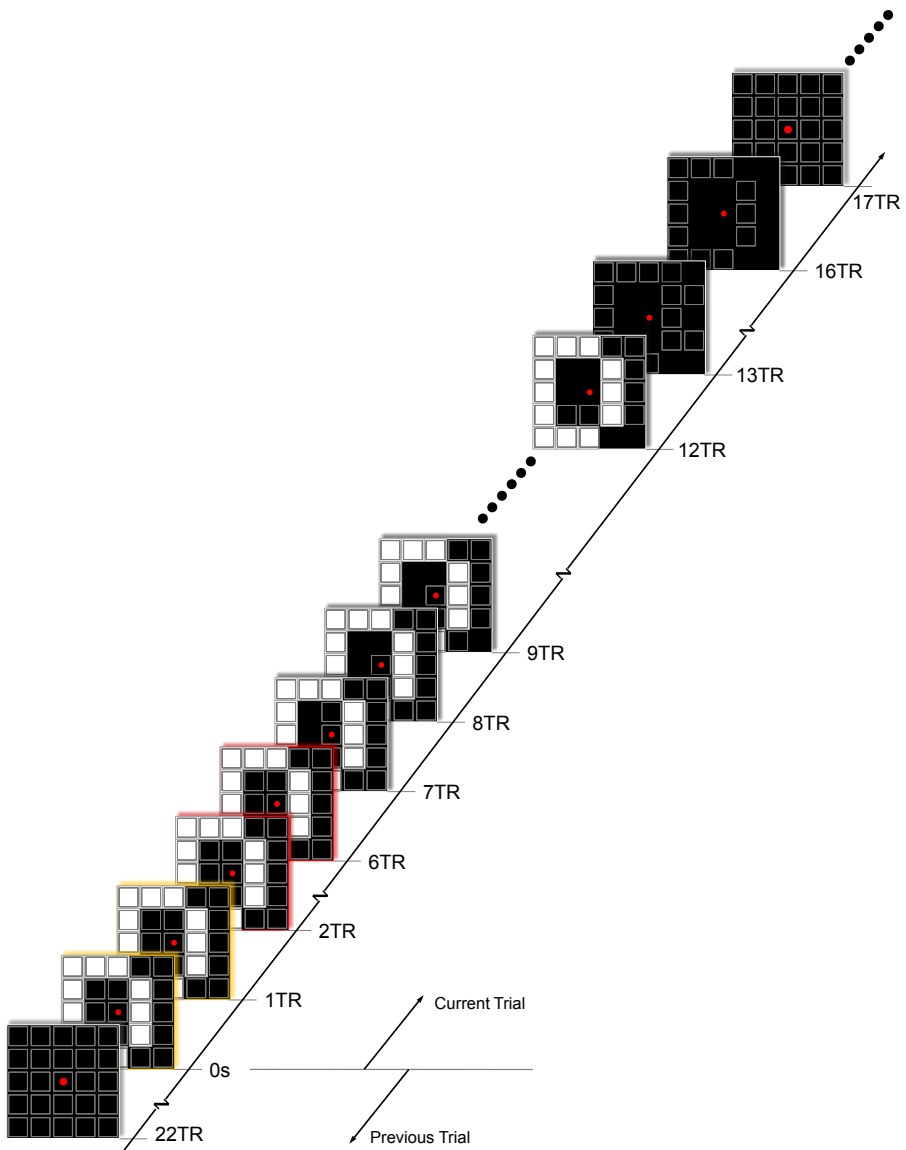


Figure 3.6 | Stimuli used in ‘Visual perception with feedback condition’. In each trial of visual perception with feedback condition, the classifier prediction is also shown to the subjects. Each trial contains 12 TRs (18 s) of task followed by 12 TRs of rest in which the subjects were allowed to close their eyes. The task consists of fixating on a letter, in this case ‘D’, flickering with 8 Hz. In the first two TRs, highlighted in yellow, there is no feedback due to pipeline delay. In the four TRs that follow, highlighted in red, there is no feedback due to hemodynamic delay. The feedback starts from 7th TR and is presented until the 16th TR although the task/visual stimulation stops after the 12th TR. This is due to aforementioned hemodynamic lag. The feedback is presented such that if the classifier prediction for the grid element is below 0.5, the corresponding feedback block is turned off and if its above 0.5 then its turn on. Sixteen trails were conducted in this manner, one trial for each of the letter in the word DONDERSINSTITUTE.

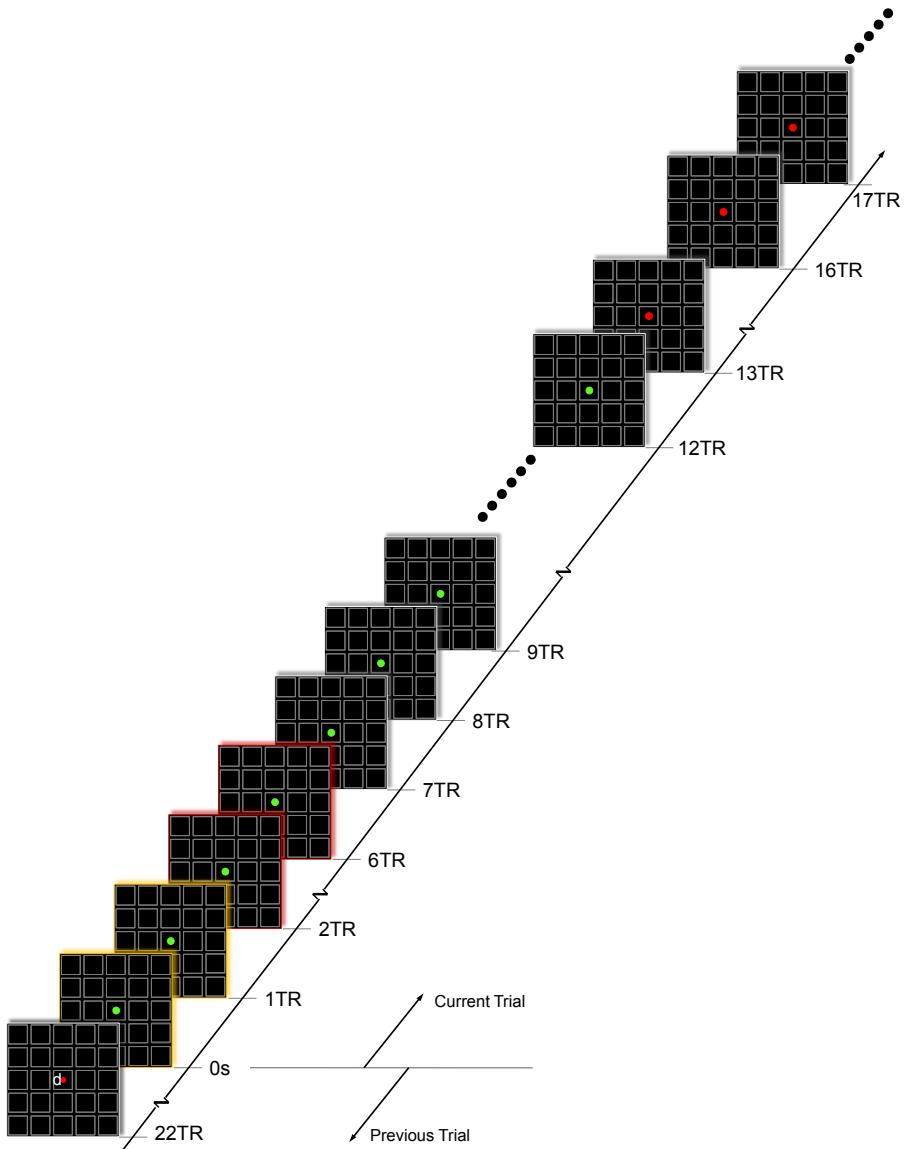


Figure 3.8 | Stimuli used in ‘Visual imagery with no feedback condition’. In each trial of visual imagery with feedback no condition, no classifier prediction is shown to the subjects. Therefore, the feedback grid remains static throughout the duration of the trial. The cue is presented two TRs before the beginning of each trial in the rest period of the preceding trial. After the cue is over, the fixation dot turns from red to green, giving an indication to subjects that they have to start imagining the capital letter corresponding to the letter they saw in the cue. The imagery task ends at the 12th TR and is indicated by a change of color the fixation dot from green to red. Thus, each trial contains 12 TRs (18 s) of task followed by 12 TRs of rest. Sixteen trails were conducted in this manner, one trial for each of the letter in the word DONDERSINSTITUTE.

hemodynamic delay. From 7th TR until the 16th TR, the feedback was shown by manipulating the visibility of the feedback blocks according to the classifier prediction. The imagery task ends at the 12th TR and is indicated by a change of color of the fixation dot from green to red. The feedback, however, was visible until the 16th TR due to hemodynamic lag. Thus, each trial contained 12 TRs (18 s) of task followed by 12 TRs of rest. Sixteen trials were conducted in this manner, one trial for each of the letter in the word DONDERSINSTITUTE.

3.2.3 Experimental protocol

Before putting subjects in the scanner, they were thoroughly briefed about the experiment. This was done to avoid any communication during real-time fMRI run when the scanner noise is too high for two-way communication between the subject and the experimenter. During this pre-screen briefing (see Appendix E for more details), subjects were shown video recordings of all five experimental conditions and the task was explained with the help of these videos. They were specifically instructed that the feedback would be delayed by about 9 seconds and that no matter what the feedback was, they were to always concentrate on the task without moving their gaze from the central fixation. Furthermore, they were allowed to close their eyes during rest periods but were advised to open their eyes a few seconds before this rest period was over. Subjects were instructed to adjust the viewing mirror in the scanner before the start of the experiment such that they were comfortably viewing the center of the screen at all times. After subjects had adjusted the mirror, they were strictly advised not to change its position through out the rest of the duration of the experiment.

Once subjects got a thorough grasp of the experiment, they were asked to memorize the patterns corresponding to 9 letters DONERSITU. These exact patterns were to be later imagined in the imagery conditions. The memorized patterns were practiced on an interactive software that had the same look and feel as the screen that subject would be seeing in the scanner during imagery conditions. Once the experimenter was sure that all patterns have been correctly memorized, the subject was put in the scanner. An eye tracker was used to monitor if the subject was awake in the scanner.

After the experiment was over, the subject was asked to fill out a computer based vividness of visual Imagery questionnaire (VVIQ) (see Appendix D for more details). The Vividness of Visual Imagery Questionnaire (VVIQ) was published in 1973 by the British psychologist David Marks [75]. The VVIQ consists of 16 items in four groups of 4 items in which the participant was asked to consider the image formed in thinking about a specific scenes and situations. The vivid-

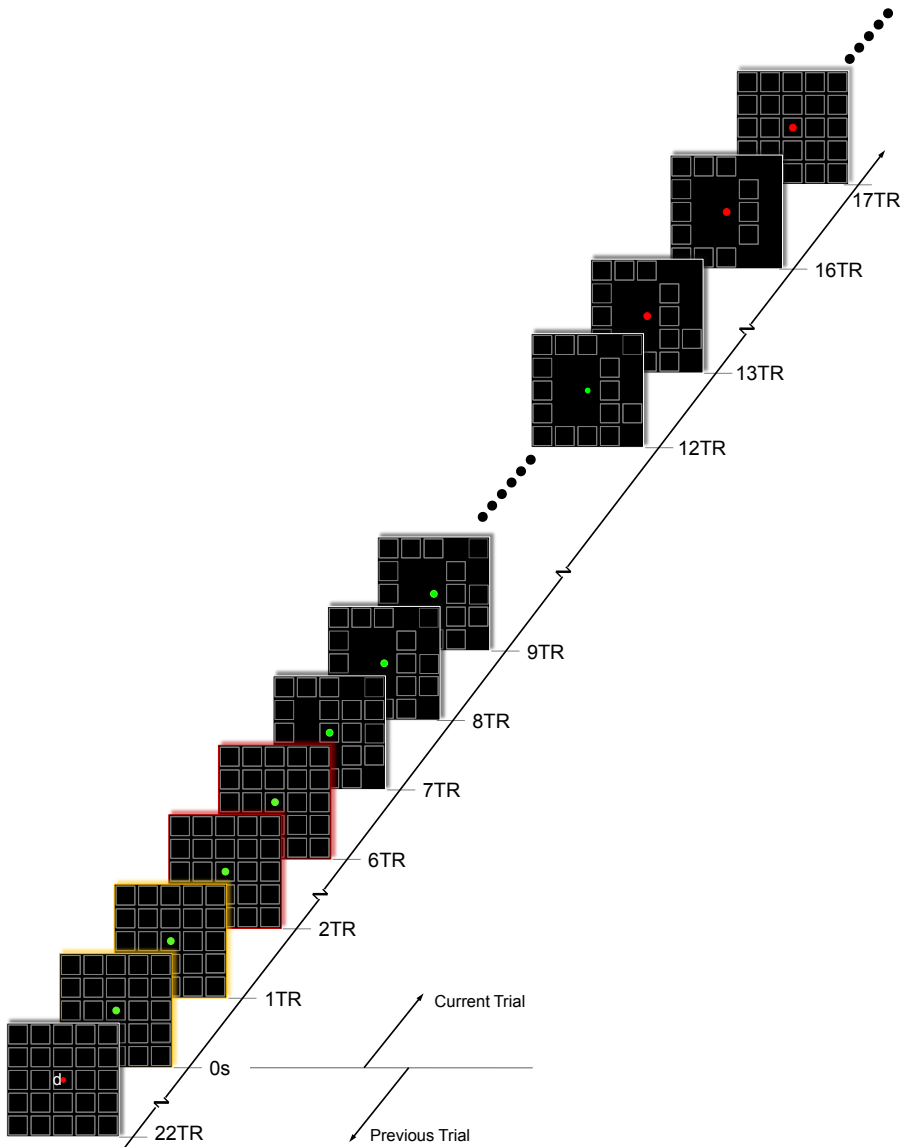


Figure 3.9 | Stimuli used in ‘Visual imagery with feedback condition.’ In each trial of visual imagery with feedback condition, the classifier feedback is also shown to the subjects. The cue is presented two TRs before the beginning of each trial in the rest period of the preceding trial. After the cue is over, the fixation dot turns from red to green, giving an indication to subjects that they have to start imagining the capital letter corresponding to the letter they saw in the cue. In the first two TRs, highlighted in yellow, no feedback is shown due to pipeline delay. Similarly, no feedback is shown in the 4TRs that follow due to hemodynamic delay. From 7th TR until the 16th TR, the feedback was shown by manipulating the visibility of the feedback blocks according to the classifier prediction. The imagery task ends at the 12th TR and is indicated by a change of color the fixation dot from green to red. The feedback is visible until the 16th TR due to hemodynamic lag. Thus, each trial contains 12 TRs (18 s) of task followed by 12 TRs of rest. Sixteen trials were conducted in this manner, one trial for each of the letter in the word DONDERINSTITUTE.

ness of the image was rated along a 5-point Likert³ scale. The questionnaire was conducted twice, once eyes open and once with eyes closed. The questionnaire has been widely used as a measure of individual differences in vividness of visual imagery. The large body of evidence confirms that the VVIQ is a valid and reliable psychometric measure of visual image vividness [21, 38].

The VVIQ was immediately followed by a short computer-based demographics questionnaire, which among the usual things, also measured how boring or interesting the participants found the experiment to be (see Appendix D for more details). Furthermore, it also inquired as to which letter patterns the subjects difficult to imagine.

3.2.4 MRI Acquisition parameters

Experiments were performed at the Donders Institute MRI lab using a Siemens MAGNETOM Tim TRIO 3.0 T scanner with a 32-channel head coil. All functional images were acquired using a single shot gradient EPI sequence (TR/TE = 1500/30 ms; Flip angle = 75°; voxel size = 3x3x3.3 mm; distance factor = 10 %). 21 axial slices were acquired, oriented typically at 30° to the AC-PC (Anterior-Posterior Commissure) line as shown in Figure 3.10. A high-resolution anatomical image was acquired using an MP-RAGE sequence (TE/TR=3.03/2300 ms; 192 sagittal slices, isotropic voxel size of 1x1x1 mm). The anatomical images were acquired before the real-time run and these high resolution images were used to position the slices.

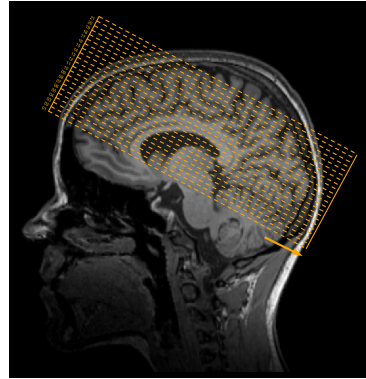


Figure 3.10 | Slice positioning. 21 axial slices were acquired orientated typically at 30° from the AC-PC line. As slice # 1 and 21 were to be masked out in the preprocessing later on, these two slices covered no brain region which was of interest in this study.

3.2.5 Real-time fMRI processing

All functional scans were acquired using the distributed real-time fMRI pipeline implementation. In this pipeline, the preprocessing, classification, and synchronization were each performed on a separate PC. For more details about this pipeline, please refer to Chapter 5, Section 5.1. The functional scans acquired

³Actually, a 6-point Likert scale was used. The default position of the pointer was 6th point on the scale that represented no rating at all. If the subject did not move the slider from this position, the test would not proceed. This was to encourage the subjects to move the slider rather than just using the default slider position and skipping ahead.

using this pipeline were preprocessed before being used for classification. The preprocessing steps included:

Slice time correction Slice time correction with trilinear interpolation was used to correct for differences in the acquisition time of various slices in each scan.

Motion correction A three pass motion correction procedure was used. In the first and second pass, the head motion was corrected by the Siemens scanner, prospectively (PACE) and retrospectively (MoCo), respectively. In the third pass, retrospective motion correction was applied by the real-time pipeline to remove any residual motion.

Boundary slice Masking The average duration of this experiment is 90 minutes. With PACE enabled, only a very small motion occurs and on average only half of the first and last slices gets damaged due to motion. Hence by masking the entire first and last slices, it was ensured that none of the damaged voxels gets used in the training and test session.

Nuisance regressors removal Five regressors were used to remove scanner drifts, offsets, and motion related activation.

Brain Extraction The skull was stripped away from all functional scans by applying a skull mask which was derived using the Brain Extraction Tool (BET) [11, 116].

3.2.6 Data analysis

After the classifier had been trained during the actual real-time experiment, the prediction was started. Because each trial contained 12 scans (or TRs) therefore, each current scan was averaged with all the previous scans of a trial in the hope that classification on averaged scans will be more robust and accurate than on individual non-averaged scans. The trained classifiers, their predictions and pre-processed fMRI data for every scan of the actual real-time experiment run were saved for any offline statistics and additional post-hoc analyses.

The saved predicted labels were used to calculate the prediction accuracy of the actual real-time experiment. Because each letter in the test conditions is constructed from 25 individual elements (5x5 grid) or building blocks therefore, there are 25 binary predictions, one for each element of the grid. By taking a ratio of the correctly predicted grid elements and the total number of grid elements, the accuracy for all 16 trials in each condition was calculated. This accuracy represents the proportion of grid elements that were correctly classified. Because each reconstructed letter is built from the predictions of *binary classifiers* therefore, the chance level accuracy for this experiment is 50%. A bi-

nomial test (p-level 0.05) was then used to find if the accuracies obtained were significantly above chance level. A binomial test can be used when data is dichotomous - that is, when each individual in the sample is classified in one of two categories (e.g. category A and category B) and when one wants to know if the proportion of individuals falling in each category differs from chance or from some pre-specified probabilities of falling into those categories. .

Additional post-hoc analyses were done by using the preprocessed data and the trained classifier. For example, during the actual real-time experiment, in each test session, every incoming scan in a trial was averaged with all the previous scans of the same trial and then classified. To find if this averaging was any superior to no averaging at all, a post-hoc analysis was done where only current scans were fed to the classifier for prediction. Similarly, in the actual experiment, voxels from the entire brain were used during classifier training and testing. To find if restricting classifiers to only grey matter voxels in occipital cortex and calcarine sulcus, would yield any better decoding performance, a post-hoc analysis was done in which a subject-specific Anatomical Automatic Labeling (AAL) mask [127] was constructed by warping the standard AAL mask in MNI (Montreal Neurological Institute) space to native space [6] using the inverse of the spatial transformation matrix obtained from the SPM8 (Wellcome Department of Cognitive Neurology, Queens Square, London, UK), unified segmentation normalization [7]. This mask was then used to find the grey matter voxels in occipital and calcarine sulcus of each subject. Then the classifiers were retrained and retested on these restricted subset of voxels for each subject and the prediction accuracies were recalculated.

Single voxel time course analysis was performed in Analyze4D (www.analyze4d.com) on MoCo series from the preprocessed data buffer. The time course was detrended by using 0.01 Hz high-pass filter. No additional processing was applied on the time courses. Furthermore, to assess distribution of classifier weights, these weights were overlaid onto first functional scan of the raw data buffer using Analyze4D.

Averaged reconstructions for each of the nine letters in DONERSITU were constructed post-hoc by averaging together the single trial reconstructions of each of these letters across subjects for each condition. As these averaged reconstructions turned out to be rather crude, an additional step of template matching was performed where each averaged raw reconstructed letter was cross-correlated with ground truth letters (i.e. perfectly shaped letters). The letter that correlated the highest with raw reconstructed letter was chosen as closest match.

3.3 RESULTS

The aim of this experiment was to find if perceived and imagined stimuli can be decoded in real-time using a classifier trained only on perceived stimuli. Furthermore, the study tried to find the effect of neurofeedback of reconstructed patterns on subject's task performance.

The reconstruction accuracy for all four test session averaged across trials across the group is shown in Figure 3.11. These results show that *visual perception without feedback* condition was decoded with an average accuracy of 55% ($SD = 6.8$), whereas *visual perception with feedback* condition was decoded with an accuracy of 52% ($SD = 4.6$). Similarly, the decoding accuracy for *visual imagination without feedback* condition was found to be 50% ($SD = 4.6$), whereas *visual imagination with feedback* condition was decoding with an accuracy of 48% ($SD = 3.8$). Contrary to our hypothesis, conditions without feedback have higher decoding accuracy than the corresponding conditions with feedback.

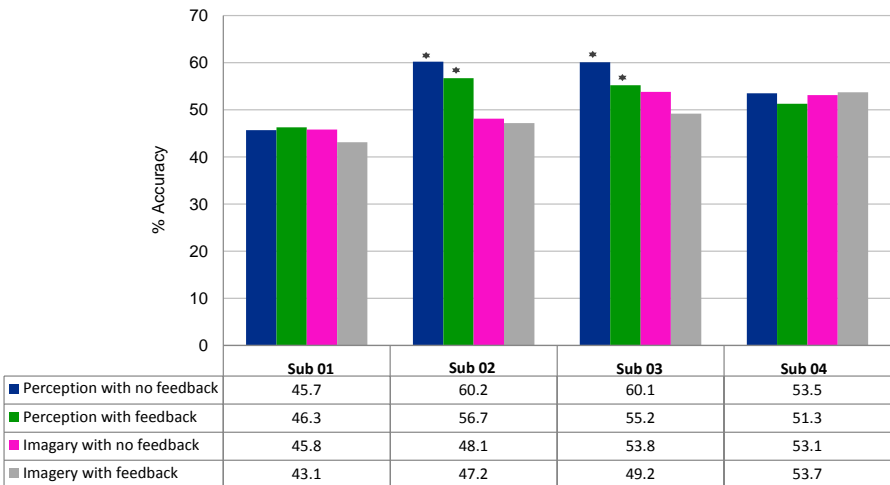


Figure 3.11 | Decoding accuracy per subject. Shows the decoding accuracy for every subject for all four experimental conditions. The decoding accuracy is statistically significant only for Subject 02 and 03 in *visual perception* condition and is marked by *. Note: The chance level performance is 50%.

Figure 3.12 shows the accuracy in all four conditions as a function of time into each trial. A linear regression analysis was conducted on the average of the accuracy(as a function of TR) for all four condition to detect any trend. The results of that analysis shows that the accuracy increases with increasing TR $\beta = 0.802$, $p = 0.02$, $\alpha = 0.05$. This is because accumulating and averaging over scan in a trial gives a more accurate measure of the BOLD activity due to reduced noise in the averaged signal.

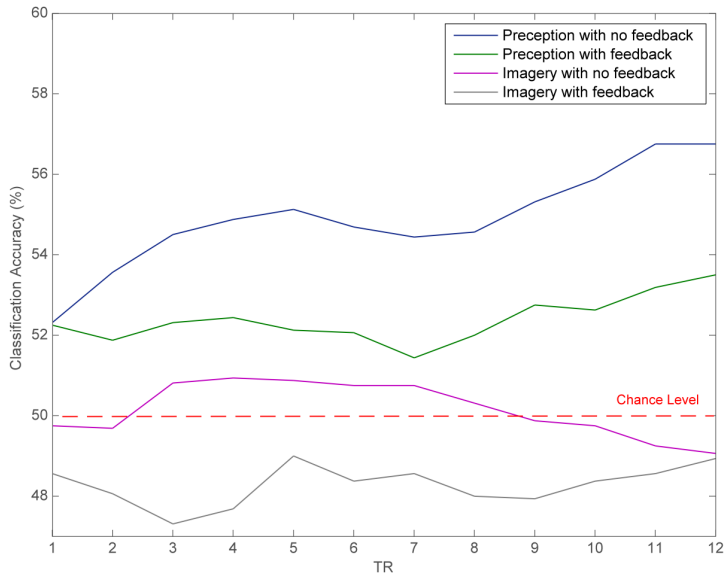


Figure 3.12 | Decoding accuracy per TR with cumulative averaging of scan data. Shows the decoding accuracy as a function TR averaged across all subjects for each condition. Decoding was done at each TR on the cumulative average of the current and all the previous scans of a trial. As more and more scans get accumulated, the decoding accuracy increases.

To further investigate the effect of accumulating and averaging scans over each trial on the classification accuracy, the analysis was repeated offline but this time instead of classifying on the average of current and all previous scans of a trial, the classification was carried out on just the current scan. The results, as depicted in the Figure 3.13, show a decreased performance compared to the previous case in which all past scans in a trial were accumulated with current scan. A linear regression analysis was conducted on the average of the accuracy (as a function of TR) of all four conditions to detect any trends in the data. The results of that analysis shows that the accuracy does not change in predictable manner with increase in TR $\beta = -0.124$, $p = 0.7$, $\alpha = 0.05$ thereby indicating that not averaging over previous scans is suboptimal. Figure 3.14 shows the VVIQ (Vividness of Visual Imagery Questionnaire) scores for all four subjects. Higher scores on this graph means a better ability to form mental imagery. To find if there is any correlation between VVIQ and decoding performance in imagery conditions, the average accuracy for each subject in both imagery conditions was correlated with the VVIQ. The two variables (VVIQ score and decoding accuracy) were found to be not correlated, $r(4) = .359$, $p = 0.64$.

The reconstructed patterns for each of the four test sessions are shown in Figures 3.15 and 3.16. The reconstructed letter don't look very recognizable. Therefore, template matching was then performed on the raw averaged reconstructed

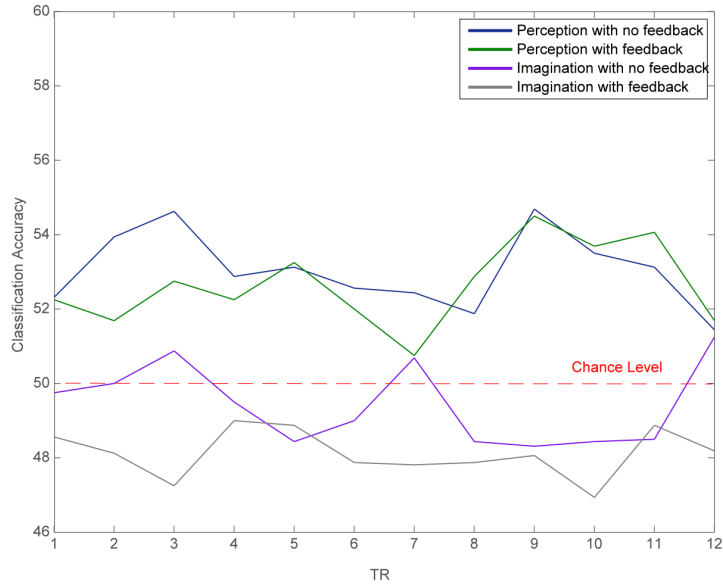


Figure 3.13 | Decoding accuracy per TR without averaging of scan data. Shows the decoding accuracy as a function TR averaged across all subject for each condition. Decoding was done at each TR using only the scan data from the current scan.

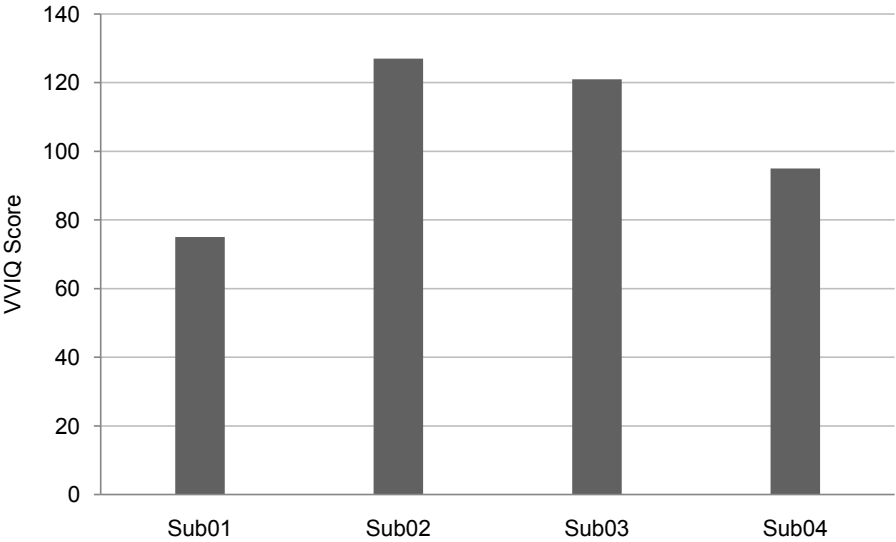


Figure 3.14 | Vividness of Visual Imagery(VVIQ) score for each subject

pattern to pick the best match in the candidate set. The candidate set for template matching contained the letters DONERSITU.

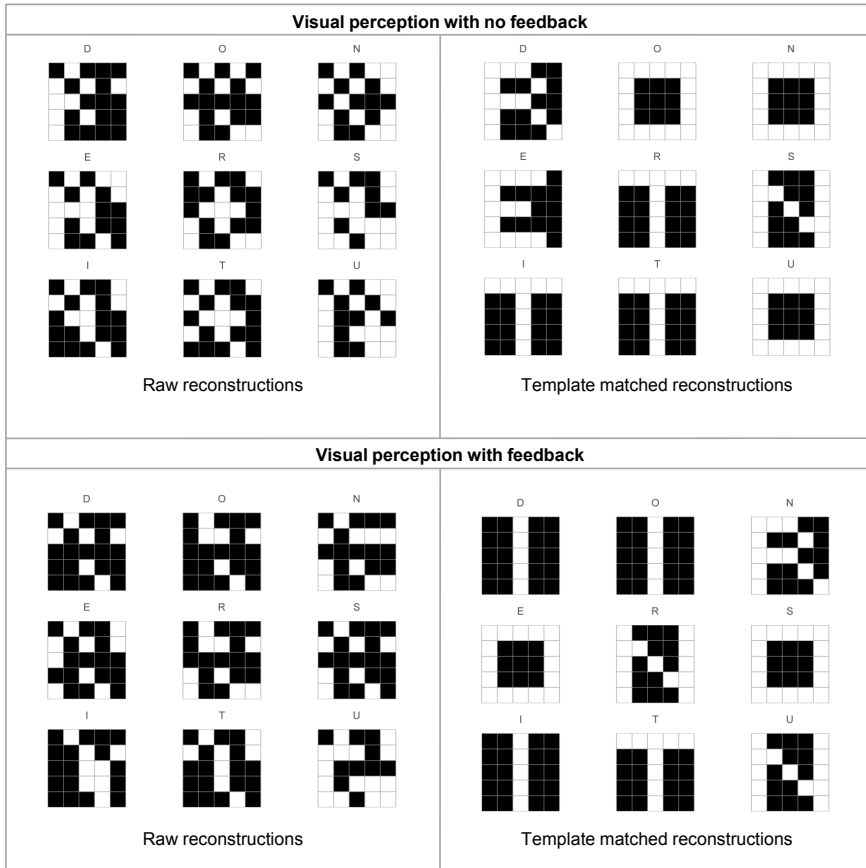


Figure 3.15 | Reconstructions for visual perception condition averaged across group. The letter on top of each pattern is the true label.

Because significant reconstruction accuracy was obtained only for subject 02 and 03 for visual perception condition, therefore, the reconstructions averaged across these two subjects was also calculated and is shown in 3.17. This was done in the hope that by excluding the worst subjects, perhaps the reconstructed might improve however this wasn't to be.

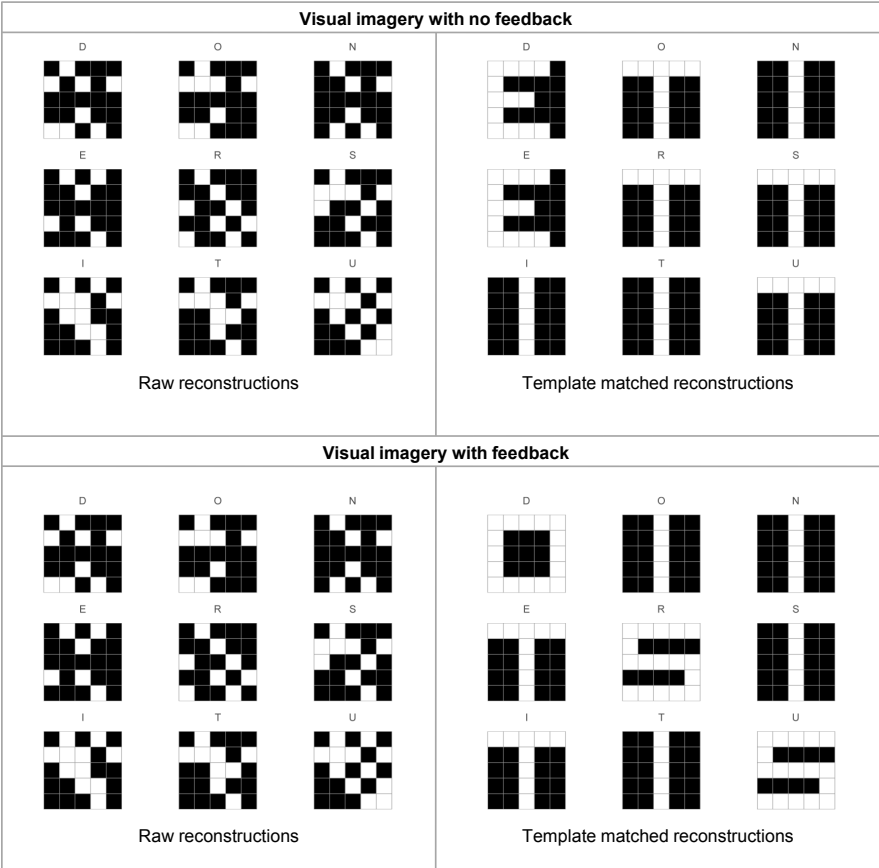


Figure 3.16 | Reconstructions for visual imagery condition averaged across group. The letter on top of each pattern is the true label.

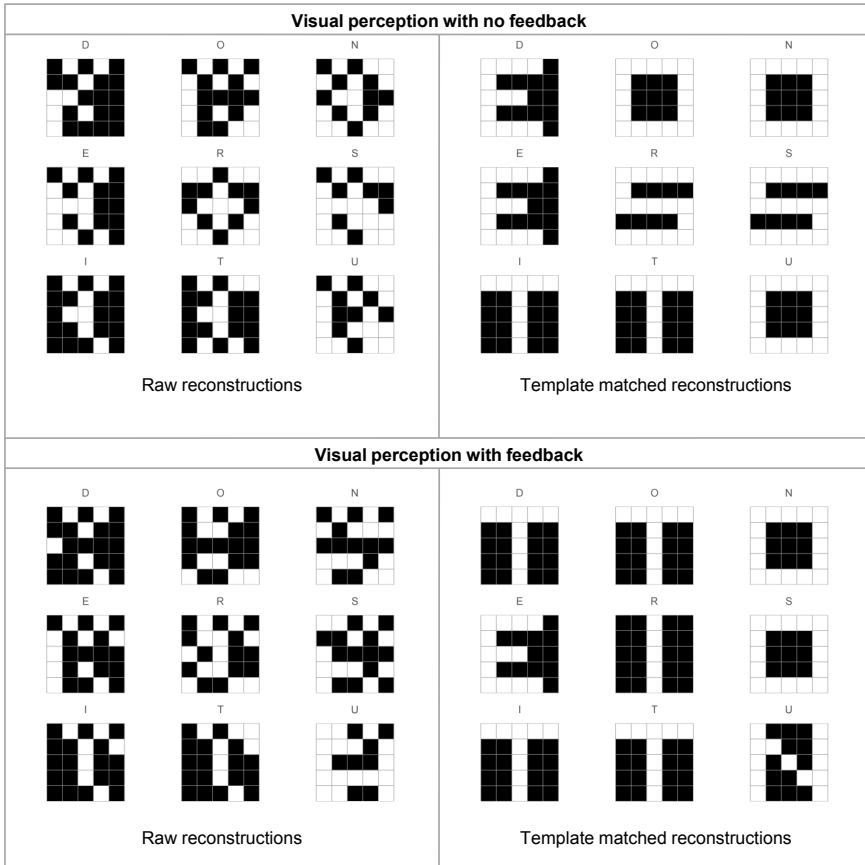


Figure 3.17 | Reconstructions for visual perception condition averaged across subject 02 and 03. The letter on top of each pattern is the true label.

3.4 DISCUSSION

The current study tried to decode perceived and imagined stimuli in real-time and investigated the effect of neurofeedback on the task performance. In two out of four subjects, the decoding performance for visual perception was significantly above chance level of 50%. However, the decoding performance for imagery condition was not found to statistically significant. There could be several reasons for these observation. First and foremost is motivation. The experiment was about 150 minutes long which is almost at the edge of legally allowed limit of continuous scanning. The subjects started to feel quite tired and weary after only 30 minutes inside the scanner as they had to perform an excruciatingly difficult task of constantly staring at flashing patterns for more than an hour. Furthermore, subjects got a fixed compensation for their participation in the experiment no matter how good or otherwise they performed in the experiment. The lack of any monetary incentive coupled with the task difficulty is made even worst by the scanner environment where subjects lie on a very cosy bed. With the head fixated by foam padding, it is very easy to go to sleep, even with all that scanner noise. One of the experiment had to be aborted prematurely because the subject was too tired to open his eyes for more than a few seconds during the stimulation periods. Similarly, other subjects also had a hard time not sleeping during the experiment and the experimenter had to intervene every now and then via intercom to warn the subjects. A conclusive proof that motivation was indeed a major factor in such low performance in the experiment, is a pilot experiment that was conducted on the author (highly motivated!) himself. The author performed *visual perception without feedback* condition at 65% accuracy, 10% higher than the best subject reported in this study. The reconstructions obtained for that session are amazingly accurate. To see of a footage of the session and the reconstructions, please refer to the video in Appendix G. Unfortunately, the remaining three conditions were not conducted by the author because of a technical malfunction. However, the video provides a convincing proof that it is possible to decode at least visual perception in real-time with acceptable levels of decoding performance, albeit, it is not reflected in performances of actual subjects.

Another reason for low decoding accuracy is some inherent design flaws which, in hindsight, could have easily been avoided. The first biggest design flaw was the length of stimulation period during training. Each random pattern was made to flicker for 12 seconds followed by 12 seconds of rest. This 12 seconds stimulation is just way too long. Studies have shown that if a stimuli stimulates the visual cortex for more than 4 seconds, then activations in the cortical areas activated by that particular stimuli might bleed into the surrounding cortical areas [14, 71]. Thus any stimulation more than 4 seconds long can severely blur the locus of the actual activation. This is exactly what we see in the time course of the training block (Figure 3.19). By looking at the time course (Figure 3.20) of one such voxel (Figure 3.19) for subject 04, it can be clearly seen that the voxel is responding

to every trial in the training session when it should only respond to only 50 % of the trials in the training session because each pixel in the training stimuli was activated no more than 50 % of the trials. This shows that when a voxel was supposed to be OFF, activations from the neighboring ON voxels crept into it and turned it ON as well. Thus the voxels presented to the classifier for training do not have much meaningful information to help it in learning any meaningful mapping from stimulus to cortical activation. This is again confirmed by looking at the classifier weight distribution in Figure 3.18. In a visual experiment such as ours, one would expect to find the majority of weights to be concentrated on the visual cortex. However, the classifier distribution obtained for all subjects show that the voxels used for training are disbursed around the whole brain. This indicates that the visual cortex voxels did not had any meaningful information in the first place to help classifier choose them to train itself on. Instead, the classifier went on a wild goose across the entire brain and picked any voxel for training that it found to be remotely correlating to the stimulus.

The second design flaw is the rather large voxel size (3 x 3 x 3 mm) used in this study. Recently a study conducted specifically to find scanning parameters for optimal decoding in early visual cortex using a 32-channel fMRI head coil. The findings of the study reveals that the best decoding performance is obtained for voxel size of 2 x 2 x 2 mm acquired using SENSE (SENSitivity Encoding) protocol [19]. For future experiments a variation of the SENSE sequence, called SENSE-EPI should be used to substantially increase speed and spatial resolution of conventional EPI-based fMRI [98].

The third design flaw is not filtering out the irrelevant voxels before training. The classifiers were trained and tested on the whole brain data which includes grey matter, CSF, and white matter voxels, when only voxels in the grey matter encode any meaningful information. This not only increase training time but may also yield suboptimally trained classifiers. In future studies, grey matter mask should be applied to confine analysis to only grey matter voxels. An even better option would be to confine analysis to only the retinotopically organized areas of the visual cortex by conducting an additional localizer experiment before the start of each experiment. Confining classifier training only to retinotopically mapped voxels has yielded much better decoding accuracies in visual cortex related experiments currently ongoing in our department. The decision to not perform grey matter masking or retinotopic mapping was based purely on the fact that real-time fMRI pipeline available at that time did not had these feature. Furthermore, retinotopic mapping would also have prolonged the experiment duration by approximately 20-25 minutes which would have made an already painfully long experiment even longer.

By looking at the decoding accuracies in the feedback and non-feedback condition, it can be observed that subjects perform better in non-feedback situations than in feedback situations. This can be explained by the fact that the feedback itself induces activity patterns in the visual cortex and this feedback if incor-

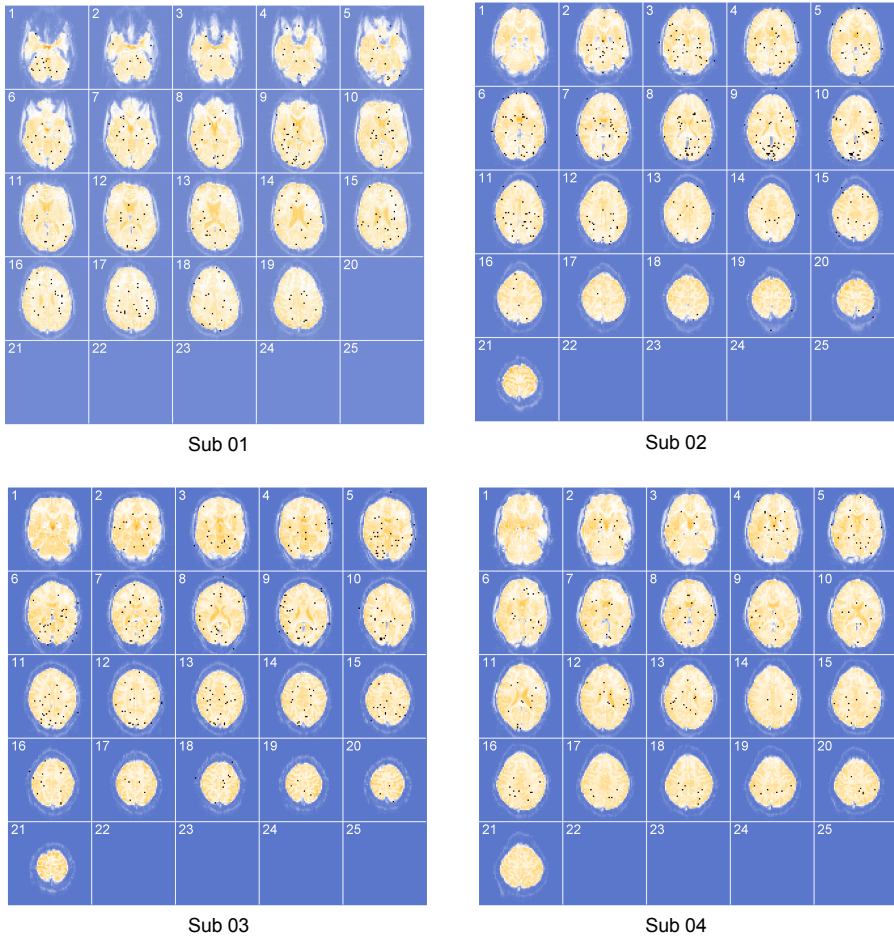


Figure 3.18 | Classifier Weights. The classifier weights shown in black color are overlayed on a functional image. The weights seem to be distributed all over the brain rather than being concentrated at the occipital cortex, indicating that not much discriminative information was present there.

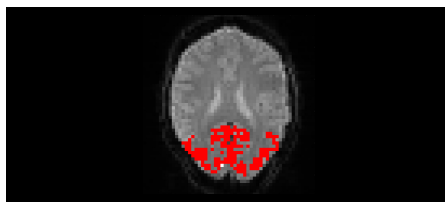


Figure 3.19 | Voxel for time course analysis. The voxel highlighted in white was chosen for plotting the time courses in Figure 3.20. The voxels highlighted in red represent the grey matter of occipital cortex and calcarine sulcus.

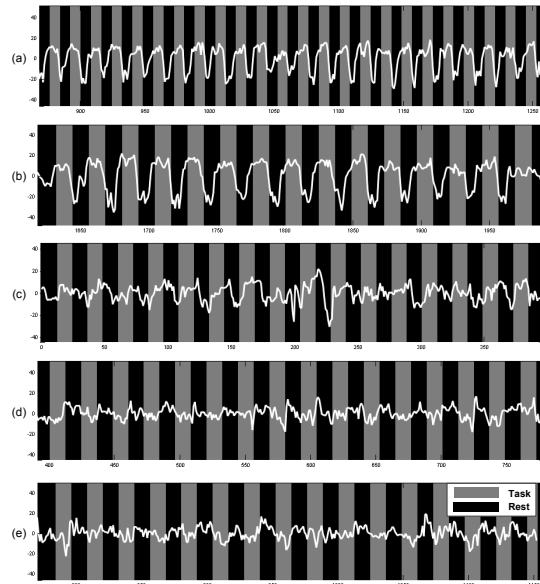


Figure 3.20 | Voxel time course. Time course of one voxel highlighted in white in Figure 3.19 for all the different experimental phases. All the time courses have been detrended and shifted by 4 TRs **(a)** Time course for 24 of the 100 training blocks **(b)** Time course for visual perception with no feedback condition **(c)** Time course for visual perception with feedback condition **(d)** Time course for visual imagery with no feedback condition **(e)** Time course for visual imagery with feedback condition

rect might negatively affect the ongoing perception or imagination by the subject. By presenting feedback while the subject is actively engaged in the perception/imagination might result in shifting of gaze which could result in shift in the voxel activity, thereby resulting in poor performance. This can be seen by comparing the voxel time courses of the visual perception with and without feedback condition. In non-feedback conditions the voxel is responding very predictably to the stimuli while the same voxel in the feedback condition has a considerably less predictable response in the feedback condition. Thus the current strategy of presenting the real-time feedback seems to negatively impacting the subject performance by being too distracting. A more clever and non-obtrusive way of presenting feedback for this kind of paradigm, therefore, needs to be developed for future experiments.

The study failed to show that imagined stimuli could be decoded. No significant decoding accuracy was obtained for any of the participants in the visual imagination sessions. This is in contrast to much of the existing research. For example, studies in visual perceptual learning (e.g., [114]) have shown that it is possible for subjects to voluntarily evoke the same activity in the visual cortex, similar to the one evoked during actual perception of the stimuli, hence demonstrating that it is possible to decode a stimuli even in its absence. However, these stud-

ies use simple stimuli like gratings and only a limited number of orientations⁴ for decoding, which makes the problem of decoding much easier. Furthermore, these studies use longer trial duration and more repetitions of the trials which helped subjects in learning the relevant strategy that assisted them in getting better decoding performance. In our study, the patterns to be imagined are too complex (compared to simple grating), the trial duration too small, and there are not enough repetitions of the trials to allow subjects to learn any effective strategy for getting the best decoding performance. The fact that the patterns to be imagined were very difficult was reported by the subjects on a questionnaire (see appendix D - demographics section) conducted after the experiment and also in informal discussions with participants after the experiment was over. In particular, subjects found E,R,and D very difficult to imagine. Future studies should therefore consider using simple characters like +, - etc. with longer trial durations and more repetitions of the same trials. Furthermore, to keep subjects motivated and attentive during the whole duration of the experiment, a reward system should be in place where the subject could receive compensation in par with their performance in the task.

3.5 SUGGESTIONS FOR FUTURE IMPROVEMENTS

The lessons learned in these experiments can be summarized a few suggestions that can help researchers in future to better design their real-time experiments.

- In any visual cortex related experiment, it's best to confine classifier training to retinotopically mapped voxels
- If retinotopic map is not available for any reason, then the classifier training should be confined to grey matter voxels in occipital cortex and calcarine sulcus. Such a mask can be constructed using the Anatomic Automatic Labeling Atlas (AAL).
- If the occipital cortex and calcarine mask is not available, then at least a grey matter mask should be used. Such mask can be extracted from SPM8 unified segmentation and normalization procedure.
- The stimulation duration of visual cortex should not exceed 4 seconds, otherwise activation will spread to neighboring voxels, thereby activating them when they shouldn't be.
- Voxel size for visual cortex experiment should be no more than 2 x 2 x 2 mm. Furthermore, an EPI-SENSE sequence should be used to acquire them for better SNR.

⁴By orientation we mean the angle which the grating makes with the horizontal axis. For example the orientation of a horizontal grating is 05 degrees and for vertical grating it's 90 degrees.

- Neurofeedback should be delivered as timely as possible.
- If the duration of real-time experiment starts to become too long, conduct the experiment in separate sessions on separate days. For example, the classifier can be trained one day and tested the other. Each scanning session should not exceed more than 70 minutes.
- If conducting the experiment in separate sessions is not feasible then conditions should be divided among groups of subjects. For example one group of subjects can perform one condition and the other group can perform the other condition. This will lead to a decrease in experiment duration because now each subject has to attempt only half of the conditions than before.
- Trials in different conditions should be randomized to avoid any systematic errors entering into on particular condition and not the others. One side effect of this would be that it would lead to a decrease in learning effect if trials from feedback and non-feedback conditions are intermixed.
- Subjects should not only be given fixed compensation for their participation but should also be motivated by the promise of a monetary reward if their performance during the experiment exceeds a certain threshold.

CHAPTER 4

ONLINE VOLUNTARY CONTROL OF CATEGORY-SELECTIVE BRAIN REGIONS

THIS chapter describes the second and the last experiment conducted during this study. The experiment tries to investigate if category of the attended stimulus in a scenario where two competing stimuli are presented, can be decoded in real-time. Furthermore, the experiment tries to investigate if presenting neurofeedback of ongoing decoding can yield any increase in task performance. The chapter begins with a literature review of pertinent studies along with the improved neurofeedback strategy which will be used in this experiment. Lessons learned with the previous experiment (Chapter 3) will be used to fine tune the implementation in this experiment. The method section describes all the details of the experimental setup along with a detailed description of the statistics carried out on both online and offline data. The chapter concludes with a discussion of the important findings of this experiment.

4.1 INTRODUCTION

In our daily life, we are always confronted with situations where multiple objects or scenes compete for our attention but somehow our brain is able to filter out the pertinent information from all the distractions present out there. When images of familiar concepts impinge on the retina, neurons in the human medial temporal encode these in an abstract and invariant manner [29, 100] as these neurons are selectively activated by remarkably different pictures of same individuals, landmarks or objects and in some cases even by letter strings with their names [101]. These representations can be activated again when subjects view [100], imagine [64] or recall these concepts or episodes [34]. But how do these neurons behave when a person is faced with competing visual inputs. In 2010, a study by Moran Cerf and colleagues [17] reported that these neurons can also fire selectively when attending to a particular face in a hybrid of two competing faces. Using intracranial recordings and a ECoG-based Brain-Computer Interface (BCI) setup, they demonstrated that subjects were able to reliably modulate the firing of these neurons to manipulate an initial 50/50 hybrid of two different faces, a target and a non-target face, towards the target face. Before each trial subjects were briefly shown target and non-target face pictures. They were then shown a 50/50 hybrid of these two pictures and were asked to enhance the target picture by focusing their thoughts on it. The firing rates of MTL neurons were fed into a real-time decoder that could change the visibility ratios until either the target was fully visible (*success*), the distractor was fully visible (*failure*), or until 10 s had passed (*timeout*). The results showed that subjects were able to reliably regulate, often on the first trial, the firing rate of their neurons, increasing the rate of some while simultaneously decreasing the rate of others. Their experiment demonstrated that despite of the presence of competing retinal sensory inputs, subjects were able to voluntarily, rapidly and differentially up- or down-regulate the firing of the MTL neurons by object-based selective attention.

In Cerf et al. study, neurons that fired for faces of particular persons such as Josh Brolin and Marilyn Monroe were identified before the experiment in a pre-screen session. The participant was then shown a 50/50 hybrid of these pictures and the firing rates from the previously identified responsive neurons were fed in a decoder which adjusted the relative mix of the target and non-target picture depending on the activity of these neurons. Because fMRI measure activity from a huge population of neurons, we want to investigate if it is also possible to decode the attended stimulus from two competing stimuli using fMRI BOLD activity. Instead of using the hybrid of two faces (as was used in the Cerf study) and trying to decode the within-category information, we will try to decode between-category information. The categories that were selected for this purpose are faces and places. Numerous studies have shown that pictures of faces and places invoke spatially distinct and dissociable cortical regions namely, Fusiform Face Area (FFA) for the face pictures and Parahippocampal Place Area (PPA) for pictures of scenes [3, 26, 53, 77]. By using activity in these category selective areas we will try to demonstrate if it is possible to decoded the attended picture cate-

gory (a face or a place), when the subject is presented with overlapping pictures of a face and a place. A recent study [133] to investigate the effect of repetition priming on activity in FFA and PPA has shown that when subjects were presented with overlapping pictures of faces and places and asked to attend to only one them, an attenuation effect was observed in the BOLD signal in the brain regions associated with the unattended category. This indicates that it might be possible for machine learning technique to detect this activity differential and predict the attended category. We therefore, hypothesize that a classifier trained on fMRI activity corresponding to the perception of faces and places will be able to predict the attended category using the fMRI activity of the brain when the subject is attending to target category in a hybrid picture of target and non-target category. We hypothesize that decoding will be very high because previous decoding studies with pictures of faces, places, objects, and tools have also demonstrated very high decoding accuracies [115].

H1: The attended category will be decoded with very high accuracy

In the experiment that we described in the previous chapter, scans in the transition period, i.e. in the first 6s on HRF curve where the BOLD activity is not fully mature, were not classified. They were simply ignored. This caused a lack or any feedback for the the scans collected in this period. The feedback was started only when this transitional period was over. It is as if you are driving a car on the road and suddenly, out of nowhere, you see a deer pop up in the middle of the road. You hit the brakes, but your car does not respond instantly. It comes to a halt 6 seconds after you have pressed the brakes. By that time, it's too late already. Timely feedback is a crucial prerequisite for operant conditioning [85, 104]. Therefore, in this experiment we will follow a different approach. Instead of ignoring the scans in the initial 6s of the BOLD activity, we will try to classify these scans as well just like scans the stable period that follow the transition period. This will completely remove lag in feedback due to hemodynamic delay. A study by LaConte et al. shows that BOLD activity in the transition period contains reliable structure that can result in a better trained classifier compared to when this transition activity is not used at all [67]. Hence, by classifying the BOLD activity in the transition period and feeding back the classification results to the subject, we will circumvent the fMRI BOLD delay effects. We hypothesize that above chance level decoding accuracies will be obtained in the transition period. We also predict that the prediction accuracies will increase in the transition period and will level off in the stable periods. This is because the BOLD signal strength increases in the transition period and levels off in stable period and the same will also be reflected in decoding performance.

H2: The decoding accuracy will be lower in the scans in transition period compared to the stable period

H3: The decoding accuracy will increase gradually increase in scans in the transition period and will level off in scans in the stable period.

Furthermore, we will investigate the effect of real-time fMRI neurofeedback on decoding performance. Trials will be conducted once with neurofeedback and

once without neurofeedback. We predict that due to feedback, subjects will perform better in a trial because they will always have a feedback available as to how good or otherwise they are doing in the trial and adjust their attention accordingly. In the non-feedback condition we expect that subjects attention will switch between the target and non-target pictures and this attentional shift might also get reflected in the trial-by-trial decoding performance.

H4: Subjects will perform better in trials with feedback compared to trials with no neurofeedback

H5: The attention will shift between target and non-target picture in trials with no feedback whereas, in trials with feedback, the attention will remain glued to the target picture for longer durations of time.

Moreover, we expect that the decoding performance for trials with face picture as a target will be the same as trials with place picture as a target. In other words, we expect the decoding to be unbiased.

H6: The decoding accuracy will be independent of the target category

4.2 METHOD

4.2.1 Subjects

Seven subjects (6 male) participated in the experiment. The average age of the sample was 23.4 ($SD = 4.6$) years. Subjects were recruited from a web-based human subject pool management system (SONA). All subjects had normal vision. For their participation, subjects received either a cash compensation or study credits. The study was approved by the ethical committee of the Donders Institute and all subjects gave a written informed consent (see Appendices B and C). To keep participants motivated throughout the task, they were promised a cash reward in case their task performance (decoding accuracy) exceeded 95%.

4.2.2 Experimental Task

Because the experiment tries to investigate if the attended picture in two overlapping pictures of a face and place could be decoded therefore, its necessary to train a classifier first to learn which brain areas respond to faces and places. Once the classifier has been been trained, we can present overlapping pictures of faces and places and ask subjects to attend one of them and then try to classify the attended category using the previously trained classifier. To find the effect of neurofeedback, trials are to be conducted twice, once with neurofeedback and

once without the neurofeedback. The modality chosen for neurofeedback for this experiment is visual because it is best suited for noisy rtfMRI environment where auditory feedback is not ideal. The neurofeedback is such that depending on the prediction of classifier at each TR, the picture of the predicted category in the hybrid is enhanced while at the same time picture of the opposite category faded out. This gives a visual indication to subjects of their task performance on a TR-by-TR and trial-by-trial basis. This particular type of feedback was selected because it is very natural and intuitive. One the most important aspects of operant conditioning is that the feedback should induce minimal cognitive load [132]. We believe that this type of feedback produces the least amount of cognitive processing load compared to scenario if we had used traditional thermometer type bar alongside the hybrid of two pictures. In that case, the subjects would not only have to attend to the target picture in the hybrid but would also need to simultaneously monitor the thermometer bar to figure out what the classifier prediction was. This increased cognitive load would have certainly resulted in suboptimal reinforcement learning.

Pictures of famous faces and places were selected for the stimulus presentation because previous studies have shown greater responses in face and place selective regions for familiar faces and places compared to pictures of unfamiliar faces and place, respectively [106, 110]. These pictures were collected from the World Wide Web. The dimensions of the picture were 450 x 450 pixels with a resolution of 95.987 pixels/inch. The pictures were not corrected for luminous, contrast, and subtended an angle of 8°. The next few sections will describe in detail how these pictures were used in different phases of the experiment.

4.2.2.1 Training phase The data collected in this phase is used for training a classifier which is used later on in the testing phase of the experiment. The training phase consists of fifteen 30 s blocks of pictures of famous faces and fifteen 30 s blocks of famous places with 12 s rest intervals interleaved in between as shown in Figure 4.1.



Figure 4.1 | Training phase. 15 face blocks and 15 place blocks were used in the training phase. Each stimulation block was followed by a rest block represented by 'R' in the figure.

In each block, 14 pictures were shown and the first picture was repeated at some random position in the block. Each picture in a block was presented for 1.5 seconds followed by a 0.5 s fixation as shown in Figure 4.2). Subjects were instructed to press a button on a button box with their right index finger when they saw the first picture repeated in that block. This was just to make sure that participants were actively engaged in the task throughout the training phase. All 14 pictures in each block were unique and used nowhere else in the experiment. The du-

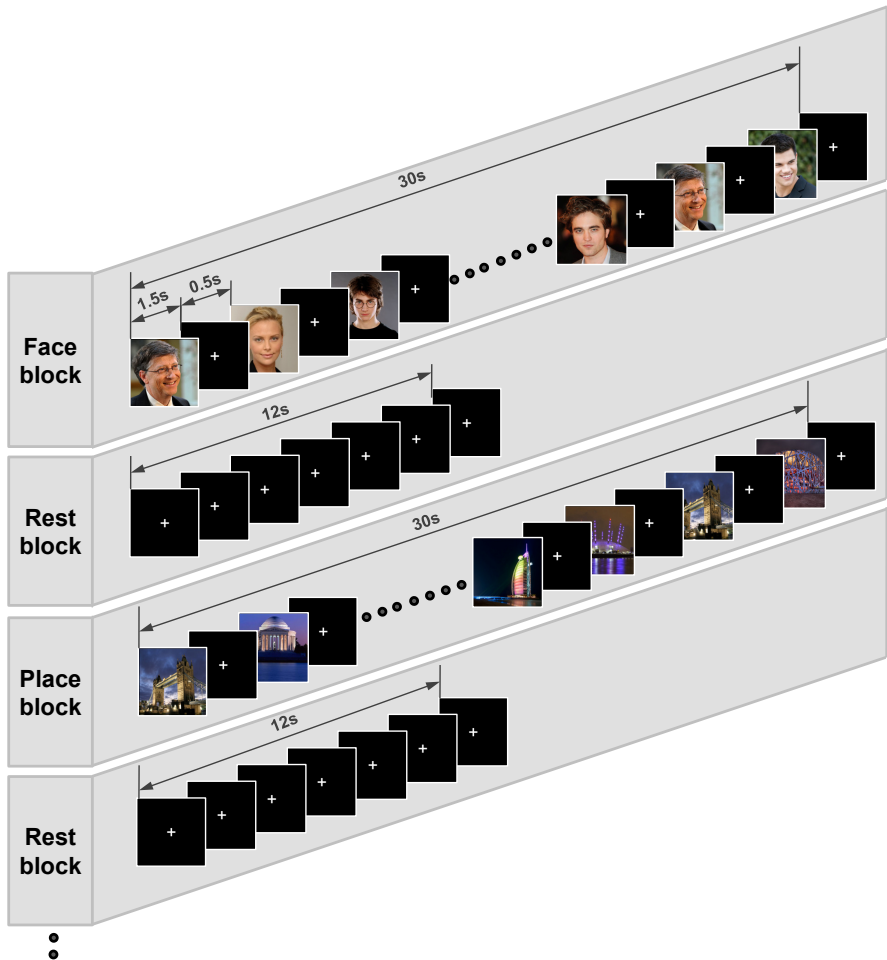


Figure 4.2 | Structure of face, place and rest blocks in the training phase. In each face or place block, 14 unique pictures were used and the first picture in each block was randomly repeated somewhere in that block and the subjects were instructed to press a button on the button box when they saw this repetition. Each picture was presented for 1.5 s followed by a fixation of 0.5 s. Each stimulation block took 30 s to complete followed by the rest block. The rest block was 12 s long to allow the hemodynamic activity to return to baseline.

ration of the entire training block was 22 minutes (1 minute instruction + 21 minute task).

4.2.2.2 Classifier Training Phase The scans collected in the training phase were shifted by 3 TRs (6 s) to account for the hemodynamic delay. After that, the 6 scans corresponding to rest periods between every consecutive face and place block were also dropped. Then all fifteen scans in each of the face and place blocks were used to train the classifier. The classifier training phase took only 30 seconds to complete during which time the subjects were shown the instructions upcoming test phase.

Classifier The classifier in this experiment was an Elastic Net Logistic Regression classifier as implemented in the Donders Machine Learning Toolbox (DMLT). The mixing parameter α parameter was fixed to 0.99. For the regularization parameter λ , the whole regularization path was calculated with maximum number of allowed iterations set to 100. Optimal setting of λ was then computed using nested cross-validation on 75% of the training data. For more details, please refer to Chapter 2, Section 2.3.

4.2.2.3 Testing Phase The purpose of this section is to quantify whether subjects can voluntarily control activation in spatially distinct cortical areas when presented with two overlapping stimuli that could invoke activity in these areas. Furthermore, this phase also investigates the effect of real-time fMRI neurofeedback. Therefore, the testing phase contains overlapping pictures of face and place in two different conditions.

1. Feedback Condition: In this condition the classifier prediction is fed back to subject on a TR by TR basis.
2. Non-Feedback Condition: In this condition the classifier prediction is not fed back to subject. The 50/50 always remains at the same contrast throughout the duration of the trial.

Both conditions have an equal number of trials with face picture as target and place picture as target and their order is random.

The basis set for the stimulus in the test phase contains 15 pairs, each containing a picture of a famous face and a place. The choice of the face and place pair in the test session is very crucial and therefore the face-place pairs for the test phase was carefully handpicked. Ideally, in the 50/50 hybrid of the face and place, both pictures should be equally salient, otherwise it will steer the user's attention towards the more prominent picture and hence bias the result towards one or the other class. To ensure that this does not happen, we applied the Graph Based Visual Saliency (GBVS) algorithm [41] on all the candidate 50/50 hybrid image pairs. Then we observed the saliency maps of each pair as shown in Figure 4.3.

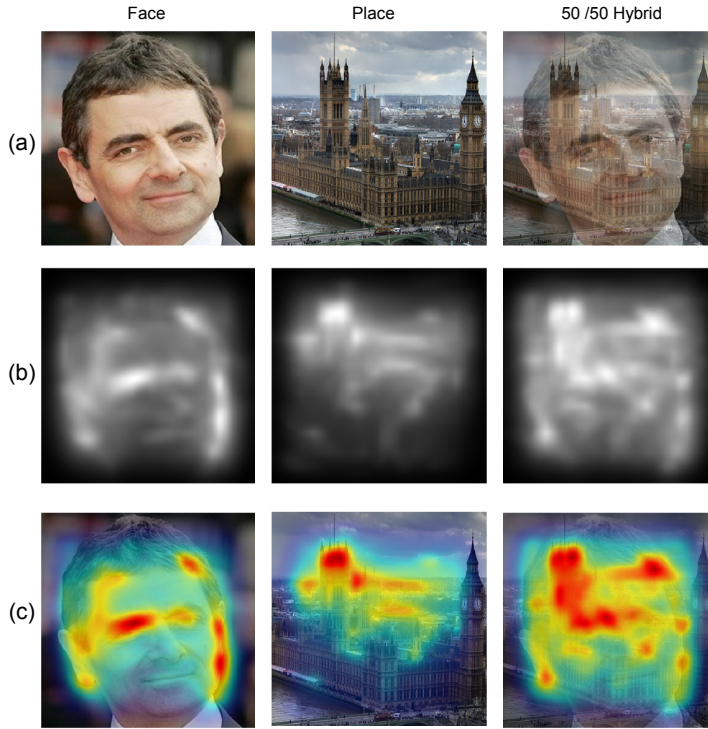


Figure 4.3 | Face-place pair selection. Graph based visual saliency (GBVS) was used to select the face-place pair such that in the 50/50 hybrid both the constituent pictures were equally salient. (a) Original face and place picture alongside their 50/50 hybrid (b) GBVS map of the face, place and hybrid pictures (3) GBVS map overlayed onto the original pictures. As can be in the saliency map of the 50/50 hybrid, none of two pictures is dominating the other. Hence, this pair is suitable for the experiment.

If a 50/50 hybrid had equal number of salient points in the face picture and an equal number of salient points in the place picture, then the face-place pair would be accepted otherwise, a new pair will be sought that fulfilled the above criteria. In this way, 15 pairs of face place pictures were made, as shown in Figure 4.4. From these fifteen pairs, 30 trials were constructed, 15 trials contained a face picture as a target and the place picture as a non-target while the remaining 15 trials contained a place picture as a target and face picture as non-target. These thirty trials were assigned to feedback blocks and also to non-feedback block. In that way the entire test phase had 60 trials in total (see Figure 4.6).

The test phase was conducted in 12 mini-blocks (feedback mini-block and non-feedback mini-block) each containing 5 trials as shown in Figure 4.6. In the feedback mini-blocks, the 50/50 hybrid was updated every TR (except the first two TR's due to pipeline delay) whereas in the non-feedback mini-blocks, it remained stationary at the 50/50 hybrid at all times. The feedback and non-feedback mini-blocks were interleaved and the ordering was counterbalanced across subjects



Figure 4.4 | Basis set of 15 picture pairs used in the test phase. These 15 picture pairs were used in the test phase of the experiment. The first picture in each pair is a famous face and the second picture is that of a famous landmark. The third pair is the 50/50 hybrid of the two pictures. Each pair was used exactly four times in the experiment in these configurations: (1) Target = Face, Non-Target = Place, Condition = Feedback (2) Target = Place, Non-Target = Face, Condition = Feedback (3) Target = Face, Non-Target = Place, Condition = Non-feedback (4) Target = Place, Non-Target = Face, Condition = Non-feedback. In this way, a total of 60 trials were obtained for the test phase. Pictures used in these 15 pairs were not used in the training set.

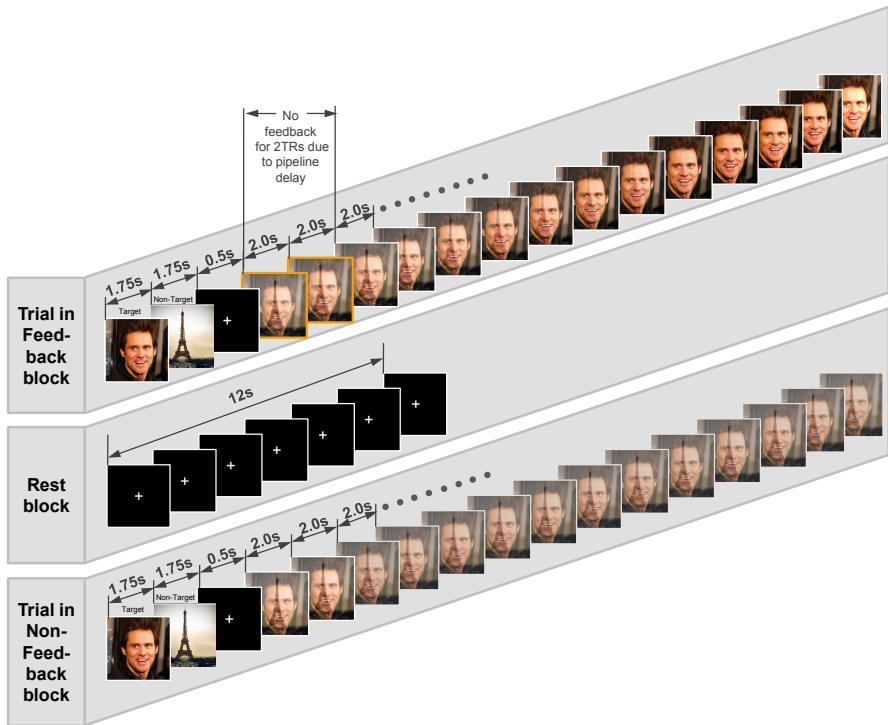


Figure 4.5 | Structure of feedback and non-feedback trial in the test phase. Each trial in the test phase began with a display of the cue pictures, one of a famous face and the other of a famous place, followed by a brief fixation period. Then a 50/50 hybrid of the two picture was shown and the subject was asked to attend only to the target picture while ignoring the non-target picture. In non-feedback trials, nothing would happen to the hybrid, whereas in feedback trials, the hybrid was updated every TR based on the prediction of the classifier. However, in the first two TRs in the feedback block, highlighted in orange, the hybrid remained at 50/50 contrast. This is because in real-time fMRI, when a stimuli is presented, the corresponding scan is generated one TR after it, and it takes an additional one TR to preprocess it. So there is a delay of 2 TRs between presentation of the stimulus and the prediction results being available. Due this lack of data in the first two TRs of each trial, highlighted in orange, the feedback remains frozen to 50/50 contrast.

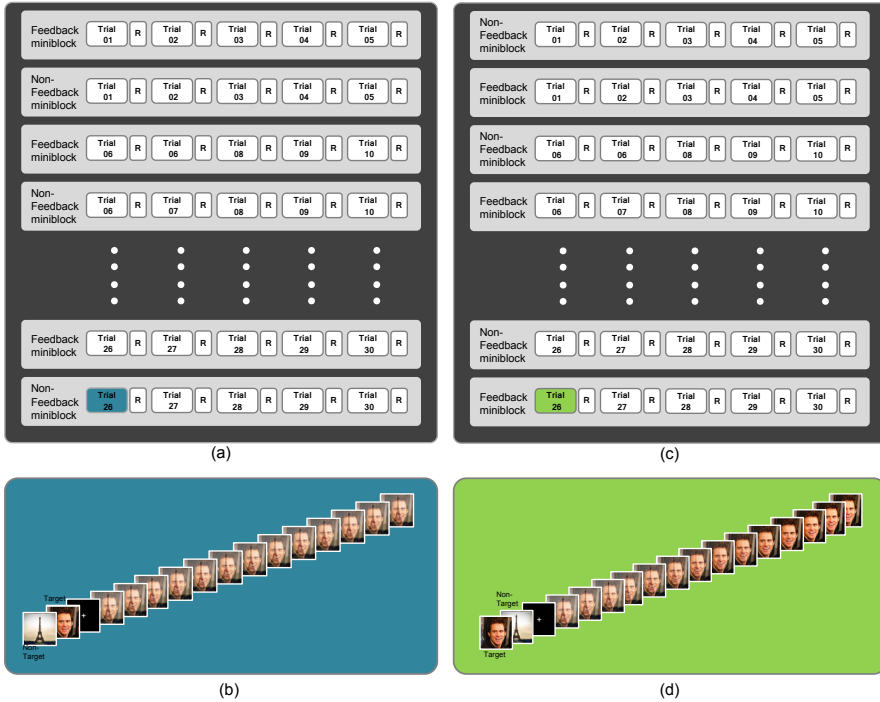


Figure 4.6 | Test phase. (a) The arrangement of feedback and non-feedback trials for even-numbered subjects. The test phase started with five feedback trials followed by five non-feedback trials and so on. In this way 60 trials were conducted, 30 in feedback and 30 in the non-feedback condition. Each condition had 15 trials in which a face was the target, and 15 trials in which a place was the target. The order of these face and place trials was random in each condition. (b) For even numbered subjects, each trial in the test phase began with a display of the non-target picture cue followed by the target picture cue. This figure shows an example of one trial in the non-feedback block highlighted in Figure a (c) For odd numbered subjects, the order of the feedback and non-feedback blocks is reversed. (d) For odd numbered subjects, the order of the cue pictures is reversed. This picture shows an example of a feedback trial highlighted in Figure c.

(see Figure 4.6 b & d). For even subjects, each trial began with presenting of the target cue for 1.75 s followed by presentation of the non-target cue for 1.75 s and a fixation period for 0.5 s. For odd subjects, the non-target cue was presented first. After presenting the cues, the 50/50 hybrid was shown. The hybrid was updated every TR based on the prediction P of the classifier. If the classifier prediction was above 0.5 then the target contrast was increased by 5%⁵ and the non-target decreased by 5%. If the classifier prediction was below 0.5 then the place contrast was increased by 5% and the face contrast decreased by 5%. This is represented mathematically in Equation 4.1.

$$\alpha_{TR} = \begin{cases} 0.5 & \text{if } TR = 1, 2 \\ \alpha_{TR-1} + 0.05 & \text{if } TR = 3, 4, \dots, 14 \text{ and } P(\text{face} \mid TR-2) > P(\text{place} \mid TR-2) \\ \alpha_{TR-1} - 0.05 & \text{if } TR = 3, 4, \dots, 14 \text{ and } P(\text{face} \mid TR-2) < P(\text{place} \mid TR-2) \end{cases} \quad (4.1)$$

$$\text{HybridPicture}_{TR} = \alpha_{TR} \times \text{Face Picture} + (1 - \alpha_{TR}) \times \text{Place Picture}$$

For non-feedback trials, the blend always remained at 50/50 for all TRs, as shown below:

$$\text{HybridPicture}_{TR} = 0.5 \times \text{Face Picture} + 0.5 \times \text{Place Picture}$$

Note that different equations cause different behavior which in the end may affect feedback vs non-feedback comparisons.

4.2.3 Experimental protocol

Before putting subjects in the scanner, they were thoroughly briefed about the experiment. This was done to avoid any communication during real-time fMRI run when the scanner noise is too high for two-way communication between the subject and the experimenter. During this pre-screen briefing (see Appendix F for more details), subjects were shown video recordings of all experimental conditions and the task was verbally explained by the experimenter with the help of these videos. Subjects were specifically instructed that the feedback would be delayed by about 4 seconds due to technical reasons and that no matter what the feedback was, they were to always think about the target picture without moving their gaze from hybrid picture. Furthermore, they were allowed to close their eyes during rest periods but were advised to open their eyes a few seconds before this rest period was over. Subjects were instructed to adjust the viewing mirror

⁵A study [51] has shown that intermittent feedback is better than a continuous feedback. That is why we decided to update the hybrid in a graded fashion every TR (2 seconds) by 5% rather than slowly and continuously updating the hybrid within 2 seconds which would have made it very to assess which direction the decoding was going.

in the scanner before start of the experiment such that they were comfortably viewing the center of the screen at all times. After subjects had adjusted the mirror, they were strictly advised not to change its position through out the rest of the duration of the experiment.

To keep participants motivated throughout the experiment, they were told that if their performance (i.e. decoding accuracy) turned out to be higher than 95%, they will receive 5 Euros for every percent above 95%. Once the experiment was over, subjects was taken out of the scanner and decoding accuracy for their experiment run was calculated. Based on the results, subjects were informed on the spot if they would be receiving any reward or not.

4.2.4 MRI Acquisition parameters

Experiments were performed at the Donders Institute MRI lab using a Siemens MAGNETOM Tim TRIO 3.0 T scanner with a 32-channel head coil. All functional images were acquired using a single shot gradient EPI sequence (TR/TE = 2000/30 ms; Flip angle = 75°; voxel size = 3x3x3.3 mm; distance factor = 10%). 28 axial slices were acquired, oriented typically at 35° to the AC-PC (Anterior-Posterior Commissure) line as shown in Figure 4.7. A high-resolution anatomical image was acquired using an MP-RAGE sequence (TE/TR = 3.03/2300 ms; 192 sagittal slices, isotropic voxel size of 1x1x1 mm).

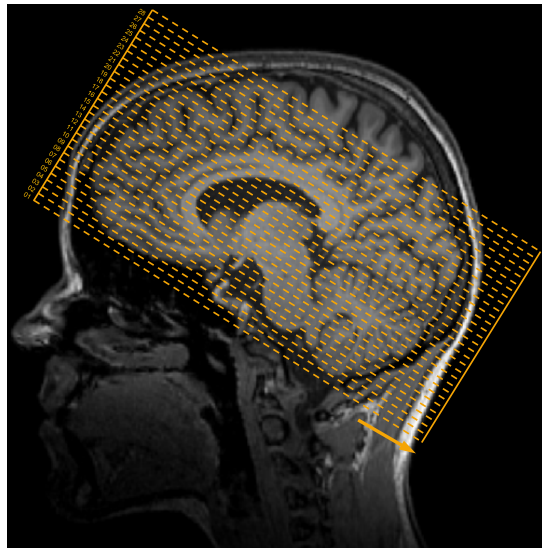


Figure 4.7 | Slice positioning. 28 axial slices were acquired orientated typically at 35° from the AC-PC line. As slice # 1 and 28 were to be masked out in the preprocessing later on, these two slices covered no regions that were of interest in the study.

4.2.5 Real-time fMRI processing

All functional scans were acquired using the Integrated real-time fMRI pipeline implementation. In this pipeline, the preprocessing, classification and synchronization were all performed on a single PC. For more details about this pipeline please refer to Chapter 5, Section 5.3. The functional scans acquired using this pipeline were preprocessed before being used for classification. The preprocessing stages used were:

Slice time correction Slice time correction with trilinear interpolation was used to correct for differences in the acquisition time of various slices in each scan.

Motion correction A three pass motion correction procedure was used. In the first and second pass, the head motion was corrected for by the Siemens scanner prospectively and retrospectively by PACE and MoCo, respectively. In the third pass, retrospective motion correction was applied by the real-time pipeline to remove any residual motion.

Boundary slice masking This average duration of this experiment is 70 minutes. With PACE enabled, only then a very small motion occurs and on average only half of the first and last slice gets damaged due to motion. Hence by masking the entire first and last slice, it was ensured that none of the damaged voxels gets used in the training and test session.

Nuisance regressors removal Five regressors were used to remove scanner drifts, offsets, and motion related activation.

Grey Matter masking The brain contains three distinct tissue types i.e. grey matter, white matter and cerebral spinal fluid (CSF). Only the voxels in grey matter respond to the experimental manipulation. The remaining voxels show only random activity patterns. Grey matter masking removes these white matter and CSF voxels. Because the brain contains more than 50% of white matter and CSF, the size of the training set after applying a grey matter mask is greatly reduced. This decreases the classifier training time dramatically. Furthermore, it improves the classifier performance because a much cleaner dataset is available after applying this procedure.

4.2.6 Data Analysis

The preprocessed data used by the classifier during the experiment along with the trained classifier and its predictions were all saved to disk and these were used in all post-hoc analyses mentioned below.

4.2.6.1 Decoding performance of each condition To calculate the decoding accuracy of each trial, it is first necessary to establish what a successful and unsuccessful trial is. Because each trial contains 12 TRs, each TR decoded individually as either as face or place and the result of the classification used to adjust the mixture of the two pictures in the hybrid, therefore a trial is regarded as successful if by the end of the these 12 scan, the hybrid has more than 50% of the target picture and less than 50% of the non-target picture. In other words, if by the end of a trial, the hybrid picture looks more like the target picture than its regarded as a success otherwise the trial is a failure. This can be mathematically written as:

$$\beta = \sum_{i=1}^{12} \log P(\text{Target} | \text{Scan}_i) - \sum_{i=1}^{12} \log P(\text{Non-Target} | \text{Scan}_i)$$

A trial was regarded as a success if β was greater than zero and a failure if β was less than zero. Using this method, the accuracy of the trails for all participants was calculated. A two-tailed t-test was then carried to find significant difference between the decoding performance of the two conditions.

4.2.6.2 Decoding performance of different trial types in each condition

Because each condition, feedback and non-feedback, contains two types of trials (one in which face picture is the target and the other in which place picture is the target) therefore, the decoding performance analysis of feedback and non-feedback conditions can be further split into the same analysis of the face and place trials within that condition to get a more in-depth view. A two-tailed t-test was then carried to find significant difference between the decoding performance for these four trial types.

4.2.6.3 Decoding performance for stable and transition periods of BOLD activity

In almost all previous real-time fMRI studies, scans corresponding to the transition period (i.e, the first 6 seconds on the HRF curve) were never decoded on grounds that the BOLD signal in this transition period is not fully mature (see [132] for a review of these studies). Our experiment specifically decoded these scans in the transition period to reduce the lag in the neurofeedback. To asses the decoding performance in the transition period versus the stable period that follow it, the decoding accuracy was calculated separately for first three TRs corresponding to the first 6s of BOLD activity and for the remaining nine TRs corresponding to 18s of stable BOLD activity. A two-tailed t-test was then carried to find significant difference between the decoding performance of the two conditions in transition and stable periods.

4.2.6.4 Decoding performance as a function of TR To find how decoding performance evolves on a TR-by-TR basis, the decoding accuracy for each

individual TR was calculated by finding the ratio of the correctly classified scans and the total number of scans. This was done for each condition and also for each trial type in these conditions.

4.2.6.5 Classification bias analysis Because the experiment contains an equal number of face and place trials therefore, one expects that if the decoding is unbiased then there will be equal number of scans (or TRs) classified as face and place. To assess this, we calculated for each subject the total number of TRs that were classified as face or place. A two-tailed t-test was then carried to find significant difference between the number of TRs classified as face and place.

4.2.6.6 Region of interest analysis For region of interest (ROI) analysis, Analyze4D (www.analyze4d.com) was used. ROIs for individual subjects were defined using the locations of the non-zero classifier weights. Then a subject-specific Anatomical Automatic Labeling (AAL) mask [127] was constructed by warping the standard AAL mask in MNI to the subject space [6] using the inverse of the spatial transformation matrix obtained from the SPM8 (Wellcome Department of Cognitive Neurology, Queens Square, London, UK) unified segmentation normalization [7]. The ROIs were then labeled by overlaying the AAL mask (in native space) over them. Then time courses for all the voxels in these ROIs were high-pass filtered (0.01 Hz) to remove very slow drifts and then detrended before averaging the time courses of all voxels in each ROI. Subsequently, percent signal change for each ROI was calculated using the mean of the entire time series as the baseline. Then the average percent signal change for each of the six different trials types¹ during the experiment was calculated. The same procedure was repeated across the group and then the results across all ROIs and conditions were averaged together across the group.

4.2.6.7 Classifier weights analysis The ROI analysis revealed the identity of anatomical regions activated during the experiment and the percent signal change analysis revealed if a particular brain region responded more strongly to faces or places. To double check if this labeling was done correctly, the classifier weights for these anatomical regions can be analyzed. Binary logistic regression will always assign positive weights to face sensitive areas and negative weights to place sensitive areas.

4.2.6.8 Voxel time course analysis To visually confirm if voxels were responding correctly to the particular experimental manipulation, their time courses were analyzed using Analyze4D. Data from the preprocessed data buffer was used

¹These trials type are: 1. Face trials/blocks in training 2. Place trials/blocks in training 3. Face trial in Feedback condition 4. Place trials in feedback condition 5. Face trials in non-feedback condition and 6. Place trials in non-feedback condition

for plotting the time courses. Voxel used for plotting the time courses was located by overlaying the classifier weights on top of the functional image and then manually picking up a particular voxel. Time courses were detrended by a high-pass filter (0.01 Hz) before plotting them. The design matrix was then overlayed to correlate the time course with experimental condition. The design matrix was shifted by 6s to account for the hemodynamic delay.

4.2.6.9 Classifier weight distribution plots Classifier weight distribution plots were made to visualize which brain regions were used by the classifier to train itself. First, a mask of the brain regions shown to be activated in the ROI analysis, was extracted from the AAL template in MNI space. This mask was then overlayed on the averaged anatomical image of the seven subjects using Analyze4D. This procedure yielded a 2D mosaic plot of the activated brain regions overlayed on the anatomical image. To visualize the activated brain regions in 3D, BrainSuite [111, 112] was used.

4.3 RESULTS

The aim of this experiment was to see if the attended category could be decoded in real-time when the subject is presented a hybrid of the target and non-target picture. Furthermore, we also wanted to investigate the effect of real-time fMRI neurofeedback on the decoding performance. The results of the decoding performance for each condition (shown in Figure 4.8) reveals that the average decoding accuracy for feedback condition and non-feedback condition is 79% and 78%, respectively. A paired samples t test failed to reveal a statistically reliable difference between the feedback ($M = 0.790$, $SD = 0.110$) and non-feedback ($M = 0.776$, $SD = 0.116$) conditions; $t_{(6)} = 0.420$, $p = .689$, $\alpha = .05$.

We hypothesized that the decoding performance for trials with face picture as target will be the same as that of trials with place picture as target. By analyzing the decoding performance for these two trial types (as shown in Figure 4.9), we observe that the face trials and place trials in feedback condition were decoded with 87% and 70%, respectively. A paired samples t test reveals no statistically significant difference between the face trials ($M = 0.876$, $SD = 0.156$) and place trials ($M = 0.705$, $SD = 0.167$) in the feedback condition; $t_{(6)} = 1.915$, $p = .104$, $\alpha = .05$. Similarly, the face trials and place trials in non-feedback condition were decoded with 84% and 71%, respectively. No statistically reliable difference was found between the face trials ($M = 0.838$, $SD = 0.143$) and place trials ($M = 0.714$, $SD = 0.153$) in the non-feedback condition; $t_{(6)} = 1.797$, $p = .122$, $\alpha = .05$.

It was also predicted that above chance level decoding accuracy will be obtained for scans in the transition period. Analysis of decoding performance for transi-

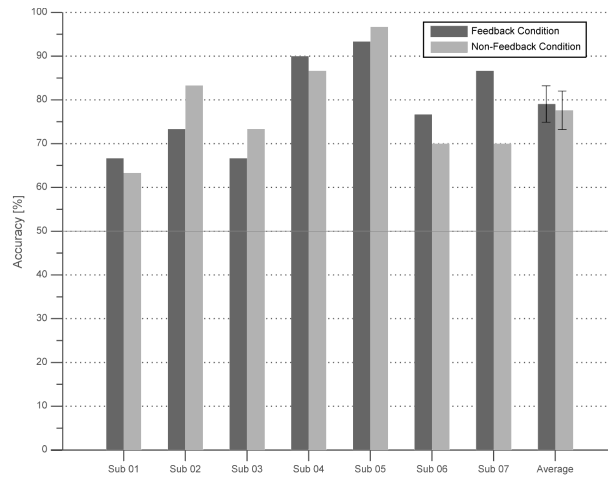


Figure 4.8 | Accuracy of feedback and non-feedback trials for all subjects. The accuracy of the feedback condition is higher than the non-feedback condition in the group average however, it is not statistically significant. Note: The chance level accuracy is 50% and the error bars represent the standard error of the mean (SEM).

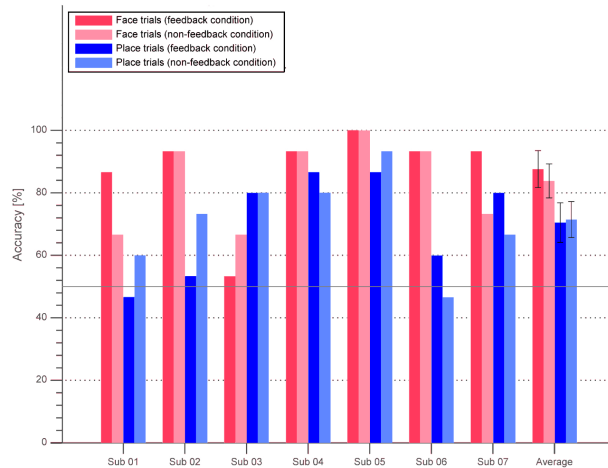


Figure 4.9 | Accuracy of face and place trials in feedback and non-feedback condition. The accuracy of the face trials is higher than place trials in the group average however, its not statistically significant. Note: The chance level accuracy is 50% and the error bars represent the standard error of the mean (SEM).

tion (Figure 4.10) and stable periods (Figure 4.11) of BOLD activity reveal that scans in transition period were decoded with above chance level (67% for feedback condition and 56% for non-feedback condition). A paired samples t test revealed a statistically significant difference between the feedback ($M = 0.671$, $SD = 0.137$) and non-feedback condition ($M = 0.561$, $SD = 0.142$) in the transition period. The scans in stable period were decoded at higher accuracy (81% for feedback condition and 80% for non-feedback condition) than scans in transition period (compare Figures 4.11 and 4.10). No significant difference was found between the feedback ($M = 0.814$, $SD = 0.096$) and non-feedback condition ($M = 0.800$, $SD = 0.109$) in the stable period; $t_{(6)} = 0.420$, $p = .689$, $\alpha = .05$.

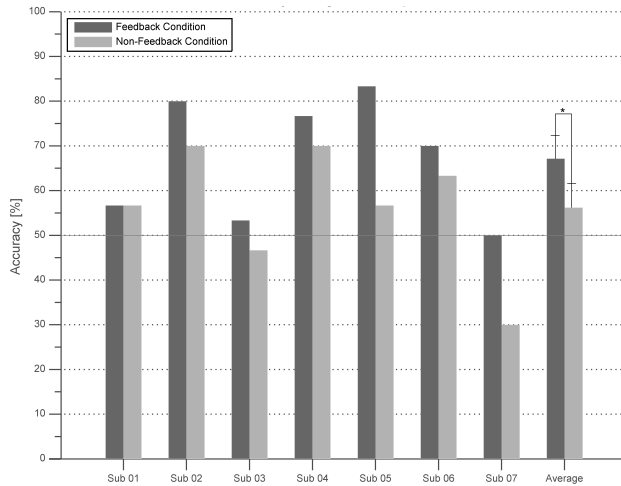


Figure 4.10 | Accuracy of feedback and non-feedback trials in transition period. The accuracy of the trials in the non-feedback condition is higher than in the feedback condition and is statistically significant. Note: The chance level accuracy is 50% and the error bars represent the standard error of the mean (SEM).

Furthermore, it was also hypothesized that the decoding performance will increase with each scan in the transition but this performance increase will eventually level off in scans in stable period of BOLD response. By analyzing the decoding performance as a function of TR (shown in Figure 4.12 and 4.13), we can see that the decoding accuracy increases in the first six seconds of BOLD activity in TR 1,2,3, and then levels off in the following eighteen seconds of BOLD activity in the stable period in TR 4 to 12.

Moreover, it was hypothesized that the classification will be unbiased, i.e., the number of scans classified as face or place during the experiment will be equal. The classification bias analysis (see Figure 4.14) indicates that this is not the case. There is bias towards the face category, in other words more scans are classified as face than place. A paired samples t test shows a statistically significant

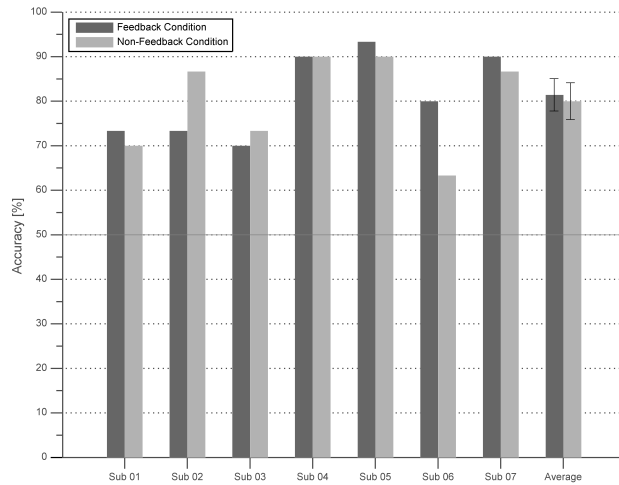


Figure 4.11 | Accuracy of feedback and non-feedback trials in stable period. The accuracy of the trials in feedback condition is higher than in non-feedback condition but is not statistically significant. Note: The chance level accuracy is 50% and the error bars represent the standard error of the mean (SEM).

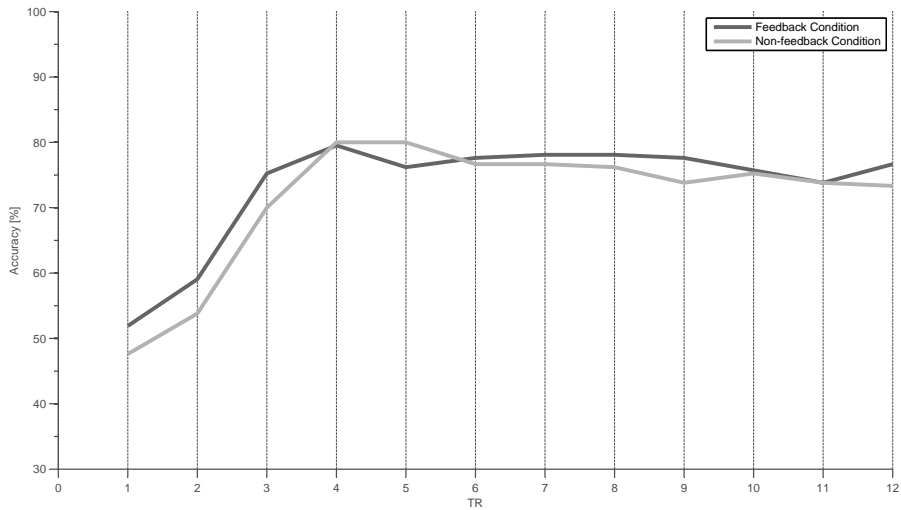


Figure 4.12 | Accuracy as a function of TR for feedback and non-feedback conditions. (Note: The chance level performance is 50%)

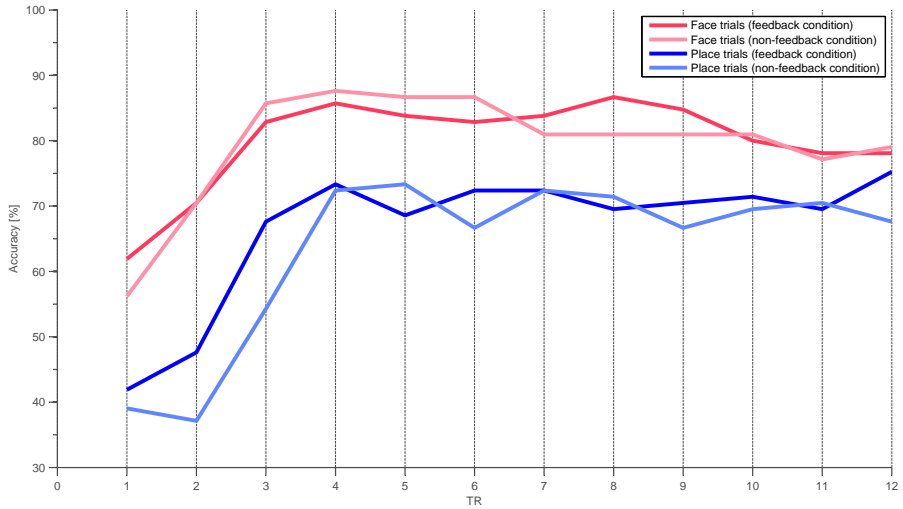


Figure 4.13 | Accuracy as a function of TR for place and face trials in feedback and non-feedback conditions. (Note: The chance level performance is 50%)

difference between scans classified as face ($M = 412.71$, $SD = 48.124$) and place ($M = 307.29$, $SD = 48.124$); $t_{(6)} = 2.898$, $p = .027$, $\alpha = .027$.

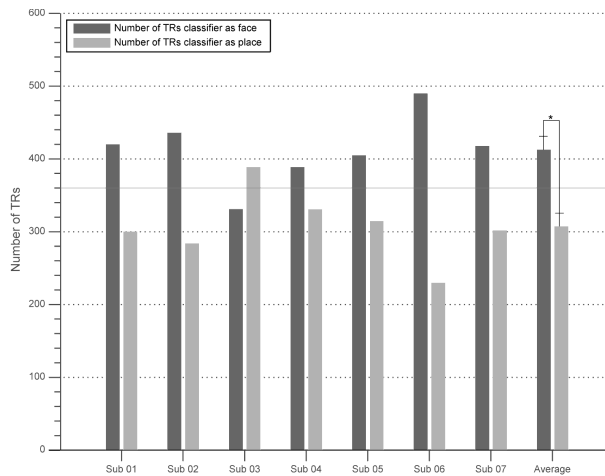


Figure 4.14 | Classifier bias. There is significant difference between the number of the scans classified as face and place. Note: The ground truth number of face and place scans is 360 each. The error bars represent the standard error of the mean (SEM).

The region of interest analysis indicates that 31 distinct brain regions were activated across all the subjects as shown in Figure 4.15. Any region that wasn't activated in more than two subjects was dropped from the further analysis leav-

ing only nine brain regions as shown in Figure 4.16 and 4.17. The areas include bilateral fusiform and lingual gyrus, right parahippocampal gyrus, left and right inferior occipital lobes, and right middle and supplementary temporal lobes. Percent signal change in these areas were calculated and a region was labeled as either face selective or place selective depending on how strongly it responded to the face and place blocks in the training session. If the percent signal change was greater in the face block of the training session than the place blocks, then the region was categorized as a face selective region else as a place selective region. Right fusiform gyrus, inferior occipital lobes(left and right), and right middle and supplementary temporal lobes responded strongly to faces and hence labeled as face sensitive regions. Left fusiform gyrus, lingual gyrus (left and right) and right parahippocampal gyrus were more responsive to the place stimuli and hence labeled as place selective regions. The results of the percent change analysis are shown in Figures 4.18 and 4.19.

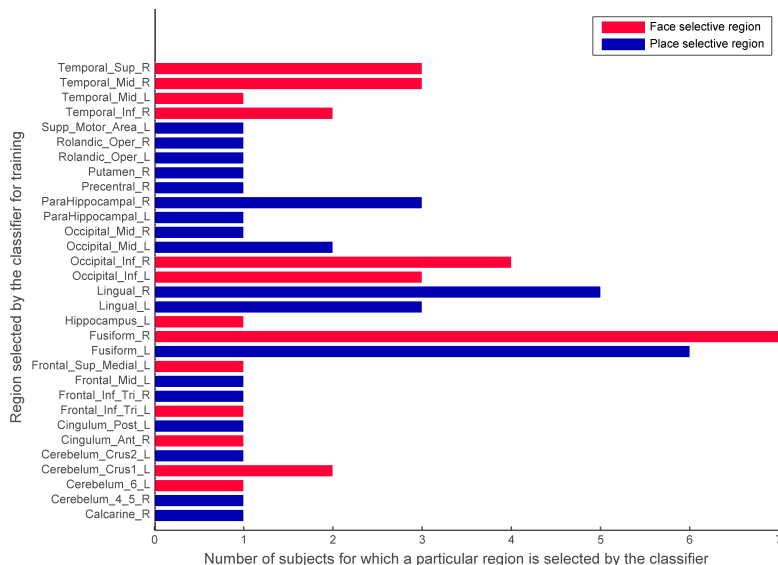


Figure 4.15 | All brain regions activated across subjects. Thirty-one distinct brain regions were activated across subjects. The regions in red showed more percent signal change in the training session compared to place blocks. The brain regions in blue showed more percent signal change in the training session compared to face blocks.

It was expected that classifier weights will be positive for face selective areas and negative for place selective areas. The classifier weights analysis confirms that this was actually the case. Face selective areas such as right fusiform gyrus, inferior occipital lobes(left and right), and right middle and supplementary temporal lobes were assigned positive weights. Place selective areas such as left fusiform gyrus, lingual gyrus (left and right) and right parahippocampal gyrus were all

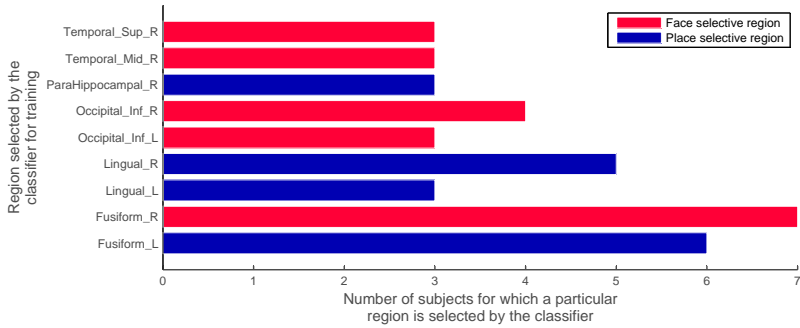


Figure 4.16 | All brain regions activated for more than two subjects. Brain regions that were activated across three or more subjects.

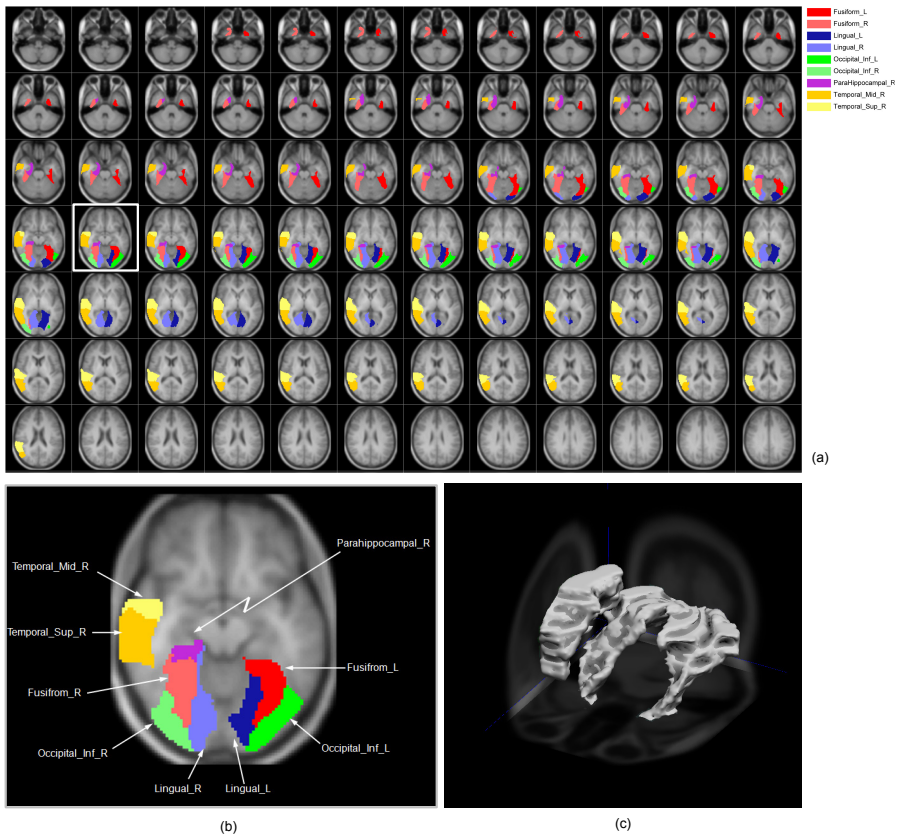


Figure 4.17 | Brain region activated during the experiment. (a) Brain regions that were activated during the experiment overlaid onto the averaged brain of all seven subjects in MNI space. (b) Zoomed version of the slice highlighted in (a) (c) 3D view of the brain regions activated during the experiment

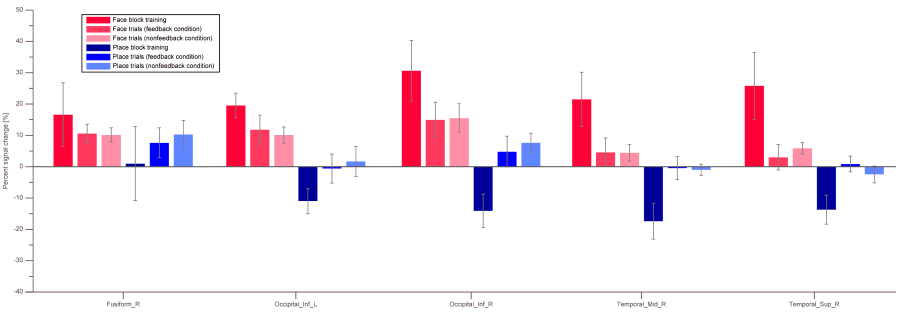


Figure 4.18 | Region of interest (ROI) analysis. Percent signal change across five different brain region averaged across the group for six distinct conditions in the experiment. These regions respond more strongly to the face pictures than place pictures. The error bars represent the standard error of the mean (SEM).

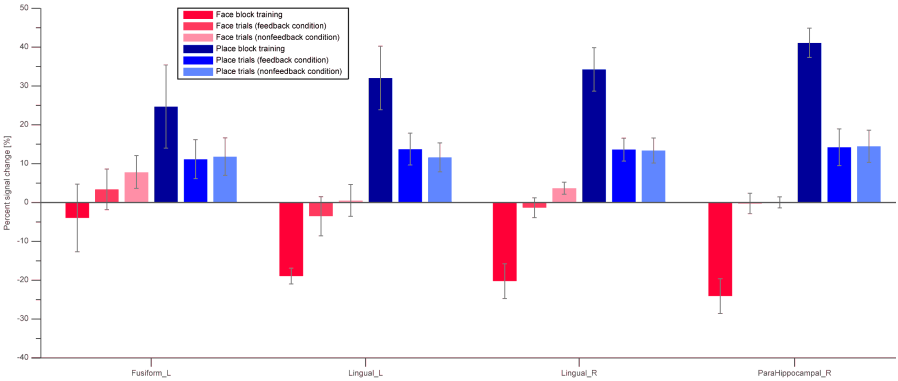


Figure 4.19 | Region of interest (ROI) analysis. Percent signal change across four different brain region averaged for the group for six distinct conditions in the experiment. These regions respond more strongly to the place pictures than face pictures. The error bars represent the standard error of the mean (SEM).

assigned negative weights. The classifier weights averaged across all subjects for all the brain regions is shown in Figure 4.20.

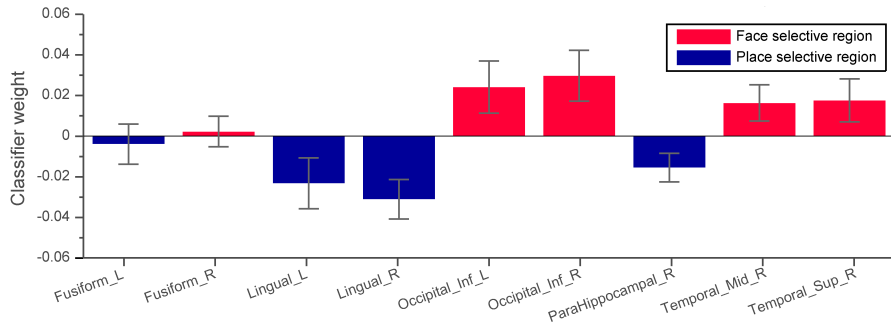


Figure 4.20 | Classifier weights. Average classifier weights in all activated brain regions across all subjects. Face selective areas have positive weights and the place selective areas have a negative weight assigned to them. The error bars represent the standard error of the mean (SEM).

To visually confirm that the experimental manipulation was having the desired effect on voxels, a time course analysis was done on voxels selected by the classifier for training. Figure 4.21 shows the time courses for two voxels, one in the face selective region and the other in the place selective region. The figure confirms that voxel in face selective regions is responding more strongly to face conditions and the voxel in the place selective region is responding more strongly to the place conditions.

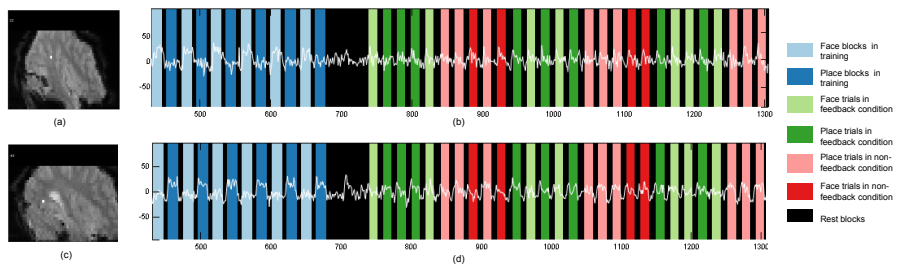


Figure 4.21 | Voxel time course. (a) A voxel (highlighted in white) in the face selective region used by the classifier for training (b) Time course of voxel in (a) (c) A voxel (highlighted in white) in the place selective region used by the classifier for training (d) Time course of voxel in (c).

4.4 DISCUSSION

The experiment was conducted to find the attended stimulus category can be decoded in real-time when two competing stimuli are presented. Furthermore, it was investigated if real-time fMRI neurofeedback of scan-by-scan classification results had any impact on the task performance. The results indicate the attended stimulus can be decoded in real-time with an average accuracy of 78.5%. The results also show the real-time neurofeedback has no influence on the decoding accuracy. The decoding accuracy for trials with and without feedback was 79% and 78%, respectively and this difference was found to be statistically insignificant. This is in contrast to our hypothesis that feedback will help drive the attention towards the target category, thereby resulting in higher decoding accuracies for trials with feedback compared to trial without feedback. By looking at the performance in feedback and non-feedback trials on an individual level (see Figure 4.8), it can be seen that four participants performed actually better on non-feedback trials than on feedback trials. One possible reason for this might be that once classifier prediction in feedback trials starts to go wrong (i.e. in the opposite direction to what the subjects are thinking about), then this wrong prediction captures their attention and these subjects just could not focus on paying attention to the target concept which, in turn, worsens the prediction in the upcoming scans. Hence an avalanche effect is seen for these subjects in feedback trials where an initial misclassification snowballs to all the rest of the scans of the trial being misclassified as well. To find if there really is such an effect, an additional analysis was performed by finding the largest continuous streak of consecutive similar classification in each trial for each condition. The results obtained are shown in Figure 4.22. The results indicate that there are longer streaks of consecutive similar classifications in feedback condition compared to non-feedback condition indicating that there is a snowball effect, where one classification triggers a stream of similar classifications in a trial (see the snowball effect in videos of feedback and non-feedback condition in Appendix H). This also gives credence to our hypothesis that attention will shift between target and non-target picture in trials with no feedback whereas, in trials with feedback, the attention will remain glued to the target picture for longer durations of time.

The snow ball effect could have been reduced with a thermometer bar type feedback alongside a static display of the 50/50 hybrid picture. But this thermometer type of feedback is riddled with some unique problems of its own. For example, it would have put huge cognitive load on subjects because they would not only need to attend to the target picture in the hybrid but would also need to covertly monitor the feedback to assess how good or otherwise they are doing in a trial. Furthermore, because the prediction could go in either direction, towards the face or place which would have needed to be color coded in the thermometer bar. For instance, red color for when prediction is going in the non-target category direction and green color for when the prediction is going in the target

category direction. Thus the subjects would have to remember what these two colors stood for, making an already difficult task, even more difficult. Therefore, the type of feedback used in the experiment was the most optimal one with least amount of cognitive load making it suitable for reinforcement learning. The duration of feedback was chosen to be 12 TR or 24 seconds which might have been too short for any significant reinforcement learning. Previous real-time studies have used trial durations ranging from 15s to 60s (see [132] for a review). Our particular choice of 24 s of neurofeedback was a compromise between number of trials and experiment duration. This is because we observed in our previous experiment (as described in Chapter 3) that subjects got exhausted as the scanning session was just too long and tiring. Therefore, in this experiment 24 s was chosen because any longer neurofeedback would have resulted in either longer experiment duration or less number of trials, none of which is what we desired.

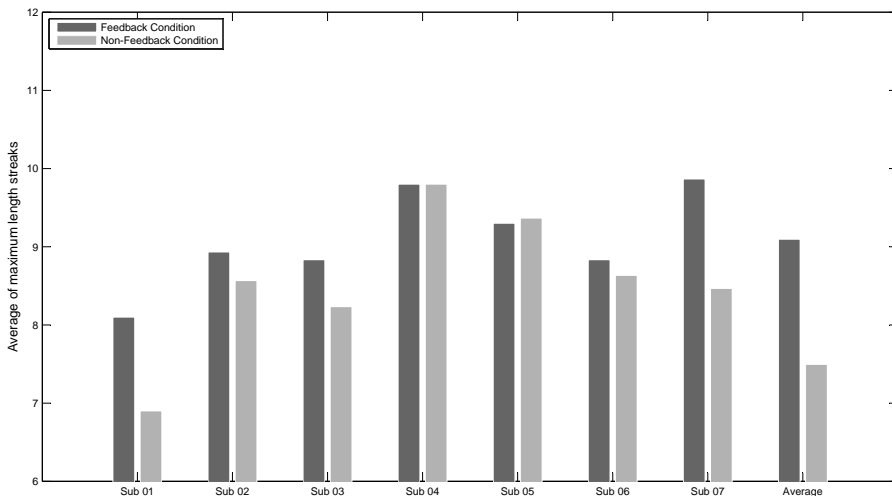


Figure 4.22 | Snow ball effect of feedback. The graph was obtained by finding the largest continuous streaks of similar classification in each trials and then averaging those for all trials in feedback and non-feedback condition.

The accuracy of the face and place trials in the feedback and non-feedback conditions (see Figure 4.9) shows that that face trials are classified with higher accuracy than place trials. This is contrast to our hypothesis that the decoding accuracy will be independent of the target category. Although, we observed saliency maps of the 50/50 hybrid to ensure that none of the two pictures, the face or the place, in a selected pair is more salient than other, the possibility that one picture was more salient than the other can not be completely ruled out and hence the observed bias towards one category. Another possible reason could be that faces are more easier to imagine and focus on as compared to pictures of places and hence a preference towards the face category. The same trend is found in the

total number of scans that were classified as face and place. Significantly more scans were classified as face than as place.

We had hypothesized that above chance level decoding accuracies would be obtained for scans in the transition period. The results seem to confirm that hypothesis. Thus our results confirm the finding of the LaConte et al. that the transition periods of the BOLD activity contains a reliable structure that can be decoded with above chance level accuracy [67]. We have therefore shown for the first time that prediction from the scans in the transition period can be used in real-time fMRI to reduce the fMRI neurofeedback delay by as much as 6s. Apart from that, it was also found that the decoding accuracy for feedback condition was significantly higher than the non-feedback condition in this transition period. This difference seem to be pronounced in the third TR of the place trials (see Figure 4.13). However, the exact cause of this observation is still unknown.

The ROI analysis revealed nine regions that responded strongly to the experimental manipulation. Among these region is the left fusiform gyrus. The left fusiform is usually associated with reading and word processing [23, 46, 76, 102]. More recently however, this area has also been suggested to be sensitive to the conjunction of object and background scene information [35]. This view has also been strengthened by invasive studies in primates that also pointed to the presence of neurons which are responsive to conjunction of object features [10, 15]. Because the pictures of famous places used in our stimulus set contained not only objects but also a wide variety of backgrounds (see Figure 4.23 (a)), that is why left fusiform is showing more activity for the place blocks then for face blocks. The pictures used in face blocks rarely had objects in them. Only a few face pictures had necklaces, earrings, glasses etc. (see Figure 4.23 (b)). The right fusiform



Figure 4.23 | Some examples of pictures of famous places and faces. a. The picture of place contains objects (man made structures) and background scenes and surroundings **b.** The pictures of faces rarely contained any objects in them except for a few items such as earrings glasses etc.

and the left parahippocampal area were also selected by the classifier during the experiment. The right fusiform showed preference for the face blocks and the left parahippocampal gyrus showed a preference for place blocks. These two regions have been implicated in many studies to be responsible for the processing of faces and place, respectively [3, 4, 26, 53, 77]. So the involvement of these two regions comes as no surprise. Two other regions that were also selected by the classifier in the study are right medial temporal lobe and right supplementary temporal lobe. A study by Tempini et al. [37] investigated the effect of fame

(famous relative to non-famous) on the activations elicited by pictures of faces and buildings. Their findings show that the category-specific activations in the fusiform and parahippocampal/lingual areas were not modulated by fame but in the left anterior middle temporal gyrus there is an effect of fame that is common to faces and buildings. Their findings also show that this effect is stronger in the left anterior middle temporal gyrus compared to the right anterior middle temporal gyrus. Our findings are contrary to this study because we find that right temporal gyrus is activated more compared to the left temporal gyrus. However this can be explained by the fact that semantic information can be retrieved by activation of either the left or the right anterior temporal cortex [37]. Furthermore, in our study the right temporal gyrus shows a preference for famous faces but not for famous places. This could be because many of the supposedly famous landmarks used in the stimulus set were not as familiar to the subjects as expected. Most participants reported that although they could recognize many of the famous faces but they could not identify many of the pictures of the famous buildings. Some of them are shown in Figure 4.24.

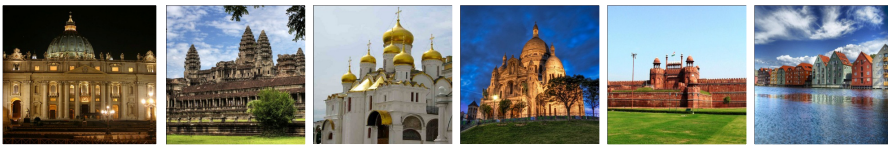


Figure 4.24 | Example pictures of supposedly famous places unfamiliar to most of the subjects. The figure shows pictures famous place that most subjects reported they were unfamiliar with.

Both left and right inferior occipital gyri were also activated in the experiment and both showed more activations for the face blocks. This region contains the occipital face area (OFA). The OFA is spatially adjacent to the FFA and preferentially represents the parts of face, such as eyes, nose, and mouth [72, 96, 97]. OFA is an essential component of the cortical face perception network and it represents face parts prior to subsequent processing of more complex facial aspects in higher face-selective cortical regions.

4.5 CONCLUSION

Our results show that it is possible for subjects to voluntarily attend to one of two simultaneously presented stimuli. This was examined by prediction of the attended stimulus category in a real-time fMRI setting. One of the most interesting findings is that above chance level decoding accuracies were obtained for TRs in the transition period of the hemodynamic response which until now had been ignored in almost all real-time fMRI studies. Our results show that we can make the real-time neurofeedback more realistic by classifying the BOLD signal in the transition periods. However, our experiment still had a delay of 4 seconds

between presenting the stimulus and its corresponding neurofeedback being presented to the subject. However, this pipeline delay can be reduced by about 50% in any future experiments. This is due to the fact that the regions of interest discovered in this study are close enough that they can all be covered with 14 slices (Voxel Size = $3 \times 3 \times 3.3$ mm) with a TR of 1 second. With new rapid parallel imaging protocols, this delay can be reduced even further. The preprocessing delay can be reduced to approximately 0.3s by sampling for scans at non-TR intervals and designing the stimulus presentation accordingly.

The study did not find any difference in the decoding accuracies obtained for conditions with and without feedback. This could be because the trials were too short and too few. Future studies should not use both conditions on same subjects. Instead one condition should be applied on one group of subjects and the other on another group. This way more trials or longer length trials could be accommodated in the same experiment duration. Furthermore, training and testing could be conducted on separate days thereby, giving an opportunity to conduct even more trials. However, in that case care would need to be taken to ensure that images functional images in both sessions align perfectly. For that purpose an AAScout sequence should be used before the real-time fMRI run of the first session to make sure that the exact same slice prescription is used for the preceding sessions as well.

Although, the current experiment shows that it is possible to decode between category information, it would be interesting to see if the same can be done for within category information. For example, presenting hybrid of two face pictures and decoding the attended face. A high resolution fMRI study [66] on 3T scanner revealed that response patterns elicited by individual face images were distinct in the anterior area but not in FFA. This study suggests that the FFA merely detects faces but anterior area is more engaged in face identification. Using the same experimental setup which we described in this chapter but with high resolution imaging on a higher strength scanner (7T or 9T), it might be possible to decode the within category information in real-time.

CHAPTER 5

HARDWARE/SOFTWARE DEVELOPMENT

DURING the entire course of this study, the architecture required to successfully execute a real-time experiment, was continually being developed and refined. In this chapter, we will first describe the *Distributed real-time fMRI pipeline* which was used to execute the first experiment. We will identify the flaws in its design and describe its successor, the *Integrated real-time fMRI pipeline*, which was used to execute the second experiment. Lastly, we will describe *Analyze4D*, a software tool developed specifically for efficient offline analysis of real-time fMRI data.

5.1 DISTRIBUTED REAL-TIME FMRI PIPELINE

This pipeline is composed of four components, each having a distinct function:

1. **Scanner Module** Scanner module directly controls the MRI scanner. Any fMRI data acquired during the experiment first becomes available on this computer. Because scanner module is a very specialized computer, dedi-

cated solely for controlling the scanner, therefore if fMRI data is to be used during the experiment, it must be transferred to another PC before it can be used.

On SIEMENS scanners, as soon as the last slice of a volume gets acquired, the raw pixel data of acquired volume gets written to a folder in the drive of the scanner console. A custom designed software, *GUI_Streamer*, constantly polls this folder for any new files and as soon as a new file is detected, its contents are read and streamed over the ethernet along with the information about the fMRI protocol which was used to acquire the scan. The protocol information helps the remote computer which receives the streaming data to reconstruct the volume.

2. **Preprocessing Module** The preprocessing module is a computer on the network that receives the raw scans and stores them in a raw data buffer (FieldTrip buffer). The scans in this buffer are then read one by one by the preprocessing pipeline which applies dummy scan rejection, motion correction, slice time correction, brain extraction, spatial smoothing, and online GLM for nuisance signal removal. The preprocessed scans are then stored in the preprocessed data buffer along with the scan numbers sent by the synchronization module. The data from preprocessed data buffer is then passed to BCI module.
3. **BCI Module** The BCI module has the responsibility to receive the preprocessed streaming data from the preprocessing module and use it in a real time BCI loop. In our setup, we used BrainStream toolbox to control the BCI loop. This module has various responsibilities as mentioned below:
 - read streaming data from the preprocessing module
 - extract features
 - classify features
 - generate stimulus based on the result of the classification (dynamic adaptive stimulus generation)

The stimulus generated in this module is sent to the Synchronization module. This is because in our setup, this computer is connected to the scanner projector.

4. **Synchronization Module** Whenever a new functional scan is acquired, the scanner generates a TTL pulse. These TTL pulse are received by BITS⁶, converted to a serial format and sent to the COM7 port of the synchronization module. The serial event corresponding to each TTL pulse is then used to increment a counter in a C application. The counter, therefore,

⁶A custom designed hardware which, among many other things, converts TTL pulses to serial format.

represents the current scan number in the functional run. These scan numbers are then sent to the preprocessing buffer in the preprocessing module where they are saved along with the corresponding preprocessed scan.

The module also receives a 'RESET' message on its UDP port # 1990 from the GUI_Streamer tool at the start of each functional run. This resets the counter. It is imperative that the counter is reset at the start of each new functional run, otherwise the FieldTrip events in the preprocessed data will not refer to the correct data.

The synchronization module also serves another purpose. Its monitor is used to display the stimulus to the experimenter.

5.2 SHORTCOMINGS OF DISTRIBUTED REAL-TIME FMRI PIPELINE

Because this pipeline contains four different PCs, each of which needs to be started in a specific order, therefore, this pipeline was prone to human error on part of the experimenter. If the experimenter made any mistake in the startup sequence, then everything needed to be manually stopped and the whole startup procedure had to be repeated all over again. Considering, that each startup attempt took approximately ten minutes to complete, any restart of the pipeline would translate into not only a loss of scanner time, but also result in subject fatigue and frustration as the subject is in the scanner during all that time.

Furthermore, in this pipeline Brain Extraction is used to remove the irrelevant skull voxel. But there still remain the white matter and cerebral spinal fluid (CSF) voxels that Brain Extraction does not remove. If these voxels are removed, then the training set and the training time can be dramatically reduced.

One major flaw of this pipeline is that it is not very portable. Apart from using four different PC, it also uses some hardware that is very specific to Donders Institute. For example, the BITS I which converts TTL pulses from scanner to serial is something very specific to Donders Institute and might not be available at other research labs. If other institutes want to use this pipeline, they will need to buy this large piece of hardware, which is not ideal, considering that it performs a trivial task of converting TTL pulses to serial format. Furthermore, modern desktop PCs and laptops do not have a legacy serial port anymore.

5.3 INTEGRATED REAL-TIME FMRI PIPELINE

To rectify the shortcomings in the distributed real-time pipeline, the *integrated real-time fMRI pipeline* was developed. It provides the following improvements:

1. **Automated operation of the real-time pipeline** In this integrated real-time pipeline, the preprocessing module and the synchronization module

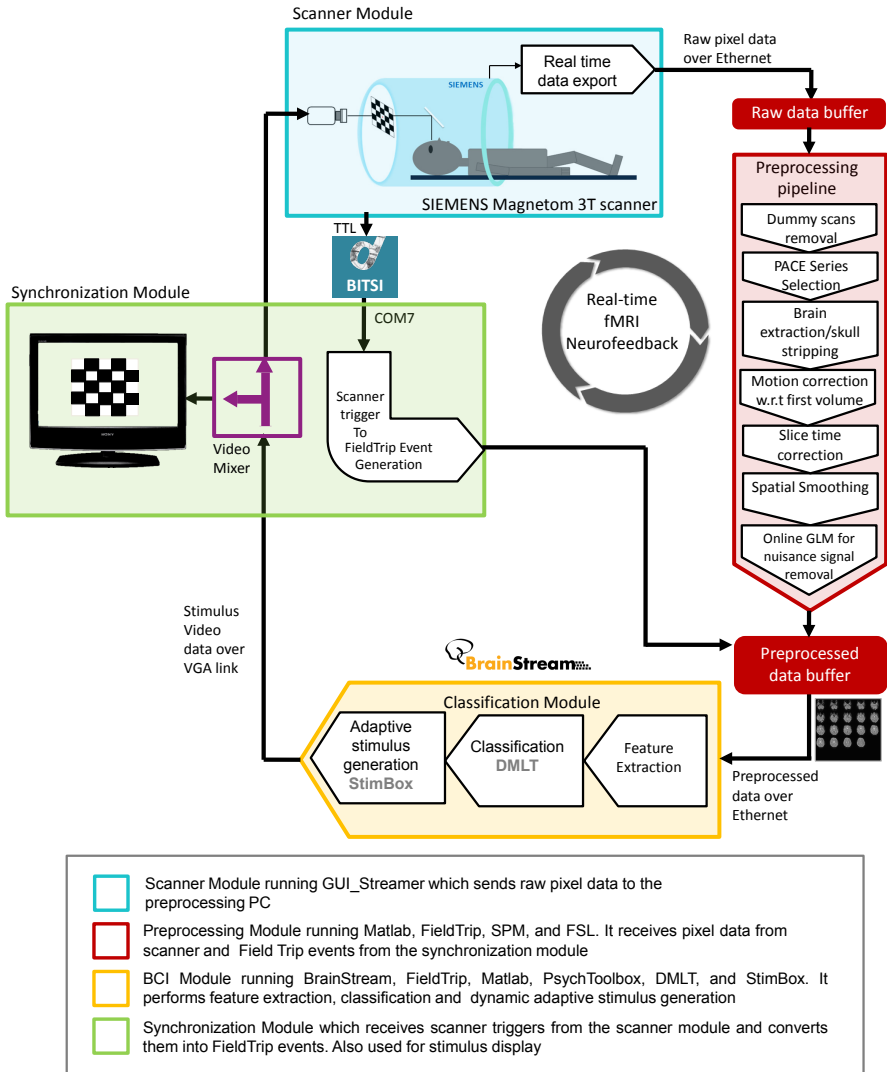


Figure 5.1 | Distributed real-time fMRI pipeline. Contains four different modules each performing a specific task in the pipeline. The scanner module acquires the functional data and forwards it in real time to the preprocessing module, where the fMRI data is preprocessed one scan at a time. The preprocessed scan is then received by the BCI module where feature extraction and classification is done. Based on the result of the classification, the stimulus (and neurofeedback) is generated, which is sent to the scanner projector and also to the monitor of the synchronization module so that the experimenter can view it. The synchronization module receives scanner triggers through BITS, converts them into FieldTrip events and passes them on to the preprocessing module.

are integrated into the BCI module, and hence the name. The whole process of starting the real-time pipeline has been automated in the BCI module. With just a click of a button, the real-time experiment can be started or stopped, giving beginners and novice users the ability to run their real-time experiment without in-depth knowledge of how it all works.

2. **Grey Matter Masking** As an improvement over Brain Extraction, *Grey Matter Masking* is introduced in this pipeline⁷. Grey matter masking uses anatomical scans to extract a grey matter mask. This mask is then applied to all functional scans to remove the white matter and CSF voxels. This reduces the size of the training set and also decreases the classifier training time. The anatomical scans that are collected on the scanner module, cannot be sent to PC having dynamically assigned IP address. Since in our implementation, the BCI module has a dynamically assigned IP address, therefore, the anatomical scans are first sent to a data transfer PC which has a static IP address. From this PC, the anatomical scans are forwarded to the BCI module. However, users can completely bypass the data transfer PC by assigning a static IP to the BCI module computer and transferring the anatomical scan directly from the scanner module to the BCI module.
3. **Portability** In this pipeline, the BITS-I has been replaced by a low cost button box designed around Arduino. It receives the TTL pulses directly from the scanner and converts it serial format. This serial data can then be received using a USB port rather than a legacy serial port. This entire solution makes the real-time pipeline highly portable.

Apart from these much of the pipeline remains the same as the distributed version.

5.4 ANALYZE4D

Visualizing voxel time courses can be a very effective tool in gaining better understanding of how brain is responding to a particular experimental manipulation. By analyzing voxel time course, one can visually verify if the stimulus is eliciting the right activity patterns in the brain.

Although most existing neuroimaging analysis softwares can do very sophisticated statistical measures on fMRI data, but when it comes to just visualizing the raw voxel time course, these software leave much to be desired. Analyze4D (www.analyze4d.com) is designed to read almost any data format and is therefore, meant to complement any of the existing neuroimaging softwares that an experimenter might be using for fMRI data analysis. So whether they are using

⁷Brain Extraction is still available in this pipeline for users who don't want to use grey matter masking

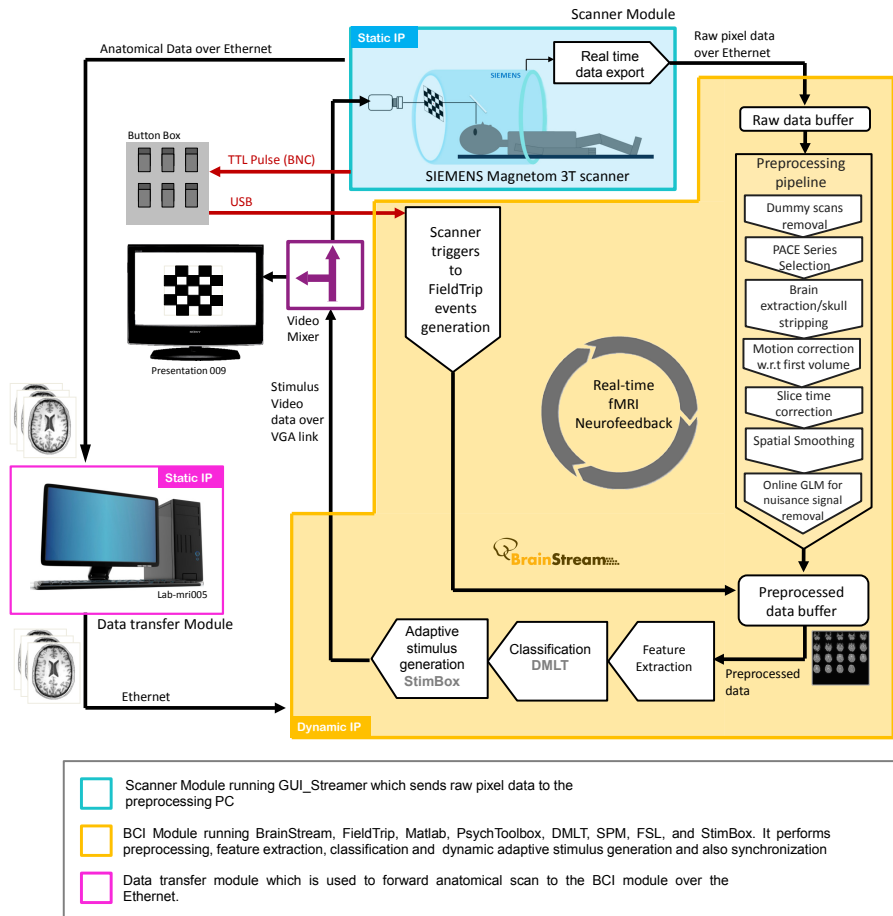


Figure 5.2 | Integrated real-time fMRI pipeline. In this pipeline, the preprocessing and the synchronization modules are integrated into the BCI module. The start up sequence is now automated in the BCI module. With just a click of button the whole pipeline can be started or stopped. The BITS1 has been replaced by a button-box which connects with the BCI module using a USB port making this implementation more general and portable. Grey matter masking has also been introduced in this pipeline to filter out the grey matter voxels from white matter, CSF, and skull voxels. The anatomical scans required to extract the grey matter mask are first passed from scanner module to a nearby computer with static IP address and from there forwarded to the BCI module, where the mask is automatically extracted and applied to the functional data.

SPM, FSL, BrainVoyager or AFNI, they can start using Analyze4D to give your analysis a fourth dimension, the dimension of time.

Analyze4D is a comprehensive tool for easy and intuitive visualization and time course analysis of functional Magnetic Resonance Imaging (fMRI) data. It has a plethora of tools to select Regions of Interest (ROI) and Volume of Interest (VOI) and analyze their time courses. Being completely GUI driven, no programming whatsoever, is needed to use it. Coupled with its ability to read virtually any neuroimaging data format, it enables anyone involved with fMRI research to use this tool for analyzing fMRI data at any stage in their analysis.



Figure 5.3 | A screenshot of Analyze4D. Analyze4D is tool for fMRI visualization and voxel time course analysis. The tool provides the ability to interactively zoom and pan into the MRI data, select the region of interests and plot the time courses of the voxels in these regions of interests. Additionally, the design matrix can be overlayed onto the time course. These are just some of the many features of Analyze4D.

5.4.1 Features of Analyze4D

Analyze4D has the following abilities:

- Supports NIFTI, Analyze 7.5, BRIK, MINC, Brainvoyager, DICOM, Matlab and Donders Real-time data formats
- Visualize functional and anatomical data
- Overlay t-maps, contrast maps, and beta maps on functional data

- Visualize the data scan-by-scan in three different mosaics i.e. Sagittal, Coronal, and axial
- Play a movie of all your functional scans
- Use intuitive zoom and pan to home in on a particular brain region or voxel
- Apply sophisticated masks during ROI and VOI analysis
- Apply interactive thresholding to imported masks such as the grey matter mask
- Apply masking from three different atlases including Anatomical Automatic Labeling (AAL) atlas to accurately perform ROI analysis on a particular anatomical region in the brain
- Overlay design matrix over voxel time courses
- Detrend the voxel time courses before plotting them
- Calculate percent signal change in the defined ROI for all the experimental conditions
- Intuitively zoom and pan the voxel time courses
- Analyze subject head motion using subtraction plots
- Import, visualize, and interact with SPM motion regressors

5.5 ANALYZE4D RT

Although the current implementation of Analyzed4D can only be used offline, a real-time version, *Analyzed4D RT*, is currently being developed. This is because the current real-time fMRI pipeline has little data visualization capabilities to offer. An experimenter cannot visualize or interact with the real-time fMRI data while it is being acquired during the experiment. The visualization capabilities of Analyze4D RT can be used to complement the existing real-time fMRI pipelines. Using Analyze4D, experimenters will be able to visualize a subject's head motion, check the real-time data for scanner spikes, perform GLM on scans while they are being acquired, and select and confine analysis to the regions of interests.

5.6 SIGNIFICANCE OF DEVELOPED HARDWARE/SOFTWARE

When this project was started, the real-time fMRI was just a bare bone implementation and had documentation that left much to be desired in terms of ease of use by complete novices. By undertaking this project, we refined that bare

bone implementation to a polished product that is now both easy to understand and design experiments with. The real-time fMRI architecture developed in this project will be used not only at Donders Institute but can be used at almost any other research institute for running real-time fMRI experiments as well. Moreover, all the tools developed are open source and free of cost unlike our competitor real-time implementations like Turbo BrainVoyager. Our pipeline is designed completely around MATLAB. Whether its dynamic stimulus generation or real-time data processing or machine learning, everything one would ever need to build a complete real-time fMRI experiment can be designed in our MATLAB-based tools, thereby enabling a user to design an entire experiment in just one easy to use language. With its open architecture anyone can modify our real-time fMRI implementation to meet their own specific needs.

With Analyze4D, researchers now have a tool that can help them in easy visualization and ROI analysis of fMRI and rtfMRI data. The software provides some of the same functionalities that are provided by commercial and proprietary softwares like BrainVoyager and MIT GabLab Timeseries Explorer, respectively. Being free and completely open source means anyone can adapt this tool for their own particular requirements. Analyzed4D which emerged as a venture from this thesis is now a Bonus deliverable for BrainGain work package 6. With continued development and improvements, our vision is to make this tool a leader in fMRI visualization and ROI analysis tools.

CHAPTER 6

SUMMARY AND GENERAL DISCUSSION

IN chapter 3, we investigated if visual perception can be decoded in real time. Our results showed that the perceived letters can be decoded but with a very low accuracy. We also investigated if a classifier trained on perceived stimuli can be used to decode imagined percepts. The results obtained suggest that it is rather difficult to get good reconstruction accuracy for imagined stimuli with classifier trained on perceived stimuli. Moreover, the experiment also investigated the effect of feedback on decoding performance. It was found that the performance was worse in the feedback conditions compared to the non-feedback conditions that preceded it. Some critical mistakes were made in the experiment design that might have contributed to rather low reconstruction accuracy. First the trials in the four conditions were not intermixed but instead were performed in four big blocks. In future designs of the experiment, the conditions should be mixed and the trial order randomized in order to rule out effect of scanner drift and other artifacts. Furthermore, the real-time neurofeedback in this experiment was not strictly real time. There was a delay of 6 TRs (9s) between the start of the task and the subject seeing the result. This is a huge amount of delay which made the neurofeedback rather useless and redundant, to say the least. More-

over, the training and testing were performed on the grey matter, CSF, and white matter voxels, when only the voxels in grey matter carry any meaningful information. In future studies, grey matter mask should be applied to confine analysis to only grey matter voxels. An even better option would be to confine analysis to only the retinotopically organized areas of the visual cortex by conducting an additional localizer experiment before the start of each experiment. Moreover, the duration of the stimulus in the training was too long which caused the bleeding of activations from activated voxels to neighboring non-activated voxels, thereby worsening the spatial localization of fMRI which was a crucial pre-requisite for this experiment.

In chapter 4, we investigated if subjects can voluntarily attend to one of the two competing overlapping stimuli and if this attended stimulus can be decoded in real time. Furthermore, the effect of neurofeedback on subject performance was also investigated. The lessons learned during the previous experiment were applied in the design of this experiment. For example, instead of performing each condition in one big block, the conditions were intermixed and the trial randomized within and across subjects. Furthermore, the scans on the transition period were also classified which reduced the feedback delay from 9s (in the previous experiment) to 4s in this experiment. The feedback was still quasi real (i.e. it had still the pipeline delay of 4s) time but still it was a huge improvement over the last experiment. The result of this experiment indicated that it is possible to decode the attended stimuli in real time with a very high accuracy. Trials in feedback condition were decoded with same accuracy non-feedback condition. The fact that feedback and non-feedback trials were intermixed might have resulted in small learning effect compared to the scenario if the two conditions were conducted in two big blocks. Further studies should be carried out to investigate if any learning effect is produced in this experiment with neurofeedback. Moreover, the results also indicate that there is a snowball effect where feedback of one classification results in a series of subsequent similar classifications.

In chapter 5, we described the hardware and software tools developed during this study. However, there is still a room for further improvement. For instance, in future experiments that might use rapid parallel imaging protocols such as 3D Flash or SENSE-EPI, the rtfMRI pipeline would need modification. Furthermore, the current pipelines provide no data visualization capabilities to the experimenter while the experiment is still running. To counter this shortcoming, an online implementation of Analyze4D can be used in future experiments to complement the existing rtfMRI pipeline with the visualization and analysis capabilities of Analyze4D.

6.1 FUTURE OF REAL-TIME fMRI

Real-time fMRI, though still in its infancy, has a great future ahead of it. Every year more and more research labs are getting involved in real-time fMRI research and some very promising developments have been made already in mind reading [117] and therapeutic interventions [18, 39, 40, 42, 69, 70] using real-time fMRI. However, these are all just experimental ventures and there is still no commercially viable application of real-time fMRI. The reason being the high cost of running an fMRI scanner and a lack of portability. In near future, we might see a shift towards the use of real-time fMRI on cheap and portable MRI scanners such as those currently being developed at UC Berkeley [48] and Fraunhofer Institute [130]. For now though, for any consumer application, MRI scanners would need to be replaced by currently available mobile technology such as fNIRS—a portable technique that is also based on the hemodynamic brain response and which should be sensitive enough for any of the applications mentioned above.

Furthermore, in future there will be a shift towards two-brain studies using hyperscanning fMRI (hfMRI). The term ‘Hyperscan’ embodies both the hardware and the software necessary to link two or more magnetic resonance scanners through the internet. Hyperscanning allows to conduct human behavioral experiments in which participants can interact with each other while functional MRI is acquired in synchrony with the behavioral interactions [84]. The advent of hyperscanning is a major breakthrough because many aspects of social behavior are not easily understood by looking at just one brain. For example, can one try to understand a bitter argument by only recording what one person said? Of course not. Hyperscanning enables us to see both sides of the equation and sheds light on behaviors that are a property of shared social behavior. A disagreement in bargaining, for example, is a shared activity that can be best understood by seeing the joint activity in two brains at the same time. Hyperscanning has already proven valuable in discovering agent-specific responses in the cingulate cortex during economic exchanges [124] and in finding the neural correlates of reputation and trust in a two-person economic exchange [55]. In future we will see more of such research studies investigating how our brains behave in complex social and economic interactions.

REFERENCES

- 1.
2. Mirzajani A, N Riyahi-Alam, M A Oghabian, K Firuznia, and H Saberi. An fMRI study of human visual cortex in response to spatiotemporal properties of visual stimuli. *Iranian Journal of Radiology*, 3(4):191–194, 2006.
3. G K Aguirre, J A Detre, D C Alsop, and M D'Esposito. The parahippocampus subserves topographical learning in man. *Cerebral Cortex*, 6(6):823–829, 1996.
4. G K Aguirre, E Zarahn, and M D'Esposito. An area within human ventral cortex sensitive to 'building' stimuli: evidence and implications. *Neuron*, 21(2):373–383, 1998.
5. G K Aguirre, E Zarahn, and M D'Esposito. The variability of human, BOLD hemodynamic responses. *NeuroImage*, 8(4):360–369, 1998.
6. Y Aleman-Gomez, L Melie-Garcia, and P Valdes-Hernandez. *IBASPM: Toolbox for automatic parcellation of brain structures*, pages 11–15. 2005.
7. J Ashburner and K J Friston. Unified segmentation. *NeuroImage*, 26(3):839–851, 2005.
8. E Bagarinao, K Matsuo, T Nakai, and S Sato. Estimation of general linear model coefficients for real-time application. *NeuroImage*, 19(2 Pt 1):422–429, 2003.
9. E Bagarinao, T Nakai, and Y Tanaka. Real-time functional MRI: development and emerging applications. *Magnetic resonance in medical sciences MRMS an official journal of Japan Society of Magnetic Resonance in Medicine*, 5(3):157–165, 2006.
10. C I Baker, M Behrmann, and C R Olson. Impact of learning on representation of parts and wholes in monkey inferotemporal cortex. *Nature Neuroscience*, 5(11):1210–6, 2002.
11. M Battaglini, S M Smith, and N Brogi, Sand De Stefano. Enhanced brain extraction improves the accuracy of brain atrophy estimation. *NeuroImage*, 40(2):583–589, 2008.
12. T Bayne. *I Know What you are Thinking: Brain Imaging and Mental Privacy*, chapter Mindreading. Oxford University Press.
13. H Benali, J Mattout, and M Pelegrini-Issac. Multivariate strategies in functional magnetic resonance imaging. *Brain and Language*, 18(2):548–559, 2003.
14. G M Boynton, S A Engel, G H Glover, and D J Heeger. Linear systems analysis of functional magnetic resonance imaging in human V1. *Journal of Neuroscience*, 16(13):4207–4221, 1996.
15. S L Brincat and C E Connor. Underlying principles of visual shape selectivity in posterior inferotemporal cortex. *Nature Neuroscience*, 7(8):880–886, 2004.
16. T A Carlson, P Schrater, and S He. Patterns of activity in the categorical representations of objects. *Journal of Cognitive Neuroscience*, 15(5):704–717, 2003.
17. M Cerf, N Thiruvengadam, F Mormann, A Kraskov, R Q Quiroga, C Koch, and I Fried. On-line, voluntary control of human temporal lobe neurons. *Nature*, 467(7319):1104–1108, 2010.

18. Heather Chapin, Epifanio Bagarinao, and Sean Mackey. Real-time fmri applied to pain management. *Neuroscience Letters*, (0):1–8, 2012.
19. A C Connolly, Y C Wu, J S Guntupalli, and J V Haxby. Scanning parameters for optimal decoding in visual cortex using a 32-channel head coil for fMRI. *Journal of Vision*, 11:822Ü822, 2011.
20. D D Cox and R L Savoy. Functional magnetic resonance imaging (fMRI) “brain reading”: detecting and classifying distributed patterns of fMRI activity in human visual cortex. *NeuroImage*, 19(2 Pt 1):261–270, 2003.
21. X Cui, C B Jeter, D Yang, P R Montague, and D M Eagleman. Vividness of mental imagery: individual variability can be measured objectively. *Vision Research*, 47(4):474–478, 2007.
22. F De Martino, G Valente, N Staeren, J Ashburner, R Goebel, and E Formisano. Combining multivariate voxel selection and support vector machines for mapping and classification of fMRI spatial patterns. *NeuroImage*, 43(1):44–58, 2008.
23. S Dehaene and L Cohen. The unique role of the visual word form area in reading. *Trends in Cognitive Sciences*, 15(6):254–262, 2011.
24. A Eklund, M Andersson, H Ohlsson, A Ynnerman, and H Knutsson. A Brain Computer Interface for Communication Using Real-Time fMRI. *2010 20th International Conference on Pattern Recognition*, 0:3665–3669, 2010.
25. A Eklund, H Ohlsson, M Andersson, J Rydell, A Ynnerman, and H Knutsson. *Using Real-Time fMRI to Control a Dynamical System*, page 3685. 2009.
26. R Epstein and N Kanwisher. A cortical representation of the local visual environment. *Nature*, 392(6676):598–601, 1998.
27. M J Farah. The neurological basis of mental imagery: a componential analysis. *Cognition*, 18(1-3):245–272, 1984.
28. G C Feigl, S Safavi-Abbasi, A Gharabaghi, V Gonzalez-Felipe, A El Shawarby, H-J Freund, and M Samii. Real-time 3T fMRI data of brain tumour patients for intra-operative localization of primary motor areas. *European journal of surgical oncology the journal of the European Society of Surgical Oncology and the British Association of Surgical Oncology*, 34(6):708–715, 2008.
29. P Foldiak. Neural coding: non-local but explicit and conceptual. *Current Biology*, 19(19):R904–R906, 2009.
30. E Formisano, F De Martino, M Bonte, and R Goebel. “Who” is saying “what”? Brain-based decoding of human voice and speech. *Science*, 322(5903):970–3, 2008.
31. E Formisano, D E J Linden, F Di Salle, L Trojano, F Esposito, A T Sack, D Grossi, F E Zanella, and R Goebel. Tracking the Mind’s Image in the Brain I: Time-Resolved fMRI during Visuospatial Mental Imagery. *Neuron*, 35(1):185–194, 2002.
32. J Friedman, T Hastie, and R Tibshirani. Regularization Paths for Generalized Linear Models via Coordinate Descent. *Journal Of Statistical Software*, 33(1):1–22, 2010.
33. G Ganis, W L Thompson, and S M Kosslyn. Brain areas underlying visual mental imagery and visual perception: an fMRI study. *Brain Research*, 20(2):226–241, 2004.
34. H Gelbard-Sagiv, R Mukamel, M Harel, R Malach, and I Fried. Internally generated reactivation of single neurons in human hippocampus during free recall. *Science*, 322(5898):96–101, 2008.

35. J O S Goh, S C Siong, D Park, A Gutchess, A Hebrank, and M W L Chee. Cortical areas involved in object, background, and object-background processing revealed with functional magnetic resonance adaptation. *Journal of Neuroscience*, 24(45):10223–10228, 2004.
36. E B Goldstein. *Sensation and Perception*. Wadsworth Pub Co, 2009.
37. M L Gorno-Tempini and C J Price. Identification of famous faces and buildings: a functional neuroimaging study of semantically unique items. *Brain: A journal of neurology*, 124:2087–2097, 2001.
38. R C Gur and E R Hilgard. Visual imagery and the discrimination of differences between altered pictures simultaneously and successively presented. *British journal of psychology London England 1953*, 66(3):341–345, 1975.
39. S Haller, N Birbaumer, and R Veit. Real-time fMRI feedback training may improve chronic tinnitus. *European Radiology*, 20(3):696–703, 2010.
40. M Hampson, T Stoica, J Saksa, D Scheinost, M Qiu, J Bhawnani, C Pittenger, X Papademetris, and T Constable. Real-time fMRI Biofeedback Targeting the Orbitofrontal Cortex for Contamination Anxiety. *Journal of visualized experiments JoVE*, (59):1–8, 2012.
41. Jonathan Harel, Christof Koch, and Pietro Perona. Graph-Based Visual Saliency. *America*, 19(2):545, 2007.
42. K J Hartwell, J J Prisciandaro, J Borckardt, X Li, M S George, and K T Brady. Real-Time fMRI in the Treatment of Nicotine Dependence: A Conceptual Review and Pilot Studies. *Psychology of Addictive Behaviors Journal of the Society of Psychologists in Addictive Behaviors*, 2012.
43. J V Haxby, M I Gobbini, M L Furey, A Ishai, J L Schouten, and P Pietrini. Distributed and overlapping representations of faces and objects in ventral temporal cortex. *Science*, 293(5539):2425–2430, 2001.
44. J D Haynes and G Rees. Predicting the orientation of invisible stimuli from activity in human primary visual cortex. *Nature Neuroscience*, 8(5):686–691, 2005.
45. J D Haynes and G Rees. Decoding mental states from brain activity in humans. *Nature Reviews Neuroscience*, 7(7):523–534, 2006.
46. A E Hillis, M Newhart, J Heidler, P Barker, E Herskovits, and M Degaonkar. The roles of the ‘visual word form area’ in reading. *NeuroImage*, 24(2):548–59, 2005.
47. R D Hoge and G B Pike. Oxidative metabolism and the detection of neuronal activation via imaging. *Journal of Chemical Neuroanatomy*, 22(1-2):43–52, 2001.
48. C Humphries. Cheap, Portable MRI. <http://www.technologyreview.com/news/406510/cheap-portable-mri/>, Sep 2006.
49. A Ishai, L G Ungerleider, and J V Haxby. Distributed neural systems for the generation of visual images. *Neuron*, 28(3):979–990, 2000.
50. P Jezzard, P M Matthews, and S M Smith, editors. *Functional MRI: An Introduction to Methods*. Oxford University Press, USA, 1 edition, 2002.
51. K A Johnson, K Hartwell, T Lematty, J Borckardt, P S Morgan, K Govindarajan, K Brady, and M S George. Intermittent “Real-time” fMRI Feedback Is Superior to Continuous Presentation for a Motor Imagery Task: A Pilot Study. *Journal of neuroimaging official journal of the American Society of Neuroimaging*, 22(1):1–9, 2010.

52. Y Kamitani and F Tong. Decoding the visual and subjective contents of the human brain. *Nature Neuroscience*, 8(5):679–685, 2005.
53. N Kanwisher, J McDermott, and M Chun. The fusiform face area: A module in human extrastriate cortex specialized for face perception. *Journal of Neuroscience*, 17:4302–4311, 1997.
54. C Kesavadas, B Thomas, S Sujesh, R Ashalata, M Abraham, A K Gupta, and K Radhakrishnan. Real-time functional MR imaging (fMRI) for presurgical evaluation of paediatric epilepsy. *Pediatric Radiology*, 37(10):964–974, 2007.
55. B King-Casas, D Tomlin, C Anen, C F Camerer, S R Quartz, and P R Montague. Getting to know you: reputation and trust in a two-person economic exchange. *Science*, 308(5718):78–83, 2005.
56. I Klein, J Dubois, J Mangin, F Kherif, G Flandin, J Poline, M Denis, S M Kosslyn, and D Le Bihan. Retinotopic organization of visual mental images as revealed by functional magnetic resonance imaging. *Brain Research*, 22(1):26–31, 2004.
57. M Knauff. Visual and spatial representations in relational reasoning, 2000.
58. M Knauff, J Kassubek, T Mulack, and M W Greenlee. Cortical activation evoked by visual mental imagery as measured by fMRI. *NeuroReport*, 11(18):3957–3962, 2000.
59. S M Kosslyn, N M Alpert, W L Thompson, V Maljkovic, S B Weise, S F Chabris, S E Hamilton, S L Rauch, and F S Buonanno. Visual mental imagery activates topographically organized visual cortex: PET investigations. *Journal of Cognitive Neuroscience*, 5(3):263–287, 1993.
60. S M Kosslyn, A Pascual-Leone, O Felician, S Camposano, J P Keenan, W L Thompson, G Ganis, K E Sukel, and N M Alpert. The role of area 17 in visual imagery: convergent evidence from PET and rTMS. *Science*, 284(5411):167–170, 1999.
61. S M Kosslyn and W L Thompson. When is early visual cortex activated during visual mental imagery? *Psychological Bulletin*, 129(5):723–746, 2003.
62. S M Kosslyn, W L Thompson, and N M Alpert. Neural systems shared by visual imagery and visual perception: a positron emission tomography study. *NeuroImage*, 6(4):320–334, 1997.
63. S M Kosslyn, W L Thompson, and G Ganis. *The Case for Mental Imagery*, volume 1. Oxford University Press, 2006.
64. G Kreiman, C Koch, and I Fried. Imagery neurons in the human brain. *Nature*, 408(6810):357–361, 2000.
65. N Kriegeskorte and P Bandettini. Analyzing for information, not activation, to exploit high-resolution fMRI. *NeuroImage*, 38(4):649–62, 2007.
66. N Kriegeskorte, E Formisano, B Sorger, and R Goebel. Individual faces elicit distinct response patterns in human anterior temporal cortex. *Proceedings of the National Academy of Sciences of the United States of America*, 104(51):20600–20605, 2007.
67. S M Laconte, S J Peltier, and X P Hu. Real-Time fMRI Using Brain-State Classification. *Human Brain Mapping*, 1044(10):1033–1044, 2007.
68. J Lee, J Ryu, F A Jolesz, Z Cho, and S Yoo. Brain-machine interface via real-time fMRI: preliminary study on thought-controlled robotic arm. *Neuroscience Letters*, 450(1):1–6, 2009.

69. X Li, K J Hartwell, J Borckardt, J J Prisciandaro, M E Saladin, P S Morgan, K A Johnson, T Lematty, K T Brady, and M S George. Volitional reduction of anterior cingulate cortex activity produces decreased cue craving in smoking cessation: a preliminary real-time fMRI study. *Addiction Biology*, 2012.
70. D E J Linden, I Habes, S J Johnston, S Linden, R Tatineni, L Subramanian, B Sorger, D Healy, and R Goebel. Real-time self-regulation of emotion networks in patients with depression. *PLoS ONE*, 7(6):e38115, 2012.
71. H L Liu, Y Pu, L D Nickerson, Y Liu, P T Fox, and J H Gao. Comparison of the temporal response in perfusion and BOLD-based event-related functional MRI. *Magnetic Resonance in Medicine*, 43(5):768–772, 2000.
72. J Liu, A Harris, and N Kanwisher. Stages of processing in face perception: an MEG study. *Nature Neuroscience*, 5(9):910–916, 2002.
73. H Lu, S Yang, Y Zuo, S Demny, E A Stein, and Y Yang. Real-time animal functional magnetic resonance imaging and its application to neuropharmacological studies. *Magnetic Resonance Imaging*, 26(9):1266–1272, 2008.
74. J Maclaren, M Herbst, O Speck, and M Zaitsev. Prospective motion correction in brain imaging: A review. *Magnetic Resonance in Medicine*, 000, 2012.
75. D F Marks. Visual imagery differences in the recall of pictures. *British journal of psychology London England 1953*, 64(1):17–24, 1973.
76. B D McCandliss, L Cohen, and S Dehaene. The visual word form area: expertise for reading in the fusiform gyrus. *Trends in Cognitive Sciences*, 7(7):293–299, 2003.
77. G McCarthy, A Puce, J C Gore, and T Allison. Face-specific processing in the human fusiform gyrus. *Journal of Cognitive Neuroscience*, 9(5):605–610, 1997.
78. A Mechelli, C J Price, K J Friston, and A Ishai. Where bottom-up meets top-down: neuronal interactions during perception and imagery. *Cerebral Cortex*, 14(11):1256–1265, 2004.
79. E Mellet, S Briscogne, N Tzourio-Mazoyer, O Ghaem, L Petit, L Zago, O Etard, A Berthoz, B Mazoyer, and M Denis. Neural correlates of topographic mental exploration: the impact of route versus survey perspective learning. *NeuroImage*, 12(5):588–600, 2000.
80. E Mellet, N Tzourio, F Crivello, M Joliot, M Denis, and B Mazoyer. Functional anatomy of spatial mental imagery generated from verbal instructions. *Journal of Neuroscience*, 16(20):6504–6512, 1996.
81. M Mishkin and L G Ungerleider. Contribution of striate inputs to the visuospatial functions of parieto-preoccipital cortex in monkeys. *Behavioural Brain Research*, 6(1):57–77, 1982.
82. T M Mitchell, R Hutchinson, R S Niculescu, F Pereira, X Wang, M Just, and S Newman. Learning to Decode Cognitive States from Brain Images. *Machine Learning*, 57(1/2):145–175, 2004.
83. Y Miyawaki, H Uchida, O Yamashita, M Sato, Y Morito, H C Tanabe, N Sadato, and Y Kamitani. Visual image reconstruction from human brain activity using a combination of multiscale local image decoders. *Neuron*, 60(5):915–929, 2008.
84. P R Montague, G S Berns, J D Cohen, S M McClure, G Pagnoni, M Dhamala, M C Wiest, I Karpov, R D King, N Apple, and et al. Hyperscanning: simultaneous fmri during linked social interactions. *NeuroImage*, 16(4):1159–1164, 2002.

85. T Mulholland, R Boudrot, and A Davidson. Feedback delay and amplitude threshold and control of the occipital EEG. *Applied Psychophysiology and Biofeedback*, 4:93–102, 1979.
86. T Naselaris, R J Prenger, K N Kay, M Oliver, and J L Gallant. Bayesian reconstruction of natural images from human brain activity. *Neuron*, 63(6):902–15, 2009.
87. S Nishimoto, A T Vu, T Naselaris, Y Benjamini, B Yu, and J L Gallant. Reconstructing visual experiences from brain activity evoked by natural movies. *Current Biology*, 21(19):1–6, 2011.
88. K M O’Craven and N Kanwisher. Mental imagery of faces and places activates corresponding stimulus-specific brain regions. *Journal of Cognitive Neuroscience*, 12(6):1013–1023, 2000.
89. K M O’Craven and N Kanwisher. Mental imagery of faces and places activates corresponding stimulus-specific brain regions. *Journal of Cognitive Neuroscience*, 12(6):1013–1023, 2000.
90. S Ogawa, T M Lee, A R Kay, and D W Tank. Brain magnetic resonance imaging with contrast dependent on blood oxygenation. *Proceedings of the National Academy of Sciences of the United States of America*, 87(24):9868–9872, 1990.
91. Y Otaka, R Osu, M Kawato, M Liu, S Murata, and Y Kamitani. Decoding Syllables from Human fMRI Activity. *Magnetic Resonance Imaging*, 4985(LNCS):979–986, 2008.
92. A J O’Toole, F Jiang, H Abdi, N Penard, J P Dunlop, and M A Parent. Theoretical, statistical, and practical perspectives on pattern-based classification approaches to the analysis of functional neuroimaging data. *Journal of Cognitive Neuroscience*, 19(11):1735–1752, 2007.
93. W D Penny, K J Friston, J T Ashburner, S J Kiebel, and T E Nichols, editors. *Statistical Parametric Mapping: The Analysis of Functional Brain Images*. Academic Press, 1 edition, 12 2006.
94. F Pereira, T Mitchell, and M Botvinick. Machine learning classifiers and fMRI: a tutorial overview. *NeuroImage*, 45(1 Suppl):S199–209, 2009.
95. F Pereira, T Mitchell, and M Botvinick. Machine learning classifiers and fMRI: A tutorial overview. *NeuroImage*, 45(1, Supplement 1):S199–S209, 2009.
96. D Pitcher, L Garrido, V Walsh, and B Duchaine. TMS disrupts the perception and embodiment of facial expressions. *Journal of Neuroscience*, 8(6):700, 2008.
97. D Pitcher, V Walsh, G Yovel, and B Duchaine. TMS evidence for the involvement of the right occipital face area in early face processing. *Current Biology*, 17(18):1568–1573, 2007.
98. C Preibisch, U Pilatus, J Bunke, F Hoogenraad, F Zanella, and H Lanfermann. Functional MRI using sensitivity-encoded echo planar imaging (SENSE-EPI). *NeuroImage*, 19(2 Pt 1):412–421, 2003.
99. A Puce, T Allison, J C Gore, and G McCarthy. Face-sensitive regions in human extrastriate cortex studied by functional MRI. *Journal of Neurophysiology*, 74(3):1192–1199, 1995.
100. R Quian Q, L Reddy, G Kreiman, C Koch, and I Fried. Invariant visual representation by single neurons in the human brain. *Nature*, 435(7045):1102–1107, 2005.

101. R Q Quiroga. Concept cells: the building blocks of declarative memory functions. *Nature reviews Neuroscience*, 2012.
102. S Z Rapsak, E S Kim, M L Henry, S M Andersen, and P M Beeson. The Contributions of the Visual Word Form Area to Skilled Reading. *Neurology*, 72(11):A265–A265, 2009.
103. L Reddy, N Tsuchiya, and T Serre. Reading the mind’s eye: decoding category information during mental imagery. *NeuroImage*, 50(2):818–25, 2010.
104. B Rockstroh, T Elbert, N Birbaumer, and W Lutzenberger. Biofeedback-produced hemispheric asymmetry of slow cortical potentials and its behavioural effects. *International Journal of Psychophysiology*, 9(2):151–165, 1990.
105. P F Rodriguez. Neural decoding of goal locations in spatial navigation in humans with fMRI. *Human Brain Mapping*, 31(3):391–397, 2010.
106. R S Rosenbaum, M Ziegler, G Winocur, C L Grady, and M Moscovitch. “I have often walked down this street before”: fMRI studies on the hippocampus and other structures during mental navigation of an old environment. *Hippocampus*, 14(7):826–835, 2004.
107. C Schwindack, E Siminotto, M Meyer, A McNamara, I Marshall, J M Wardlaw, and I R Whittle. Real-time functional magnetic resonance imaging (rt-fMRI) in patients with brain tumours: preliminary findings using motor and language paradigms. *British journal of neurosurgery*, 19(1):25–32, 2005.
108. E W Sellers, D J Krusienski, D J McFarland, T M Vaughan, and J R Wolpaw. A P300 event-related potential brain-computer interface (BCI): the effects of matrix size and inter stimulus interval on performance. *Biological Psychology*, 73(3):242–252, 2006.
109. M I Sereno, S Pitzalis, and A Martinez. Mapping of contralateral space in retinotopic coordinates by a parietal cortical area in humans. *Science*, 294:1350–1354, 2001.
110. N J Shah, J C Marshall, O Zafiris, A Schwab, K Zilles, H J Markowitsch, and G R Fink. The neural correlates of person familiarity. A functional magnetic resonance imaging study with clinical implications. *Brain: A journal of neurology*, 124(Pt 4):804–815, 2001.
111. D W Shattuck and R M Leahy. Brainsuite: an automated cortical surface identification tool. *Medical Image Analysis*, 6(2):129–142, 2002.
112. D W Shattuck, S R Sandor-Leahy, K A Schaper, D A Rottenberg, and R M Leahy. Magnetic resonance image tissue classification using a partial volume model. *NeuroImage*, 13(5):856–876, 2001.
113. R N Shepard and J Metzler. Mental rotation of three-dimensional objects. *Science*, 171(972):701–703, 1971.
114. K Shibata, T Watanabe, Y Sasaki, and M Kawato. Perceptual Learning Incepted by Decoded fMRI Neurofeedback Without Stimulus Presentation. *Science*, 334(6061):1413–1415, 2011.
115. I Simanova, R Oostenveld, P Hagoort, and M van Gerven. Modality-Independent Decoding of Semantic Information from the Human Brain. 2011.
116. S M Smith. Fast robust automated brain extraction. *Human Brain Mapping*, 17(3):143–155, 2002.

117. B Sorger, J Reithler, B Dahmen, and R Goebel. A Real-Time fMRI-Based Spelling Device Immediately Enabling Robust Motor-Independent Communication. *Current Biology*, 22(14):1333–1338, 2012.
118. M Stokes, R Thompson, R Cusack, and J Duncan. Top-down activation of shape-specific population codes in visual cortex during mental imagery. *Journal of Neuroscience*, 29(5):1565–1572, 2009.
119. L Subramanian, J V Hindle, S Johnston, M V Roberts, M Husain, R Goebel, and D Linden. Real-time functional magnetic resonance imaging neurofeedback for treatment of Parkinson’s disease. *Journal of Neuroscience*, 31(45):16309–16317, 2011.
120. S Thesen, O Heid, E Mueller, and L R Schad. Prospective acquisition correction for head motion with image-based tracking for real-time fmri. *Magnetic Resonance in Medicine*, 44(3):457–465, 2000.
121. B Thirion, E Duchesnay, E Hubbard, J Dubois, J Poline, D Lebihan, and S Dehaene. Inverse retinotopy: inferring the visual content of images from brain activation patterns. *NeuroImage*, 33(4):1104–1116, 2006.
122. W L Thompson, S M Kosslyn, K E Sukel, and N M Alpert. Mental imagery of high- and low-resolution gratings activates area 17. *NeuroImage*, 14(2):454–64, 2001.
123. R Tibshirani. Regression shrinkage and selection via the lasso. *Journal of the Royal Statistical Society Series B Methodological*, 58(1):267–288, 1996.
124. D Tomlin, M A Kayali, B King-Casas, C Anen, C F Camerer, S R Quartz, and P R Montague. Agent-specific responses in the cingulate cortex during economic exchanges. *Science*, 312(5776):1047–1050, 2006.
125. R B Tootell, M S Silverman, E Switkes, and R L De Valois. Deoxyglucose analysis of retinotopic organization in primate striate cortex. *Science*, 218(4575):902–904, 1982.
126. L Trojano and D Grossi. A critical review of mental imagery defects. *Brain and Cognition*, 24(2):213–243, 1994.
127. N Tzourio-Mazoyer, B Landeau, D Papathanassiou, F Crivello, O Etard, N Delcroix, B Mazoyer, and M Joliot. Automated anatomical labeling of activations in SPM using a macroscopic anatomical parcellation of the MNI MRI single-subject brain. *NeuroImage*, 15(1):273–289, 2002.
128. L G Ungerleider and J V Haxby. ‘what’ and ‘where’ in the human brain. *Current Opinion in Neurobiology*, 4(2):157–165, 1994.
129. M A J Van Gerven, P Kok, F P De Lange, and T Heskes. Dynamic decoding of ongoing perception. *NeuroImage*, 57(3):950–7, 2011.
130. F Volke. Pocket-sized magnetic resonance imaging. . <http://www.archiv.fraunhofer.de/archiv/pi-en-2004-2008/EN/press/pi/2008/07/ResearchNews072008Topic1.html>, 2008.
131. V Q Vu, P Ravikumar, T Naselaris, K N Kay, J L Gallant, and B Yu. Encoding and decoding V1 fMRI responses to natural images with sparse nonparametric models. *The Annals of Applied Statistics*, 5(2B):1159–1182, 2011.
132. N Weiskopf, F Scharnowski, R Veit, R Goebel, N Birbaumer, and K Mathiak. Self-regulation of local brain activity using real-time functional magnetic resonance imaging (fMRI). *Journal Of Physiology Paris*, 98(4-6):357–373, 2004.

133. D Yi, T A Kelley, R Marois, and M M Chun. Attentional modulation of repetition attenuation is anatomically dissociable for scenes and faces. *Brain Research*, 1080(1):53–62, 2006.
134. H Zou and T Hastie. Regularization and variable selection via the elastic net. *Journal of the Royal Statistical Society - Series B: Statistical Methodology*, 67(2):301–320, 2005.

Appendices

APPENDIX A

Experiment 1 - Informed consent form

Please consider this information carefully before deciding whether to participate in this research.

Purpose of the research: The experiment uses fMRI to predict what you see and imagine. Furthermore, this prediction will be done in real time, which in simple terms means that you will be able to see if the computer makes correct or wrong prediction.

What you will do in this research: In the first 30 minutes of the experiment, we will brief you about the whole experiment. Then we will put you in the scanner and start the experiment. For the next 45 minutes, you will see various random flickering patterns on a screen inside the MRI scanner. During this time, the computer trains itself and learns your brain activity. This training part would be extremely boring for you because you would constantly need to stare at flickering patterns on the screen, but you needn't worry because the fun part is just about to begin.

Once the computer is trained, it can start predicting your visual perception. You will see an alphabet on the screen and the computer will predict what alphabet you are seeing. You will be able to see the computer's prediction. After this, the computer will start to predict your visual imagination. You will be asked to imagine an alphabet and the computer will make a prediction as to what alphabet you were thinking about. Again, you will be able to see if the computer makes a right or a wrong prediction, which make this experiment very interesting. More detailed information about the experiment will be given to you in the pre-scan briefing.

Time required: The experiment will take 2.5 hours from start to finish.

Risks: Because you will be staring at flickering patterns for about 90 minutes, therefore tears may come out of your eyes during the experiment. You may experience mild headache after the experiment as well.

Benefits: At the end of the study, we will provide a thorough explanation of the study and of our hypotheses. We will describe the potential implications of the results of the study both if our hypotheses are supported and if they are disconfirmed. If you wish, you can send an email message to adnaniazi@gmail.com and we will send you a copy of any manuscripts based on the research (or summaries of our results).

Compensation: You will receive 25 Euros or 2.5 Study Pool credits for your participation in this study. As a souvenir for your participation in the experiment,

you will also be given a video of your brain anatomy and a video of your skull in 3D. These will be emailed to you within two weeks after your participation in the experiment.

Eligibility Requirements: Normal or corrected to normal vision, no family history of epilepsy, no tattoos on the neck, no braces, no metal implants, no piercing, must be at least 18 or older and must be able to understand English.

Participation and withdrawal: Your participation in this study is completely voluntary, and you may withdraw at any time without penalty. You may withdraw by informing the researcher that you no longer wish to participate (no questions will be asked).

Confidentiality: Your participation in this study will remain confidential and there will be no link between your responses and your identity. Participation and withdrawal: You can withdraw from the study at anytime without giving a reason. How to contact the researchers: If you have questions or concerns about your participation or payment, or want to request a summary of research findings, please contact the researcher:

Name: Adnan Niazi
 Email: adnaniazi@gmail.com
 Mobile: *****

Whom to contact about your rights in this research: For questions, concerns, suggestions, or complaints that are not being addressed by the researcher, or research-related harm: Committee on the Use of Human Subjects in Research (Commissie Mensgebonden Onderzoek) at UMC St. Radboud.

<http://www.cmoregio-a-n.nl/>

Agreement

The nature and purpose of this research have been sufficiently explained and I agree to participate in this study. I understand that I am free to withdraw at any time without incurring any penalty.

Signature: _____

Date: _____

Name: _____

APPENDIX B

Experiment 2 - Informed consent form

Please consider this information carefully before deciding whether to participate in this research.

Purpose of the research: The experiment uses fMRI to ascertain whether you can voluntarily attend to one stimulus when presented with two overlapping stimuli and if this attended stimulus could be decoded.

What you will do in this research: In the first 30 minutes of the experiment, we will brief you about the whole experiment. Then we will put you in the scanner and start the experiment. For the next 25 minutes, you will see pictures of famous faces and famous places. During this time the computer will train itself.

Once the computer is trained, we will present you two overlapping pictures, one of a famous person such as Michael Jackson and the other of a famous landmark such as Eiffel Tower. Your task will be to focus only on one of the picture. Depending on which picture you are focusing on, the attended picture will become more and more visible whereas the unattended picture will fade out. This task will take about 45 minutes

Time required: The experiment will take 2 to 2.5 hours from start to finish.

Risks: There are no risk involved in taking part in this experiment.

Benefits: At the end of the study, we will provide a thorough explanation of the study and of our hypotheses. We will describe the potential implications of the results of the study both if our hypotheses are supported and if they are disconfirmed. If you wish, you can send an email message to adnaniazi@gmail.com and we will send you a copy of any manuscripts based on the research (or summaries of our results).

Compensation: You will receive 25 Euros or 2.5 Study Pool credits for your participation in this study. As a souvenir for your participation in the experiment, you will also be given a video of your brain anatomy and a video of your skull in 3D. These will be emailed to you within two weeks after your participation in the experiment.

Eligibility Requirements: Normal eyesight without glasses or contact lenses, no tattoos on the neck, no braces, no metal implants, no piercing, must be at least 18 or older and must be able to understand English.

Participation and withdrawal: Your participation in this study is completely voluntary, and you may withdraw at any time without penalty. You may withdraw

by informing the researcher that you no longer wish to participate (no questions will be asked).

Confidentiality: Your participation in this study will remain confidential and there will be no link between your responses and your identity. Participation and withdrawal: You can withdraw from the study at anytime without giving a reason. How to contact the researchers: If you have questions or concerns about your participation or payment, or want to request a summary of research findings, please contact the researcher:

Name: Adnan Niazi

Email: adnaniazi@gmail.com

Mobile: *****

Whom to contact about your rights in this research: For questions, concerns, suggestions, or complaints that are not being addressed by the researcher, or research-related harm: Committee on the Use of Human Subjects in Research (Commissie Mensgebonden Onderzoek) at UMC St. Radboud.

<http://www.cmoregio-a-n.nl/>

Agreement

The nature and purpose of this research have been sufficiently explained and I agree to participate in this study. I understand that I am free to withdraw at any time without incurring any penalty.

Signature: _____

Date: _____

Name: _____

APPENDIX C

General Informed Consent Form

**STUDYSPECIFIC INFORMED CONSENT FORM**

For participation in:*

☐

MEG

☐

EEG

☐

MRI

☐

Behavioural

*tick the applicable box(es)

To be filled out by the PARTICIPANT prior to the start of the experiment:

I confirm that:

- I was satisfactorily informed about the study concerned both verbally and in writing by means of the general information brochure and additional study specific information brochure(s) (versions 6.1, February 2012)
- I have had the opportunity to put forward questions regarding the study and that these questions have been answered satisfactorily
- I have carefully considered my participation in the experiment.
- I participate of my own free will.

I agree that:

- My data will be acquired and stored for scientific purposes as mentioned in the general information brochure.
- I will be informed by a designated physician about any new information which is of medical relevance to me.

I understand that:

- I have the right to withdraw from the experiment at any time without having to give a reason.
- My privacy is protected according to Dutch law.
- My consent will be sought every time I participate in a new experiment.

I give my consent to take part in this experiment:

Name:.....

Date of birth:..... (dd/mm/jj)

Signature:.....

Date and place:.....

I agree that my experimental and coded data for strict scientifically reasons will be shared with others:

YES / NO*

*encircle preference

To be filled by the RESEARCHER prior to the start of the experiment:

The undersigned declares that the person named above has been informed both in writing and in person about the experiment. He /she guarantees subjects' privacy protection according to Dutch law.

Name:.....

Project number:

Signature:.....

Date and place:.....

APPENDIX D

Vividness of Visual Imagery Questionnaire (VVIQ)

The VVIQ questionnaire was designed in Inquisit 2.0.60616 [Computer software]. (2006). Seattle, WA: Millisecond Software and conducted on a computer after the experiment was over. The VVIQ contains sixteen questions and these are asked twice, once with eyes open and once with eyes closed. Subjects have to rate the imagery corresponding to each question on a 5 point Likert scale. The rating 5 was assigned to most vivid imagery and the rating 1 was assigned when no mental image could be formed by the subject⁸. The total VVIQ score was calculated by adding the rating on all 32 question. Given below are the screenshots of instructions and the entire questionnaire.

The entire questionnaire will take about 10 minutes of your life.
Please do not rush through the questionnaire.
(if you try to rush, the software will automatically detect it and will slow down the rate at which the questionnaire progresses)

The aim of this test is to judge your ability to imagine.
The questions in this test will ask you to form mental pictures of something in your mind. You will then be asked to rate how clearly or vividly you were able to form that mental image.


You can assign this rating on a 5 point scale, shown below.

Perfectly clear & vivid as if I was actually seeing it	Reasonably clear and vivid	Moderately clear and vivid	Vague and dim	No image at all
---	-------------------------------	-------------------------------	------------------	--------------------

So for example, if the you are able to form the mental image, such that its reasonably clear and vivid, then drag the slider to the position shown below

Perfectly clear & vivid as if I was actually seeing it	Reasonably clear and vivid	Moderately clear and vivid	Vague and dim	No image at all
---	-------------------------------	-------------------------------	------------------	--------------------

We will now begin the questionnaire
Please imagine with your eyes OPEN
Press Next to begin



NEXT

⁸In the original VVIQ test the rating is assigned in the opposite way i.e, rating 5 for no mental image and rating 1 for the most vivid mental image.



In answering items 1 to 4, think of some relative or friend whom you frequently see and consider carefully the picture that comes before your mind's eye.

- 1). The exact contour of face, head, shoulders and body.

Perfectly clear & vivid as if I was actually seeing it	Reasonably clear and vivid	Moderately clear and vivid	Vague and dim	No image at all

- 2). Characteristic poses of head, attitudes of body etc.

Perfectly clear & vivid as if I was actually seeing it	Reasonably clear and vivid	Moderately clear and vivid	Vague and dim	No image at all

- 3). The precise carriage, length of step, etc. in walking.

Perfectly clear & vivid as if I was actually seeing it	Reasonably clear and vivid	Moderately clear and vivid	Vague and dim	No image at all

- 4). The different colours worn in some familiar clothes.

Perfectly clear & vivid as if I was actually seeing it	Reasonably clear and vivid	Moderately clear and vivid	Vague and dim	No image at all

Next



Imagine the items mentioned in the following questions and rate the vividness of your imagination

- 5). The sun is rising above the horizon into a hazy sky.

Perfectly clear & vivid as if I was actually seeing it	Reasonably clear and vivid	Moderately clear and vivid	Vague and dim	No image at all

- 6). The sky clears and surrounds the sun with blueness.

Perfectly clear & vivid as if I was actually seeing it	Reasonably clear and vivid	Moderately clear and vivid	Vague and dim	No image at all

- 7). Clouds. A storm blows up, with flashes of lightening.

Perfectly clear & vivid as if I was actually seeing it	Reasonably clear and vivid	Moderately clear and vivid	Vague and dim	No image at all

- 8). A rainbow appears.

Perfectly clear & vivid as if I was actually seeing it	Reasonably clear and vivid	Moderately clear and vivid	Vague and dim	No image at all

Back

Next



In answering items 9 to 12, think of the front of a shop which you often go to. Consider the picture that comes before your mind's eye.

9). The overall appearance of the shop from the opposite side of the road.

Perfectly clear & vivid
as if I was actually seeing it

Reasonably clear
and vivid

Moderately clear
and vivid

Vague
and dim

No image
at all

10). A window display including colours, shape and details of individual items for sale.

Perfectly clear & vivid
as if I was actually seeing it

Reasonably clear
and vivid

Moderately clear
and vivid

Vague
and dim

No image
at all

11). You are near the entrance. The colour, shape and details of the door.

Perfectly clear & vivid
as if I was actually seeing it

Reasonably clear
and vivid

Moderately clear
and vivid

Vague
and dim

No image
at all

12). You enter the shop and go to the counter. The counter assistant serves you. Money changes hands.

Perfectly clear & vivid
as if I was actually seeing it

Reasonably clear
and vivid

Moderately clear
and vivid

Vague
and dim

No image
at all

Back

Next



In answering items 13 to 16, think of a country scene which involves trees, mountains and a lake.

13). The contours of the landscape.

Perfectly clear & vivid
as if I was actually seeing it

Reasonably clear
and vivid

Moderately clear
and vivid

Vague
and dim

No image
at all

14). The colour and shape of the trees.

Perfectly clear & vivid
as if I was actually seeing it

Reasonably clear
and vivid

Moderately clear
and vivid

Vague
and dim

No image
at all

15). The colour and shape of the lake.

Perfectly clear & vivid
as if I was actually seeing it

Reasonably clear
and vivid

Moderately clear
and vivid

Vague
and dim

No image
at all

16). A strong wind blows on the trees and on the lake causing waves.

Perfectly clear & vivid
as if I was actually seeing it

Reasonably clear
and vivid

Moderately clear
and vivid

Vague
and dim

No image
at all


Back

Finish

We will now repeat the same questionnaire but this time while answering the questions, you have to imagine with your eyes closed

Please do not rush through the questionnaire.
(if you try to rush, the software will automatically detect it and will slow down the rate at which the questionnaire progresses)

Please remember to imagine with your eyes CLOSED
Press Next to begin



NEXT



In answering items 1 to 4, think of some relative or friend whom you frequently see and consider carefully the picture that comes before your mind's eye.

- 1). The exact contour of face, head, shoulders and body.

Perfectly clear & vivid
as if I was actually seeing it

Reasonably clear
and vivid

Moderately clear
and vivid

Vague
and dim

No image
at all

- 2). Characteristic poses of head, attitudes of body etc.

Perfectly clear & vivid
as if I was actually seeing it

Reasonably clear
and vivid

Moderately clear
and vivid

Vague
and dim

No image
at all

- 3). The precise carriage, length of step, etc. in walking.

Perfectly clear & vivid
as if I was actually seeing it

Reasonably clear
and vivid

Moderately clear
and vivid

Vague
and dim

No image
at all

- 4). The different colours worn in some familiar clothes.

Perfectly clear & vivid
as if I was actually seeing it

Reasonably clear
and vivid

Moderately clear
and vivid

Vague
and dim

No image
at all

Next



Imagine the items mentioned in the following questions and rate the vividness of your imagination

5). The sun is rising above the horizon into a hazy sky.

Perfectly clear & vivid
as if I was actually seeing it

Reasonably clear
and vivid

Moderately clear
and vivid

Vague
and dim

No image
at all

6). The sky clears and surrounds the sun with blueness.

Perfectly clear & vivid
as if I was actually seeing it

Reasonably clear
and vivid

Moderately clear
and vivid

Vague
and dim

No image
at all

7). Clouds. A storm blows up, with flashes of lightning.

Perfectly clear & vivid
as if I was actually seeing it

Reasonably clear
and vivid

Moderately clear
and vivid

Vague
and dim

No image
at all

8). A rainbow appears.

Perfectly clear & vivid
as if I was actually seeing it

Reasonably clear
and vivid

Moderately clear
and vivid

Vague
and dim

No image
at all

Back

Next



In answering items 9 to 12, think of the front of a shop which you often go to. Consider the picture that

9). The overall appearance of the shop from the opposite side of the road.

Perfectly clear & vivid
as if I was actually seeing it

Reasonably clear
and vivid

Moderately clear
and vivid

Vague
and dim

No image
at all

10). A window display including colours, shape and details of individual items for sale.

Perfectly clear & vivid
as if I was actually seeing it

Reasonably clear
and vivid

Moderately clear
and vivid

Vague
and dim

No image
at all

11). You are near the entrance. The colour, shape and details of the door.

Perfectly clear & vivid
as if I was actually seeing it

Reasonably clear
and vivid

Moderately clear
and vivid

Vague
and dim

No image
at all

12). You enter the shop and go to the counter. The counter assistant serves you. Money changes hands.

Perfectly clear & vivid
as if I was actually seeing it

Reasonably clear
and vivid

Moderately clear
and vivid

Vague
and dim

No image
at all

Back

Next



In answering items 13 to 16, think of a country scene which involves trees, mountains and a lake.

13). The contours of the landscape.

Perfectly clear & vivid
as if I was actually seeing it

Reasonably clear
and vivid

Moderately clear
and vivid

Vague
and dim

No image
at all

14). The colour and shape of the trees.

Perfectly clear & vivid
as if I was actually seeing it

Reasonably clear
and vivid

Moderately clear
and vivid

Vague
and dim

No image
at all

15). The colour and shape of the lake.

Perfectly clear & vivid
as if I was actually seeing it

Reasonably clear
and vivid

Moderately clear
and vivid

Vague
and dim

No image
at all

16). A strong wind blows on the trees and on the lake causing waves.

Perfectly clear & vivid
as if I was actually seeing it

Reasonably clear
and vivid

Moderately clear
and vivid

Vague
and dim

No image
at all

Back

Finish

UNIVERSITEIT TWENTE

Thank you. You are almost done
Please take a few more moments to fill in a demographic questionnaire

This task wouldn't take more than 1 minute

Press 'Start' to go to the questionnaire

Start

Demographic Questionnaire (Page 1 of 3)

1). What is your age

2). Sex

- ☐ Female
☐ Male

3). Country/Region of Primary Citizenship

4). How interesting or boring was this experiment for you? (move the slider)



5). Do you normally use glasses or contact lenses?

- ☐ Yes
☐ No

6). If your answer to the previous question was 'Yes', then how much is the deviation in your left and right eye? If you don't remember it exactly just write a rough estimate.

Demographic Questionnaire (Page 2 of 3)

7). Have you used contact lenses during the experiment?

- ☐ Yes
☐ No

8). Have you used glasses during the experiment?

- ☐ Yes
☐ No

9). Are you feeling any headache after the experiment?

- ☐ Yes
☐ No

10). Which of the following alphabets did you find difficult to imagine? (you can check multiple boxes, if you want to).

- ☐ D
☐ O
☐ N
☐ E
☐ R
☐ S
☐ I
☐ T
☐ U

Back

Next


Demographic Questionnaire (Page 3 of 3)

11). Would you like to receive an MRI video of your brain and your face in 3D, as a souvenir for your participation in the experiment?

- ☐ Yes
☐ No


12). If your answer to the previous question was 'Yes', then please write down your GMAIL or YAHOO or MSN email address. We will email you the video on that address.

13). If you have any comments or questions, please write them down.



UNIVERSITEIT TWENTE


**Radboud Universiteit
Nijmegen**




**Great
You are done !**

We appreciate your participation

Adnan Niazi,
Marcel van Gerven,
Philip van den Broek, Peter Desain, Mannes Poel



Donders Institute
for brain, cognition and behaviour

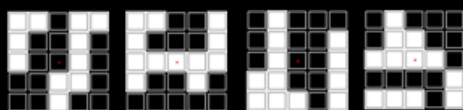


Real time decoding of visual and imagined percepts
For any queries or comments contact
 Adnan Niazi, Room B.00.74, Spinozagebouw Laag, Montessorilaan 3,
 Radboud University, Nijmegen (Email: adnaniaz@gmail.com)

APPENDIX E

Experiment 1- Pre-scan briefing and instructions

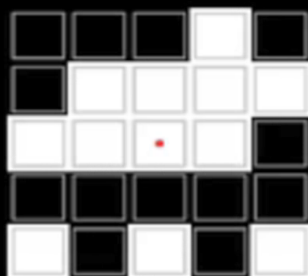
You will now be presented with random flashing patterns, some of which are shown below




Please fixate on the red fixation dot • in the middle of the screen, at all times

This task will take approx. 45 minutes

READY !!



Click  to run the video.

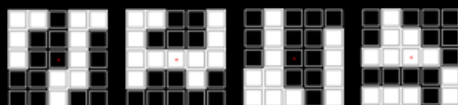
Processing training data and training classifier. This is required for the following test sessions.

This will take about 5 minutes...

Instructions for the next task will follow.

....

Previously you saw various random flashing patterns

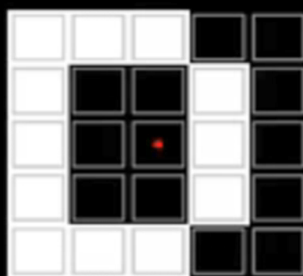


Now you will see flashing *alphabets* on the screen, as shown below



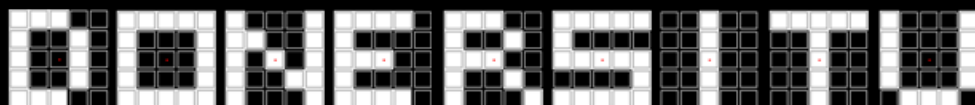
This task will take approx. 10 minutes

Please fixate on the red fixation dot ● in the middle of the screen, at all times



Click  to run the video.

You will again see various flashing *alphabets* on the screen, as shown below

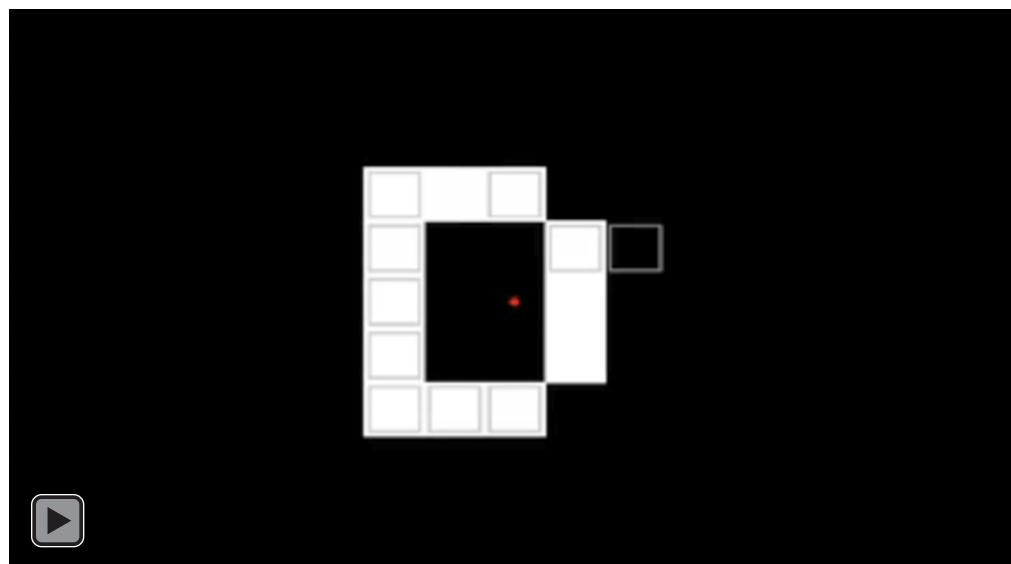



After 9 seconds into each letter, the grey boxes would start to disappear. The aim is to make all the grey boxes disappear that do not represent part of the flashing alphabet, as see examples below)



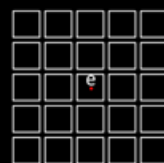
This task will take approx. 10 minutes

Please fixate on the red fixation dot ● in the middle of the screen, at all times



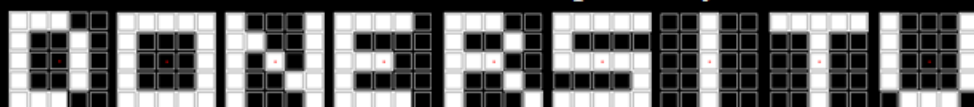
Click  to run the video.

At the beginning of each trial, you would be presented a cue alphabet in the middle of the screen. Suppose the cue is letter e.



The cue letter e would then disappear and the red fixation dot will turn green. This is an indication that you have to start imagining the capital E on the grid. You have to stop imagining when the fixation dot turns red again.

Note: For each of letter presented, you have to imagine its corresponding capital letter on the grid. The example below shows the pattern you have to imagine for the cue letters d o n e r s i t u respectively

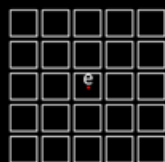


Please fixate on the fixation dot at all times



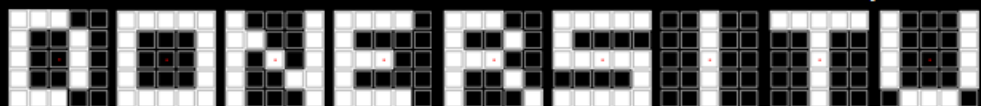
Click  to run the video.

At the beginning of each trial, you would be presented a cue letter in the middle of the screen. Suppose the cue is letter e.



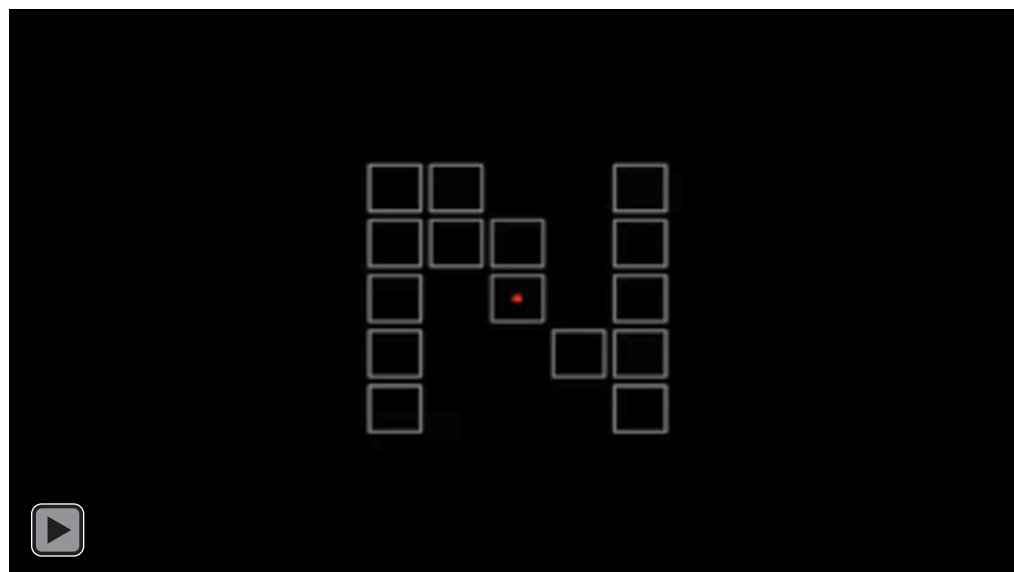
The cue letter e would then disappear and the red fixation dot will turn green. This is an indication that you have to start imagining the capital E on the grid. Stop imagining once the fixation dot turns red again.

Note: For each of letter presented, you have to imagine its corresponding capital letter on the grid. The example below shows the pattern you have to imagine for the cue letters d o n e r s i t u respectively



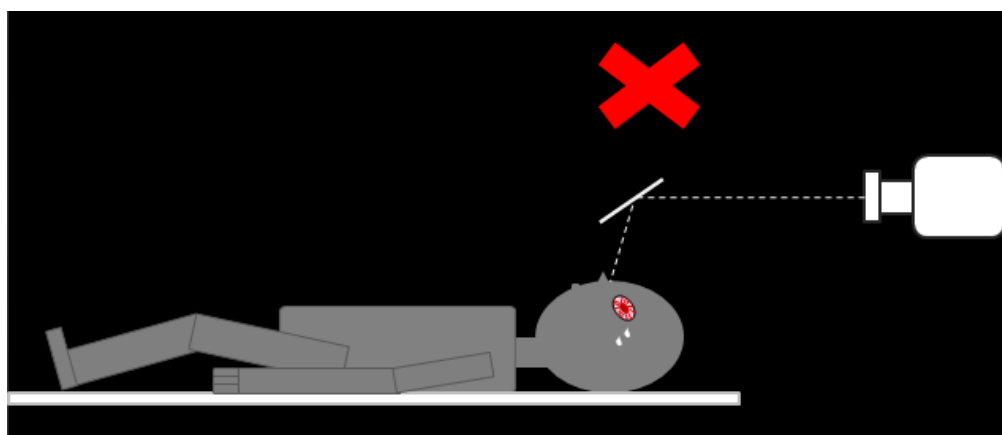
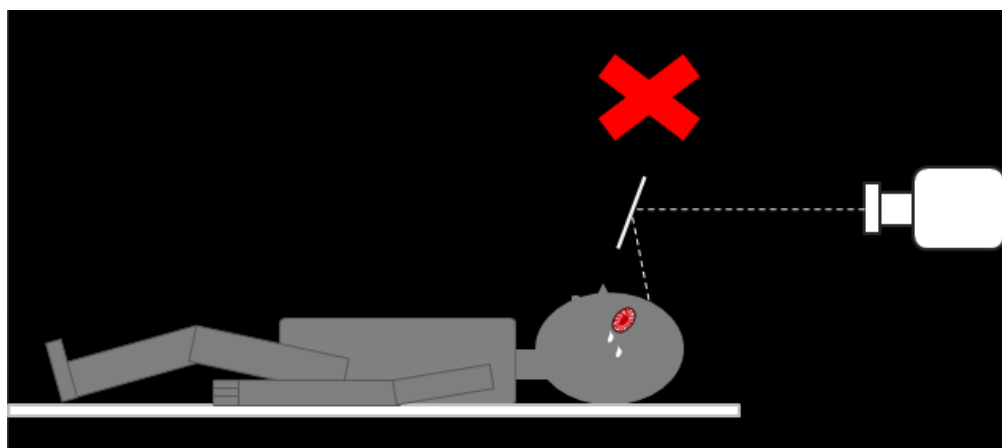
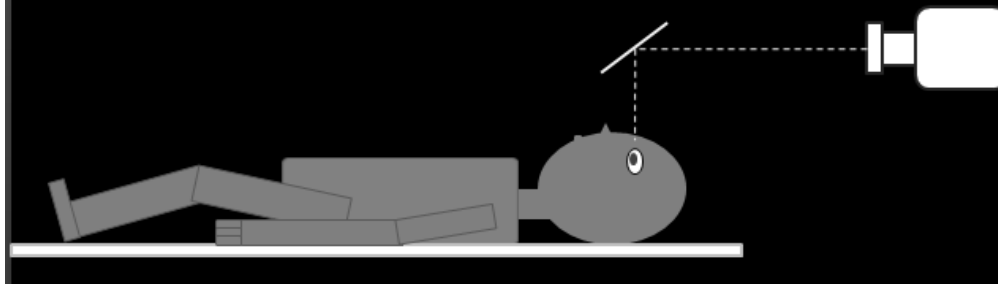
After 9 seconds into each trial, the grey rectangles that do not represent the imagined letter, would start to disappear. This gives you feedback about your imagination performance.

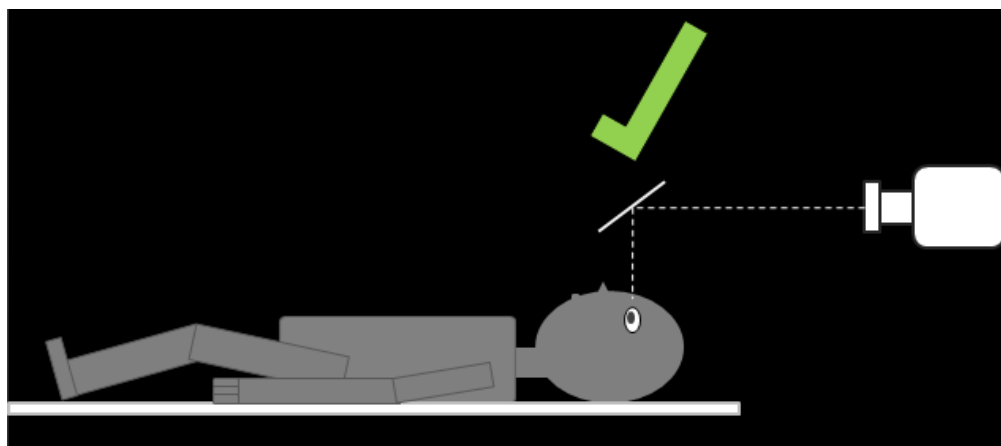
Please fixate on the fixation dot at all times.



Click  to run the video.

Please adjust the mirror properly in the scanner, so that you are conformably viewing the middle of the screen





Do this adjustment **only at the start** of the experiment



APPENDIX F

Experiment 2- Pre-scan briefing and instructions


You will be presented with blocks of pictures of famous faces and famous places. Between each two consecutive blocks is a 12 second rest period in which only a fixation cross + will be shown.

In every block, the first picture is repeated somewhere in that block. Your task is to press any button on the Button Box whenever you see the first picture repeated in a block. The whole scenario is depicted below

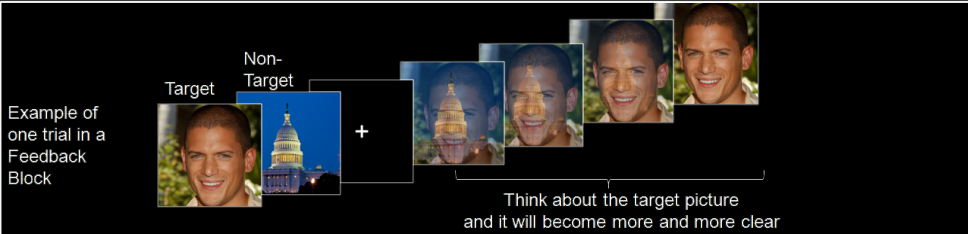


This task will take about 25 minutes




Click  to run the video.

Every trial will begin with a brief display of a target picture, followed by a brief display of a non-target picture. You will then be shown the two images overlapped over each other. Your task is to always think about the target picture. If the trial is in the *Feedback block* then the target picture will start to become more and more clear as the time progresses where as the non-target picture will fade away (shown below).

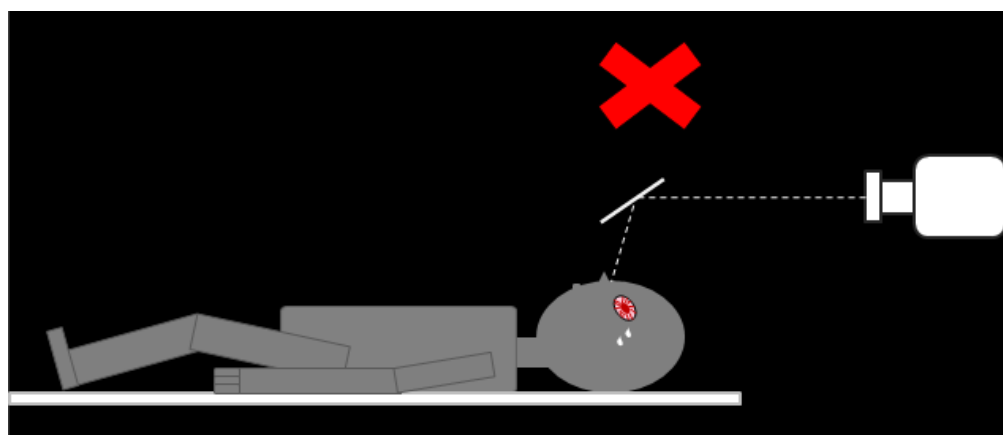
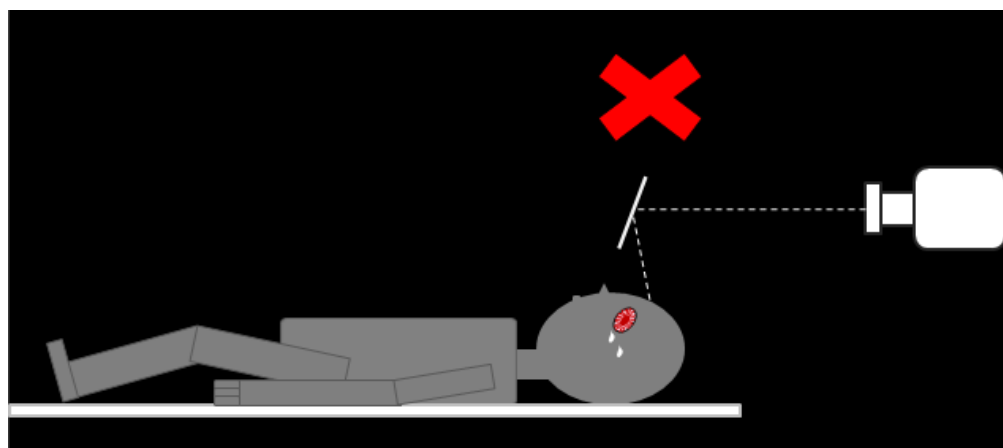
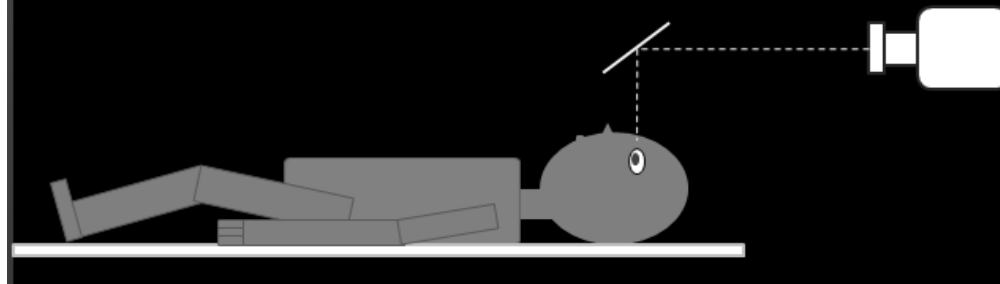


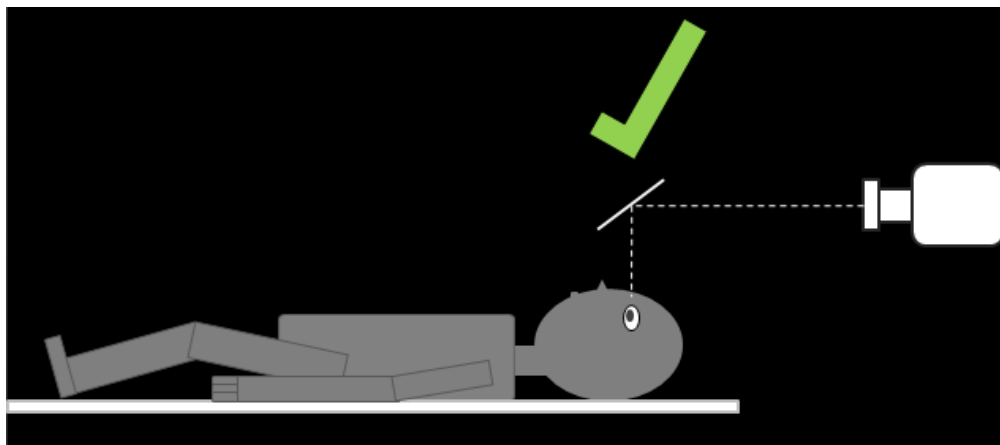
If the trial is in is Non-Feedback Block, then nothing will happen to the overlapped pictures (as shown below). But you still always need to think of the target picture.



Click  to run the video.

Please adjust the mirror properly in the scanner, so that you are conformably viewing the middle of the screen





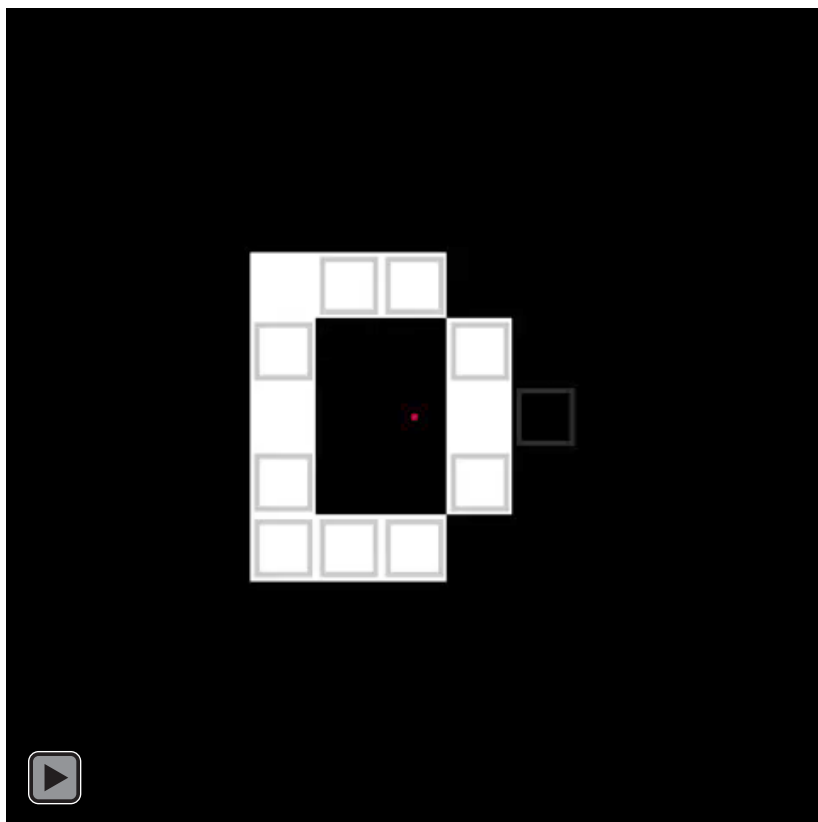
Do this adjustment **only at the start** of the experiment



APPENDIX G

Experiment 1- Best results

The video below shows the reconstruction for 'Visual perception without feedback condition' in a pilot experiment with author as the test subject. The decoding obtained in this pilot was the best we ever recorded (64%). Unfortunately, due to a technical malfunction, the remaining 3 conditions had to be aborted. At that time, only author and Philip van den Broek knew how to operate the real-time fMRI. Because of non availability of Philip, it was not possible to run a full experiment AGAIN with author in the scanner. But this video alone is a proof that it is possible to decode perceived stimuli in real time and that the reconstructions are not just some random patterns but are quite structured and do represent the perceived character.



Note: The white letter is the perceived letter. Its flickering has been stopped in this video for easy viewing by the viewer. The empty grey rectangles show the reconstructed letter. The reconstruction is updated every TR. The video is running at three times the normal speed. The rest periods and the hemodynamic lag have been removed. Decoding accuracy is 64%.

APPENDIX H

Experiment 2- Post-hoc analysis video of real-time fMRI experiment for Subject 07

Please follow the click the links below to find videos of the feedback and non-feedback blocks of the actual experiment run for subject 07.

Video of feedback condition

http://www.analyze4d.com/misc_adnan/feedback_blocks.html

Video of non-feedback blocks

http://www.analyze4d.com/misc_adnan/nonfeedback_blocks.html

Video Information: The video shows trial-by-trial rerun of the actual experiment. On the left hand side, the graph shows the α_{TR} as it evolves during the 12 scans of a trial. If the graph is colored green then it means the dominate picture in the hybrid is the target. If the graph is red then it mean the dominate picture is the non-target and that the classification is going in the wrong direction. The bar labeled 'Prob' shows the probability of the prediction made by the classifier. Green means that the prediction is right and red means that prediction is wrong. The rest is self explanatory.

Note: The first two TRs where the feedback remains static due to pipeline delay are not shown in this video.